R. & M. No. 3722

MINISTRY OF DEFENCE (PROCUREMENT EXECUTIVE)

AERONAUTICAL RESEARCH COUNCIL
REPORTS AND MEMORANDA

Measurements of the Boundary Layer and Wake of Two Aerofoil Sections at High Reynolds Numbers and High-Subsonic Mach Numbers

By T. A. Cook

Aerodynamics Dept., R. A. E., Farnborough

LONDON: HER MAJESTY'S STATIONERY OFFICE

1973

PRICE £3·30 NET

Measurements of the Boundary Layer and Wake of Two Aerofoil Sections at High Reynolds Numbers and High-Subsonic Mach Numbers

By T. A. Cook

Aerodynamics Dept., R. A. E., Farnborough

Reports and Memoranda No. 3722*
June, 1971

Summary

Boundary layer and wake surveys have been made on two cambered lifting aerofoils and integral parameters and skin-friction data have been extracted from the measurements. Skin-friction results obtained, using four integral laws and results from a 'Clauser' analysis of profile data, are consistent but values obtained, using Preston tubes, are 8 per cent higher than these, probably due to uncertainties in the compressibility corrections required, and results from razor-blade measurements are 5 per cent lower. Momentum thickness, shape parameter and skin friction (using an integral law) are compared with boundary-layer estimates made, using (i) Green's extension to compressible flow of Head's entrainment method and (ii) Bradshaw's turbulent-energy method. Agreement is generally good, though both methods under-estimate momentum thickness at the trailing edge on the upper surface, where the boundary layer is close to separation. Wake estimates were made, using Green's entrainment method, and agreement is again generally good. However, there are discrepancies between measurements and Green's method regarding the entrainment parameter used in the boundary layer.

* Replaces R.A.E. Technical Report 71127—A.R.C. 33 660.

LIST OF CONTENTS

1. Introduction

2. Experimental Details

3. Data Reduction and Corrections

   3.1. Velocity profiles and integral parameters

   3.2. Preston tube measurements

   3.3. Skin friction by Clauser's method

   3.4. Skin friction from boundary-layer integral parameters

   3.5. Razor-blade technique

4. Comparisons of Skin-Friction Results

5. Two-Dimensional Momentum Integral Equation

6. Comparisons of Boundary-Layer Estimates with Measurements

7. Comparisons of Wake Estimates with Measurements

   7.1. Extension of Squire and Young wake law

   7.2. Green's method

8. Conclusions

Acknowledgements

Symbols

References

Tables 1–20

Illustrations, Figs. 1 to 34

Detachable Abstract Cards

1. Introduction

An important feature of the pressure distribution on many recent aerofoil sections, which have been used in the design of swept-winged aircraft, has been a region of near-critical or supercritical flow on the upper surface followed by a very large adverse pressure gradient. In some instances where a moderate or large degree of rear loading is aimed for, there may be severe adverse pressure gradients on the lower surface also. Thus in order to avoid separating flow and in order to predict section drag characteristics accurately, designers must have at their disposal turbulent boundary-layer prediction techniques which are reliable in compressible flow and in strong pressure gradients up to separation. An assessment of any one such technique can only be made by comparisons with actual measurements, since exact calculations, even for special cases, are not available. In addition, profile drag prediction and, very often measurement, depend on some knowledge of the wake development aft of an aerofoil and here too there is a need for experimental data relating to modern aerofoil sections. Thus the recent research programme undertaken by the Royal Aircraft Establishment to provide sound experimental backing for swept-wing design and prediction methods has included detailed measurements of two-dimensional boundary layer and wake characteristics.

This Report describes boundary layer and wake surveys made in the 8ft × 8 ft wind tunnel at R.A.E. Bedford using two aerofoil sections of recent design. Pitot traverses across the viscous layers were made, from which velocity profiles and boundary layer and wake integral parameters were derived. Skin-friction distributions were obtained from this data by several methods, *viz.* (i) the Preston tube technique, when the survey pitot was in contact with the wing surface, (ii) the Clauser method, assuming a law of the wall, and (iii) various skin-friction laws employing measured integral parameters. Skin-friction measurements were also made independently by the razor-blade technique. The results of all these measurements are presented in tabular form, primarily for the benefit of the boundary-layer enthusiast who may wish to use and analyse the data in his own way. Some comparisons with prediction methods are included in the analysis.

The two aerofoil sections used for this work are referred to as Sections R.A.E. 2814 and 2815, though both were in fact designed outside the R.A.E. At its design condition, each section had a near-sonic 'rooftop' pressure distribution back to 50 per cent chord in the case of Section 2814 and 30 per cent chord in the case of Section 2815. Turbulent boundary layer and wake surveys were made at the design condition in each case; surveys were also made on Section 2815 at a pressure distribution which included a supercritical region on the upper surface terminated by a weak shock wave. In all cases the flow on the upper surface was close to separation at the trailing edge. Measurements on Section 2814 were made at $M = 0{\cdot}725$, $R = 15 \times 10^6$ (based on chord length) and $C_L = 0{\cdot}42$; those on Section 2815 were made at (i) $M = 0{\cdot}661$, $R = 15{\cdot}6 \times 10^6$, $C_L = 0{\cdot}51$ (rooftop case), and (ii) $M = 0{\cdot}664$, $R = 15{\cdot}6 \times 10^6$, $C_L = 0{\cdot}70$ (supercritical case).

The experimental work on Section 2814 was done in June 1967, and that on Section 2815 during October 1966, and October 1969. Further reports will discuss the overall force and pressure characteristics of both aerofoils, and also the characteristics of a 'three-dimensional' swept-wing design using Section 2814.

2. Experimental Details

Photographs of the rig used for the present work are shown in Figs. 1 and 2 and more detailed diagrams follow in Figs. 3 and 4. The main features of the wing and its support system were dictated by the intention to make balance measurements of the loads on spanwise panels of the wing (which are not discussed in this Report), by the large lift loads on the wing, and by the constructional details of the tunnel working section. Each wing spanned the R.A.E. 8 ft × 8 ft (2·4 m × 2.4 m) wind tunnel* and had a 762 mm (30 in)

* This tunnel has solid walls.

chord, chosen after examination of tunnel interference effects and acceptable maximum loadings. The wing was mounted in an inverted position so that the weight of the model and positive normal force acted in the same sense (this maintained the twin support struts in tension down to the small negative lift coefficients required during other work with these models). The support struts were designed to carry 73 per cent of the loading while the remainder was carried by the tunnel side-walls. The struts were 1107 mm (43·59 in) apart and had a 16·6 per cent thick elliptic section and a chord of 76 mm (3 in). The leading edges of the struts were at 31·7 per cent wing chord for the RAE 2814 section, and at 25 per cent chord for the 2815 section. Small gaps were present between the balance-mounted wing panels (*see* Fig. 3) during balance measurements, but these were sealed using a rubber compound for boundary-layer survey work. The gaps between the outer panels and the tunnel side-walls were also sealed, except for a small part near the trailing edge to avoid any form of contact with the tunnel schlieren windows. The wing surface panels were manufactured from Dural.

The incidence of the wing was measured using a strain-gauged dead-weight device installed in the wing near mid-span. After a suitable pressure distribution for survey work has been selected by examination of measured surface pressures, incidence was kept constant to within about $\pm 0{\cdot}04$ degrees, while all the surveys at a given condition were made.

The position of boundary-layer transition on each wing surface was fixed using roughness bands which consisted of ballotini particles attached to the wing by a thin film of adhesive. The particles were carefully sieved to have diameters between 0·104 and 0·125 mm (0·0041 and 0·0049 in), the size being chosen using the criterion of Ref. 29. On the upper surface of each section the leading edge of the band was located at 4 per cent chord and on the lower surface at 6 per cent chord ; the bandwidth in all cases was 0·7 per cent chord. The transition positions were thought to be sufficiently far ahead of the most forward boundary-layer surveys for these to be made in fully-developed turbulent flow*. On the upper surface the band was located just aft of the region where there is a steep favourable pressure gradient, and on the lower surface the band position was chosen as approximately that at which minimum roughness size was required. Transition position was also fixed on the vertical support struts.

Details of the wing section geometry, pressure distributions and boundary-layer survey stations are given in Tables 1, 2 and 3. Pressure distributions are also shown in Figs. 6 to 10. Surface pressure-plotting holes were drilled 0·5 mm in diameter normal to the wing surface ; all the holes were located at one span-wise station near mid-span. These pressures were measured using self-balancing capsule manometers and the ratio of measured pressure to tunnel stagnation pressure is estimated to be accurate to within $\pm 0{\cdot}0003$.

The rig used for making boundary-layer and wake surveys is shown in Figs. 1, 2 and 4. The probe used for all surveys on the R.A.E. 2814 section and wake surveys on the R.A.E. 2815 section comprised a 4 tube pitot rake and a single static tube, and the arrangement of this probe is included in Fig. 4. Boundary-layer surveys on the R.A.E. 2815 section were made using a 5 tube pitot rake, which is shown in Fig. 2. All pressure tubes were manufactured from hypodermic tubing. The pitot tubes had an outside diameter of 0·5 mm and an internal diameter of 0·3 mm ; the spacing between the tubes of each pitot rake was approximately 2·5 mm. The static tube diameter was 1 mm. These pressures were measured using a single $\pm 70\,kN/m^2$ (± 10 psi) transducer installed in a pressure switch which scanned the rake pressures. The ratio of measured pressure to tunnel stagnation pressure is estimated to be accurate to within $\pm 0{\cdot}001$.

As is shown in Fig. 4, the rake and/or static probe were mounted on 76 mm (3 in) arms from the axis of a support tube, which could be positioned in the vicinity of a survey station at the appropriate pitch angle and fore-and-aft position using the quadrant pitch, primary and secondary rotations and fore-and-aft traverse movements indicated. The surveys were made by traversing the rake in planes normal

* That transition was properly fixed at the roughness bands was confirmed by balance measurements of drag over a range of Reynolds number.

to the wing surface or, in the wake, normal to the free stream direction* using the tertiary rotation movement only. On the wing, surveys were commenced at a point at which one of the rake tubes just contacted the wing surface (this contact point was found by using the rake and wing to complete an electric circuit). In the wake an arbitrary starting point was chosen with the rake just clear of the wake. Measurements were then made as the rake was rotated in small steps through the boundary layer or wake. The position of each tube in the rake was calculated relative to the starting position along normals to the wing surface or stream direction using digitised records of the various rig movements. These positions are thought to be accurate to within $\pm 0{\cdot}04$ mm ($\pm 0{\cdot}0015$ in).

Mean total temperature in the tunnel was 296·5 K during survey work on Section 2814 and 298 K during work on Section 2815. Temperature variations from survey to survey were within ± 4 K of these mean values, (tunnel total pressure was regularly adjusted during the tests to maintain constant Reynolds number).

In addition to obtaining skin-friction data from analysis of profile data, skin-friction measurements were also made by the razor-blade technique described in Refs. 1 and 2. These measurements were made independently of the surveys described above, without the survey rig installed in the tunnel. Static pressures at the wing surface were measured during one test run; razor-blades cut to the appropriate geometry were then attached over the static holes in accordance with Fig. 5, and surface pitot pressures were measured during a second test run. In calculating Δp, the difference between a pair of corresponding surface pitot and static pressures (this difference is used in the calibration expression), allowance was made for small differences in tunnel total pressure and free stream Mach number between the two runs by suitable scaling of the static pressure measurements. Mean tunnel total temperature was 293 ± 1 K during razor-blade measurements on the R.A.E. 2814 section and 296 ± 2 K during measurements on R.A.E. 2815. While the nominal height, h, of the leading edge of each blade above the wing surface was 0·13 mm (0·005 in) the actual height varied from 0·10 mm to 0·15 mm (0·004 to 0·006 in) due to different blade and adhesive thicknesses.

3. Data Reductions and Corrections

The effective free stream Mach number at the position of the model was obtained by correcting a value measured far upstream of the model for the blockage effect of the model, its support system and the wakes of these items. This correction was made by representing the model, etc., by suitable distributions of sources and sinks and then calculating the ratio between

(i) the sum of centre line pressure increments due to image arrays of the model, etc., in the tunnel walls, and

(ii) the sum of roof or floor pressure increments due to both image arrays and the direct effect of the model, etc.

A selection of measured roof and floor pressures and a knowledge of the 'empty tunnel' calibration[3] then permitted the corrected Mach number to be calculated. These calculations also showed that the mean corrected Mach number at mid-span of the model did not differ from that at any particular chordwise point at the same spanwise position by more than 0·0015. The mean corrected Mach number is that quoted as the free stream Mach number for each survey condition and is that used in computing force and pressure coefficients.

Lift coefficients quoted are those obtained by balance measurements during separate tests. These are in fact very close to those obtained by the integration of surface pressures. Because of interference of the

---

* This technique, as opposed to that of attempting to measure local flow direction and subsequently aligning the probe with the flow for each pressure reading, was thought to be sufficiently accurate in the present case. The pitot tubes were found to record total pressure accurately at the outer limits of the viscous layer, even close to the trailing edge, so that errors in pitot readings due to misalignment appear to be negligible. Static pressure variations were measured, which would include any alignment errors, but these variations did not appear to affect calculated integral parameters significantly (*see* Section 3.1).

survey rig with surface pressures, the lift coefficients quoted apply only to the case where the rig is removed from the neighbourhood of the model.

Incidence angles quoted in Tables 1, 2 and 3 have been corrected for tunnel constraint effects[4] and are therefore those expected to apply in interference-free conditions at the same C_L. However, tunnel constraint also results in an effective camber change of the wing, which modifies the pressure distribution compared with that which would be obtained in free air. Since boundary-layer and wake surveys were made under this modified pressure distribution no corrections have been made to surface pressure measurements for this effect. Corrections would be small, in any case, and no more than 0·01 in terms of pressure coefficient.

3.1. Velocity Profiles and Integral Parameters

The static pressure at each boundary-layer survey station has been assumed constant* across the boundary layer and has been obtained from surface pressure measurements made with the survey rig in position for the appropriate traverse. This static pressure is generally different from that measured with the rig removed from the vicinity of the model (*see* Figs. 6, 8 and 9 and further discussion below). From the static pressure, the value of the local Mach number was obtained at the outer limit of the boundary layer and at each point at which pitot pressure was measured within the layer. A similar procedure was adopted for wake surveys, though here static pressure measured by the static probe near the position of minimum pitot pressure was used. To obtain velocity and density distributions it has been assumed, following other boundary-layer work (e.g. Ref. 5), that total temperature is constant across the viscous layer. Velocities and densities so calculated have been non-dimensionalised with respect to mean values at the outer limits of the boundary layer or wake. Wing chord has been chosen as the unit of length. Chordwise position, X, is measured downstream from the wing leading edge, while distance across a boundary layer, Y, is measured from and normal to the wing surface. In the wake, the origin of Y is simply an arbitrary datum used in data reduction. The results of these calculations are tabulated, for all surveys made, in Tables 4 to 12. Not all the experimental data obtained for each profile are listed, but sufficient are included to define the profile accurately.

The most significant parameters derived from the velocity profile data are values of displacement thickness, δ_1, and momentum thickness, δ_2. For a boundary layer these are defined as:

$$\delta_1 = \int_0^{\delta} \left(1 - \frac{\rho u}{\rho_1 u_1}\right) dY,$$

and

$$\delta_2 = \int_0^{\delta} \frac{\rho u}{\rho_1 u_1}\left(1 - \frac{u}{u_1}\right) dY,$$

where suffix 1 refers to values at the outer limit of the layers, i.e. at $Y = \delta$. In the case of a wake, integration is across the complete viscous layer with appropriate limits of integration inserted. The integrals have been computed using the trapezium rule between survey points. For each boundary-layer survey this computation began at the first survey point, normally taken with a pitot tube in contact with the surface. Therefore, if pitot displacement effects are ignored, the part of the boundary layer between the surface and a position at half the pitot tube diameter from the surface has been omitted from the integration. Allowance has been made for this by assuming that in the omitted region the boundary layer profile consists of a laminar sublayer given by

$$\frac{u}{u_\tau} = \frac{Yu_\tau}{\nu_w}, \quad \text{for } \frac{Yu_\tau}{\nu_w} < 11,$$

* This assumption is commented on below.

and Coles' law of the wall[6]*, i.e.

$$\frac{u}{u_\tau} = 5 + 5{\cdot}62 \log_{10}\left(\frac{Yu_\tau}{\nu_w}\right), \quad \text{for } \frac{Yu}{\nu_w} > 11.$$

Here u_τ is the friction velocity and ν_w is kinematic viscosity evaluated at wing surface temperature, calculated assuming a recovery factor of 0·885. u_τ was determined from measurements of local skin friction made by the razor-blade technique. This addition to the integration is small when compared with the final result near the trailing edge of each section, but at the more forward surveys on Section 2814, for example, where the boundary layer is very thin, the contribution can amount to as much as 35 per cent of displacement thickness and 9 per cent of momentum thickness.

Other integral parameters have been evaluated, with similar allowances for the region near the wall, for each boundary-layer survey. These integrals and their definitions are as follows:

$$\delta_3 = \int_0^\delta \frac{\rho u}{\rho_1 u_1}\left(1 - \left(\frac{u}{u_1}\right)^2\right) dY \qquad \text{– energy thickness,}$$

$$\delta_1^i = \int_0^\delta \left(1 - \frac{u}{u_1}\right) dY,$$

$$\delta_2^i = \int_0^\delta \frac{u}{u_1}\left(1 - \frac{u}{u_1}\right) dY,$$

$$\delta_3^i = \int_0^\delta \frac{u}{u_1}\left(1 - \left(\frac{u}{u_1}\right)^2\right) dY,$$

$$\delta_0 = \int_0^\delta \frac{\rho u}{\rho_1 u_1} dY \qquad \text{– mass flow thickness,}$$

$$\delta_0^i = \int_0^\delta \frac{u}{u_1} dY,$$

and

$$\delta_1^t = \int_0^\delta \frac{\rho}{\rho_1}\left(1 - \frac{u}{u_1}\right) dY.$$

A precise definition of δ is required in evaluating δ_0 and δ_0^i; in accordance with other workers, δ has been defined as the value of Y at which $u/u_1 = 0{\cdot}995$. These parameters, together with δ_1 and δ_2, are listed in Tables 13, 14 and 15. For surveys made in the wake of Section 2814 values of δ_1 and δ_2 are summarised in Table 16, which also includes the total width of the wake $\delta^{(0{\cdot}995)}$, defined as the distance between points on either side of the wake at which $u/u_1 = 0{\cdot}995$. Wake results for Section 2815 are listed in Table 17.

Further corrections to the results are now discussed. These affect velocity and density profiles as well as the integral parameters, but corrections to only the latter are made here. The interference of the survey rig is considered first. The rig produced a three-dimensional pressure interference field which extended upstream of each survey station and which therefore influenced boundary layer or wake characteristics

* The choice of constants in the law of the wall, from the many pairs of constants published, is not important in this context. No significantly different results would be obtained if, for example, the form of the law of the wall given in Ref. 18 were used.

measured at the station. On the wing the pressure distributions with and without the survey rig were measured directly. In the wake the only measurements of static pressure were those at the survey stations with the rig present, and the upstream distributions with and without rig interference were derived from these measurements and estimates of the interference pressure distributions. The latter were made by representing the various components of the rig by source-sink distributions and including tunnel wall blockage terms for the larger components. The accuracy of these calculations was checked to some extent by examination of the wing surface pressure distributions near the trailing edge of Section 2814 for various configurations of the wake survey rig, and close agreement was obtained. The opportunity was also taken to correct for the variation of 'empty-tunnel' centre line pressure along the wake*, since this was almost certainly a very similar three-dimensional effect of the sting support quadrant and fairing in the tunnel (*see* Fig. 4). Pressure distributions with and without interference effects are illustrated for both wing and wake survey stations in Figs. 6 to 10, and these show that interference effects on the wing increase considerably as the survey station is moved forward. Allowances for increased Mach number and the interference between probe support and model flow fields, made on the assumption that subsonic relations are still valid, offer only a partial explanation for these effects. The remainder may be due to the development of supercritical flow and a shock system between the probe support and the model, which is likely to have a similar upstream effect to that of a support of increased size.

A first approximation for the corrections required to boundary-layer and wake parameters in order to account for these pressure interference fields would be to assume that the interference, like the basic wing flow, is two-dimensional and to compare two-dimensional boundary layer and wake estimates with and without the interference present. In Ref. 7, however, Johnston describes some boundary-layer measurements made in the plane of symmetry of a three-dimensional flow and it can be deduced from his work that, over the range of interference pressure coefficient with which the present work is concerned, the additional momentum thickness due to the imposition of a three-dimensional pressure field on a flat plate is about 54 per cent of that calculated for the same two-dimensional pressure field. This result suggests that 'two-dimensional' corrections will be larger than those actually required in the present case. Now, although the surveys were not made in the plane of symmetry of the interference field but a short distance to one side of it, it is thought that the application of a factor of 0·54 to corrections calculated for two-dimensional flow will result in more realistic corrections than the use of unfactored values. Some justification for using this factor in the present case is that Johnston found that the more important of the two additional terms he incorporated in the two-dimensional momentum integral equation in order to explain his results, depended only on the continuity of flow upstream of the obstruction and not on the precise nature of the obstruction. The same factor has been used to evaluate corrections to wake data in order to maintain consistency. The absolute values of the corrections are found to be small (*see* Tables 13 to 17), which provides further justification for using a fairly crude technique. Two-dimensional estimates of boundary layer and wake development with and without survey rig interference were made using Green's procedure[8], the computer program of which evaluates δ_1 and δ_2. Other integral parameters were evaluated using relations obtained from Refs. 8, 9 and 10. The two-dimensional corrections thus obtained were all factored by 0·54 on the further assumption that the ratios between integral parameters were unchanged by three-dimensional effects.

Pitot tube displacement corrections are now considered. Several investigators have explored this phenomenon, both in wakes and in boundary layers, with conflicting results. Examination in log-law form of some boundary-layer profiles obtained during the present work suggests that a displacement correction is necessary if a linear 'law of the wall' form is to be followed, and it was decided to apply a simple displacement correction of $0{\cdot}15d$, where d is the outside diameter of a pitot tube, to all results. The displacement is in the sense towards the region of higher velocity. This correction was obtained independently by MacMillan[15] and Hall[12] in a boundary layer, but not close to the wall. Near the wall both workers found smaller or negative corrections but since corrections are being made here only to integral results, the effect near the wall can be ignored. The same correction has been made in the wake.

* Variations at the position of the wing itself were negligible[3].

Pressure measurements in turbulent flows should also be corrected for an effect due to fluctuating velocities. This results in a small error in pitot measurement and a small variation in static pressure across the boundary layer. Corrections for flat-plate boundary layers are presented in Ref. 13 and these have been applied to the present boundary-layer measurements. Although most of the surveys were made under conditions far from 'flat-plate' the corrections were all small (about 1 per cent at forward stations and decreasing towards the trailing edge) and this has been taken as sufficient justification for using them. Because of the lack of a corresponding correction method no such corrections have been made to wake measurements, though these would be expected to be negligible if extrapolation of the wing corrections is any guide. Tables 13 to 17 include boundary-layer and wake integrals after displacement and fluctuating velocity corrections have been made to previous data.

It will be recalled that velocity and density distributions and integrals have been evaluated on the assumption that static pressure is constant across the viscous layer (apart from the small fluctuating velocity correction to integrals mentioned in the last paragraph). Near the trailing edge of an aerofoil there can be measurable variations of static pressure across the viscous layer due to rapid changes in the direction of flow coupled with the relatively-large thickness of the boundary layer or wake. (Misalignment of the static probe will also contribute to such variations.) Some measurements of static pressure near the trailing edge of Section 2814 are shown in Fig. 11 and, to check the effect on δ_1 and δ_2 of the variations shown there, calculations were made of these integrals by Myring's method[14] and the results compared with those already obtained. These calculations showed that, for surveys nearest the trailing edge ($x = 0{\cdot}9970$ and $1{\cdot}020$), taking account of static pressure variations at most increases δ_1 by 1 per cent and decreases δ_2 by 1 per cent. Changes in other integrals have not been considered and no corrections have been made for this effect in any of the tables.

3.2. Preston Tube Measurements

When the boundary-layer survey-pitot rake touches the wing surface, the contact pitot can be regarded as a Preston tube and hence skin friction can be calculated. Two alternative Preston tube calibrations were initially used for this purpose. The first is that published by Hopkins and Keener[15], which can be written:

$$\log_{10}[f_2(T_1)R_d^2(M_s/M_1)^2] = 1{\cdot}517 + 1{\cdot}132\log_{10}[f_2(T_1)R_d^2C_f] \tag{1}$$

where

$$f_2(T_1) = \left[\frac{T_1(1 + 0{\cdot}1142M_1^2) + 110{\cdot}4}{T_1 + 110{\cdot}4}\right]^2 \frac{1}{(1 + 0{\cdot}1142M_1^2)^4},$$

$$R_d = \rho_1 u_1 d/\mu_1,$$

d = pitot tube outside diameter

and

M_s = Mach number indicated by surface pitot and static pressures.

Suffix 1 refers to conditions at the edge of the boundary layer; temperature T is expressed in degrees Kelvin. Compressibility effects are taken into account in the calibration by the Sommer and Short reference temperature method, which is incorporated in the factor $f_2(T_1)$. The calibration expression (1) is considered valid within the range $5 \times 10^5 \lesssim f_2(T_1)R_d^2(M_s/M_1)^2 \lesssim 2 \times 10^8$, which embraced all the present data. Hopkins and Keener obtained their calibration at supersonic speeds under 'flat-plate' conditions, using an absolute skin-friction balance as reference*.

* A further calibration expression was derived from the data of Kopkins and Keener in the course of the present analysis—*see* Section 4.

The other calibration used is that of Patel[16] which was obtained in 'incompressible' pipe flow. For the range of conditions of interest here, two analytic expressions describe the calibration, viz.:

$$\left.\begin{aligned} y &= 0{\cdot}8287 - 0{\cdot}1381x + 0{\cdot}1437x^2 - 0{\cdot}0060x^3, \quad 2{\cdot}9 < x < 5{\cdot}6 \\ \text{and} \qquad & \\ x &= y + 2\log_{10}(1{\cdot}95y + 4{\cdot}10), \qquad\qquad 5{\cdot}6 \leqslant x \lesssim 7{\cdot}6 \end{aligned}\right\} \tag{2}$$

where

$$x = \log_{10}(\rho d^2 \Delta p/4\mu^2)$$

and

$$y = \log_{10}(\rho d^2 \tau_w/4\mu^2).$$

In order to use this calibration where compressibility effects are significant, a transformation (due to Winter and Gaudet and following the work of Ref. 18) has been employed identical to that incorporated in the razor-blade calibration described in Section 3.5. With this transformation the calibration expression still holds with x and y re-defined as $\log_{10}(\rho_w d^2 \Delta p/4\mu_w^2)$ and $\log_{10}(\rho_w d^2 \tau_w (1 + 0{\cdot}2M_1^2)^{\frac{1}{2}}/4\mu_w^2)$ respectively, where suffix w refers to wall conditions, calculated on the assumption of a recovery factor of 0·885, and M_1 is Mach number at the outer edge of the boundary layer.

Since corrections to measured static pressure for the finite diameter of the static pressure orifice do not appear to have been considered in either of the above calibrations, some checks were made on their magnitude using Shaw's data[17]. Corrections to the present measurements, with no corrections to the calibration data, increase C_f by 0·0004 at most. Since corrections to the calibration data will be in the opposite sense and of the same order of magnitude*, it may be assumed that net corrections are negligible.

Corrections to skin-friction coefficients for the upstream influence of the survey rig were estimated in the same way as corrections to the boundary-layer integral parameters, i.e. by factoring estimated two-dimensional corrections by 0·54. At the most forward survey stations these corrections were up to 0·00013, i.e. up to about 4 per cent, and were negligible at stations near the trailing edge. The corrected results show some scatter (Tables 18 to 20), probably due to the fact that the surface pitot tube was not rigidly attached to the wing. The error in C_f due to this source is thought to be about $\pm 0{\cdot}00015$.

3.3. Skin Friction by Clauser's Method

Given a law of the wall, measured boundary-layer profile data can be used to yield surface shear stress by Clauser's method. Recently, Winter and Gaudet[18] have derived a convenient form for the law of the wall, with suitable constants, applicable at Mach numbers up to at least 2·8. This is written:

$$\frac{u}{u_\tau^i} = 4{\cdot}05 + 6{\cdot}05\log_{10}\left(\frac{Yu_\tau^i}{\nu_1}\right),$$

where $u_\tau^i/u_1 = (C_f/2)^{\frac{1}{2}}(1 + 0{\cdot}2M_1^2)^{\frac{1}{4}}$.

Suffix 1 refers to conditions at the outer edge of the boundary layer, and Y is distance from, and normal to, the wing surface. Clauser's technique is to compare a plot of u/u_1 against $\log_{10}(Yu_1/\nu_1)$, for a given experimental profile, with similar plots of the law of the wall, into which various, constant values of C_f have been inserted, and thus find a suitable C_f to fit the measurements. In this case it is convenient to

* The precise magnitude of corrections to the calibration data could not be determined, since the static hole diameters were not published.

plot the law of the wall for constant values of $C_f^i = C_f(1 + 0{\cdot}2M_1^2)^{\frac{1}{2}}$, and thus obtain C_f via C_f^i; the law of the wall is then:

$$\frac{u}{u_1} = \left(\frac{C_f^i}{2}\right)^{\frac{1}{2}}\left(4{\cdot}05 + 3{\cdot}025\log_{10}\left(\frac{C_f^i}{2}\right) + 6{\cdot}05\log_{10}\left(\frac{Yu_1}{\nu_1}\right)\right). \tag{3}$$

Before the comparison is made, it is necessary to consider pitot displacement corrections and the effect on pressure measurements of fluctuating velocities in a turbulent flow. MacMillan's displacement corrections have again been used[11]; these take into account both wall effect and velocity gradient effect. In the present case it was found to be sufficiently accurate to assume constant $u_\tau d/\nu = 200$ and constant $u_1/\nu_1 = 16 \times 10^6$ per chord, thus giving constant corrections for any given value of Yu_1/ν_1. Rather than add these corrections to the measurements, in practice it is more convenient to subtract them from the plots of Winter and Gaudet's log-law.

Landweber's method[13] was used to correct for fluctuating velocity effects. Since the region of interest is restricted to that where the log-law is a valid fit to the measurements and to values of $Yu_\tau/\nu_w \gtrsim 80$, it can be assumed that the velocity—fluctuation parameter

$$\frac{\overline{u'^2} - \overline{v'^2} + \overline{w'^2}}{u_\tau^2}$$

is a constant, viz. 4·75. Landweber's correction formula then reads,

$$\left(\frac{u}{u_\tau}\right)_m = \left(\frac{u}{u_\tau}\right)_c\left\{1 + 4{\cdot}75\Big/\left(\frac{u}{u_\tau}\right)_c^2\right\}^{\frac{1}{2}},$$

where suffix m refers to measured velocities and suffix c to corrected velocities. Since the correction is small it is assumed that the same form of correction applies to u/u_τ^i; this correction too can be incorporated into the log-law plots by writing equation (3) as:

$$\left(\frac{u}{u_1}\right)_m = \left(\frac{C_f^i}{2}\right)^{\frac{1}{2}}\left\{4{\cdot}05 + 3{\cdot}025\log\left(\frac{C_f^i}{2}\right) + 6{\cdot}05\log\left(\frac{Yu_1}{\nu_1}\right) + 2{\cdot}375\Big/\left(4{\cdot}05 + 3{\cdot}025\log\left(\frac{C_f^i}{2}\right) + 6{\cdot}05\log\left(\frac{Yu_1}{\nu_1}\right)\right)\right\}.$$

Some plots of experimental data are shown in Fig. 12 and compared with log-law plots amended as above. The majority of cases were similar to those shown at $x = 0{\cdot}6608$ and 0·9119, in that a skin-friction coefficient could be chosen without difficulty to give good agreement between the log-law and experimental data. It was noted, however, that the first few points of each profile near the wall did not follow the log-law but lay above a line of constant C_f^i drawn through subsequent points. This suggests that the corrections discussed above could be improved upon, for example by increasing displacement corrections close to the wall. Errors in the corrections are unlikely to affect the values of C_f^i deduced, provided reliance does not have to be placed on the first few points; this, unfortunately, has to be done at the most forward surveys where the boundary layer is very thin, (e.g. the survey at $x = 0{\cdot}3516$ shown in Fig. 12). In some other instances it is doubtful if a log-law region exists at all, e.g. on the upper surface near the trailing edge (*see* Fig. 12, $x = 0{\cdot}9878$), and on the lower surface at forward stations where there is a strong favourable pressure gradient. Though values of C_f^i have been deduced in these cases they must obviously be in doubt. Elsewhere it is thought that a value of C_f^i can be chosen to suit the data to within $\pm 0{\cdot}00002$; this does not include possible systematic errors in the profile data plotted.

Derived values of C_f have been corrected for survey rig interference in the same way as Preston tube results; the corrected data is listed in Table 18 to 20.

3.4. Skin Friction from Boundary-Layer Integral Parameters

A number of skin-friction laws are available which express skin-friction coefficient in terms of integral parameters of the compressible, turbulent boundary layer. Four of these have been used here with fully-corrected measured parameters as input.

Two of the laws used are based on the incompressible law of Ludwieg and Tillmann[19] which seems to be valid for a wide range of pressure gradient. The incompressible law reads:

$$C_f = 0{\cdot}246 \exp(-1{\cdot}561 H_{12}) R_{\delta_2}^{-0{\cdot}268}$$

where H_{12} is shape parameter ($=\delta_1/\delta_2$), and $R_{\delta_2} = \rho_1 u_1 \delta_2/\mu_1$.

A compressible form of this law has been suggested by Winter, Rotta and Smith[9] which reads:

$$C_f = 0{\cdot}246 \exp(-1{\cdot}561 H_{12}^i)(R_{\delta_2})_w^{-0{\cdot}268}\left(\frac{2\delta_2}{\delta_2^i} - 1\right) \tag{4}$$

where $H_{12}^i = \delta_1^i/\delta_2^i$, and $(R_{\delta_2})_w = \rho_1 u_1 \delta_2/\mu_w$, μ_w being coefficient of viscosity evaluated at wall temperature.

An alternative transformation of the Ludwieg–Tillmann law is published by Green in Ref. 10, making use of a procedure proposed by Spence. An intermediate temperature T_m is defined as $T_m = 0{\cdot}72T_w + 0{\cdot}28T_1$, for zero heat transfer. Then:

$$C_f = \frac{T_1}{T_m}\{0{\cdot}246 \exp(-1{\cdot}561 \bar{H}) \bar{R}_{\delta_2}^{-0{\cdot}268}\} \tag{5}$$

where $\bar{H} = \delta_1^t/\delta_2$ and $\bar{R}_{\delta_2} = \rho_1 u_1 \delta_2/\mu_m$, μ_m being coefficient of viscosity evaluated at temperature T_m.

In Ref. 20 Nash and MacDonald put forward a different form of skin-friction law, which is essentially a flat-plate law modified to take non-zero pressure gradients into account. The relations used are:

$$\left(\frac{2}{C_f}\right)^{\frac{1}{2}} = (1 + 0{\cdot}066M_1^2 - 0{\cdot}008M_1^3)\left\{2{\cdot}4711 \log_e\left[(1 - 0{\cdot}134M_1^2 + 0{\cdot}027M_1^3)\frac{u_1\delta_2}{\nu_1}\right] + 4{\cdot}75\right\} + 1{\cdot}5G + 1724/(G^2 + 200) - 16{\cdot}87$$

and

$$G = \left(\frac{T_1}{T_w}\frac{2}{C_f}\right)^{\frac{1}{2}}\left(1 - \frac{\delta_2^i}{\delta_1^i}\right). \tag{6}$$

The second relation follows from Nash and MacDonald's definition of G, viz.

$$G = \frac{1}{u_\tau}\int_0^\infty (u_1 - u)^2\, dY \Big/ \int_0^\infty (u_1 - u)\, dY,$$

assuming here that $u_\tau = (\tau_w/\rho_w)^{\frac{1}{2}}$.

For the purpose of the present calculations G was given an initial value of 6·8, which is an acceptable 'flat-plate' value; an iteration procedure between C_f and G was then followed until successive values of G differed by less than 0·01, by which time C_f was effectively constant.

The fourth law used has been suggested by Green[8] as an alternative to his version of the Ludwieg–Tillmann law mentioned above. This approach is similar to that of Nash and MacDonald in that Green

starts from the 'flat-plate' case and subsequently introduces pressure gradients. If C_{f_0} and $\bar{H}_0$ are skin-friction coefficient and transformed shape parameter (i.e. δ_1'/δ_2) respectively for a flat-plate boundary layer, then the following relation has been derived by Green from the results of Spalding and Chi:

$$F_c C_{f_0} = \{0{\cdot}012/(\log_{10}(F_R R_{\delta_2}) - 0{\cdot}64)\} - 0{\cdot}00093 \tag{7a}$$

where, assuming zero heat transfer,

$$F_c = 0{\cdot}2rM_1^2/[\arctan(0{\cdot}2rM_1^2)^{\frac{1}{2}}]^2, \qquad F_R = (0{\cdot}2rM_1^2)^{-0{\cdot}702},$$

and r is recovery factor. From a relation similar to that given by Nash and MacDonald's parameter G:

$$\frac{1}{\bar{H}_0} = 1 - 6{\cdot}8\left(\frac{C_{f_0}}{2}\right)^{\frac{1}{2}}. \tag{7b}$$

For non-zero pressure gradients Green has used results obtained by Nash and MacDonald and by Thompson to derive the relation:

$$\left(\frac{C_f}{C_{f_0}} + 0{\cdot}5\right)\left(\frac{\bar{H}}{\bar{H}_0} - 0{\cdot}4\right) = 0{\cdot}9. \tag{7c}$$

In using these four laws a recovery factor r of 0·885 has been assumed in calculating wall temperature, T_w.

The results of calculations of skin friction using equations (4), (5), (6) and (7) are included in Tables 18 to 20.

3.5. Razor-Blade Technique

Basic details of the razor-blade method of measuring skin friction at supersonic speeds have been published by Smith, Gaudet and Winter[1] and at low subsonic speeds by East[2]. Each of these references includes a calibration; that derived by the former workers was based on use of a 'flat-plate' skin-friction law, while that of East depended on prior knowledge of a Preston tube calibration*. However, in later work, Smith *et al.* have obtained a further, absolute razor-blade calibration, using a strain-gauged floating-element device mounted on a sidewall of the R.A.E. (Bedford) 8 ft × 8 ft wind tunnel to measure surface shear stress directly. Opportunity was taken at the same time to extend the Mach number range from supersonic down to low subsonic speeds, and also the Reynolds number range. From an analysis of this later information, a single expression has been derived to fit the calibration data for Mach numbers up to 2·7 and for razor-blade heights h (*see* Fig. 5 for the definition of h) between 0·05 mm and 1 mm (0·002 in and 0·04 in). This formula reads,

$$y = 0{\cdot}7353 - 0{\cdot}36600856x + 0{\cdot}58672050x^2 - 0{\cdot}16079678x^3 + 0{\cdot}02068768x^4 - 0{\cdot}00097736x^5,$$

where $x = \log_{10}\{\rho_w(h + \Delta)^2\Delta p/\mu_w^2\}$ and $y = \log_{10}\{\rho_w(h + \Delta)^2\tau_w(1 + 0{\cdot}2M_1^2)^{\frac{1}{2}}/\mu_w^2\}$.

Here μ_w and ρ_w are viscosity and density, evaluated at wall temperature; τ_w is surface shear stress; M_1 is local Mach number at the outer limit of the boundary layer; Δp is the difference between pressures recorded at a surface static hole, with and without a razor-blade in position; Δ is a constant, equal to 0·10 mm (0·004 in). This calibration is valid over the range $2 < x < 7$, for the configuration shown in Fig. 5 with one exception. The exception is that the calibration was made using a surface static hole of diameter 0·76 mm (0·030 in), whereas for the present work a diameter of 0·50 mm (0·020 in) was used. The results of Ref. 2 suggest that this difference is not significant. Another feature of this and previous

* In fact Patel's calibration, which was described in Section 3.2.

calibrations is that all were obtained in the presence of negligible pressure gradients, so that any effects of pressure gradient on the calibration used are unknown.

A check on inter-blade interference was made by removing alternate razor-blades from the wing and repeating some of the measurements. This showed that such interference was small and that its effects were indistinguishable from random errors. The probable accuracy of C_f measurements made with a full complement of blades is thought to be about $\pm 0{\cdot}00010$, taking account of scatter and interference. Further possible errors which may arise from using this technique in conditions differing from calibration conditions (i.e. in very thin boundary layers and in severe pressure gradients) are discussed in Section 4 in comparison with other skin-friction results.

4. Comparisons of Skin-Friction Results

Skin-friction results obtained by the techniques just described are listed in Tables 18 to 20 and compared in Fig. 13. For brevity the two integral laws due to Green are labelled (1) and (2), the former denoting his transformation of the Ludwieg–Tillmann law[10] and the latter his more recent formulation[8]. It is apparent from the tables that all the integral laws give very similar results. The Nash-MacDonald law (Fig. 13*a*) tends to give slightly larger values than the Green (1) law except at low C_f (i.e. less than about 0·00050) where the opposite occurs; the two laws of Winter, Rotta and Smith and Green (2) give results which are very similar to each other and which average about 0·00005 less than Green (1). Thus, within the accuracy of the present results, it is concluded that no law is any better or worse than the others and that they all appear equally valid within the range $0{\cdot}0005 \lesssim C_f \lesssim 0{\cdot}0033$. The Green (1) law has been taken as typical of the four laws and has been used in comparisons with the other techniques.

A few points on the 'rooftop' regions of the aerofoils can be regarded as being in 'flat-plate' boundary layers, since surface curvature and pressure gradients are small. Skin friction has therefore been evaluated at these points using a flat-plate skin-friction law, that of Winter and Gaudet[18] being chosen here. The positions at which this has been done are indicated in Tables 18 and 19, and the results compared with the Green (1) integral law in Fig. 13b. This shows satisfactory agreement, confirming the consistency of results produced by integral laws.

Skin-friction results obtained by the Clauser technique are compared with results using the Green (1) law in Fig. 13*c*. Agreement is seen to be very close over most of the range covered, though 'Clauser' results are greater than the integral law results at values of C_f above about 0·0030 and below about 0·0008. However, the 'Clauser' data at these extreme ends of the range is that which is in doubt in any case because of the apparent absence of a log-law region from the velocity profiles, (Section 3.3).

Razor-blade results are shown in Fig. 13d. Considerably greater scatter is exhibited on comparison with Green (1) data than has been seen in previous comparisons. This is partly due to the fact that previous comparisons have all used the same initial data so that similar errors tended to appear in corresponding results, whereas the razor-blade results were obtained quite independently. Also, as has been noted earlier, probable errors in the razor-blade results are greater than those in the results already discussed. The razor-blade results are seen to be lower than corresponding Green (1) results by roughly 5 per cent on average.

The Preston tube data show that use of Patel's calibration with the Winter–Gaudet compressibility transformation gives values of C_f about 3 per cent greater than those obtained using Hopkins and Keener's published calibration. In Fig. 13e the Hopkins and Keener results are compared with Green (1) results and, except for $C_f \lesssim 0{\cdot}001$, are seen to be approximately 5 per cent greater. Patel results are thus about 8 per cent higher than Green (1) results. The 3 per cent difference between the two sets of Preston tube data may be due to the different compressibility transformations used or to a more fundamental difference between the sets of data on which the calibrations are based, (e.g. a different calibration may be obtained from supersonic data due to shock-boundary layer interaction ahead of the pitot tube). Accordingly the published data of Hopkins and Keener were re-analysed using the Winter–Gaudet compressibility transform (as used here in conjunction with Patel's calibration) to obtain a new calibration. The coordinates x, y used are exactly the same as those defined in describing Patel's calibration and a comparison of the re-analysed Hopkins and Keener data showed close agreement with Patel's calibration

over the range of interest. A 'best straight line' fit to the revised data yielded the calibration expression:

$$y = 0{\cdot}8353x - 1{\cdot}1128, \qquad 5{\cdot}5 < x < 7{\cdot}3.$$

The close agreement means, of course, that results using the new Hopkins and Keener calibration are now also about 8 per cent higher than Green (1) results as is shown in Fig. 13f. Better agreement between Preston tube results and the Green (1) integral law would therefore have been obtained if Hopkins and Keener's intermediate temperature approach had been applied to Patel's calibration data, but this would imply different calibrations in their incompressible forms. A point worth making here is that Hopkins and Keener chose their intermediate temperature formulation on the basis of its providing close agreement with Preston's original calibration, whereas later workers have produced calibration curves which give higher values of C_f than Preston's. There is therefore some reluctance to place too much faith in Hopkin's and Keener's calibration formula.

If skin-friction results obtained using integral skin-friction laws or by Clauser analysis of profile data are assumed to be the most likely 'correct' values*, then Preston tube results employing the Winter–Gaudet transformation at 8 per cent too high and razor-blade results are 5 per cent low. Confirmation that the first of these differences at least is due to uncertainty in the compressibility correction, rather than to any systematic errors peculiar to the present experiment, has been obtained from the results of later tests[30] made in the 9 in × 8 in wind tunnel at R.A.E., Bedford, under 'flat-plate' conditions. These results, presented here in Figs. 13(g) and 13(h), show comparisons between the four methods of skin friction measurement at Mach numbers of 0·3, 0·5 and 0·7 and at two different total pressures: the value of $u_1\delta/\nu_1$ at $M = 0{\cdot}7$ was approximately $4{\cdot}5 \times 10^4$ for Fig. 13(g) and 3×10^5 for Fig. 13(h). For convenience, C_f derived from an integral skin-friction law was taken as the 'true' value, with which to compare the other estimates and, as before, the Clauser method agrees closely with the integral law. The Preston tube results using the Patel calibration and the Winter–Gaudet compressibility factor, i.e., $(1 + 0{\cdot}2M_1^2)^{\frac{1}{2}}$, are 'high' by about 5 per cent at $M_1 = 0{\cdot}7$ but appear to tend to the 'true' value as Mach number tends to zero, as they should. The factor $(1 + 0{\cdot}2M_1^2)^{\frac{1}{2}}$ is also plotted in Figs. 13(g) and 13(h) and it can be seen that the error in the Preston tube results is roughly equal to this factor. The conclusion to be drawn, therefore, is that the Winter–Gaudet factor does not adequately account for compressibility effects on Preston tube measurements: empirically changing the factor to $1 + 0{\cdot}2M_1^2$ would satisfy the data better, at least up to a Mach number of 0·7.

The razor blade results shown in Figs. 13(g) and 13(h) are inconclusive as only two points were obtained, viz. at $M_1 = 0{\cdot}5$. The point obtained at the lower total pressures is about 3 per cent high while that at the higher total pressure (which is probably experimentally the more accurate point) is about 5 per cent low. It may be that the original razor-blade calibration is inaccurate at subsonic Mach numbers.

5. Two-Dimensional Momentum Integral Equation

In its usual simplified form the two-dimensional momentum integral equation reads:

$$\frac{d\delta_2}{ds} = \frac{C_f}{2} - (H_{12} + 2 - M_1^2)\frac{\delta_2}{u_1}\frac{du_1}{ds} \tag{8}$$

where s is streamwise distance and $H_{12} = \delta_1/\delta_2$. Terms involving turbulent normal shear stress and normal static pressure gradient have been ignored. Thompson[21] has observed that most boundary-layer measurements in supposedly two-dimensional flow do not satisfy this equation, and that the primary explanation

* The only significant systematic error likely to affect the validity of this assumption would be one in the procedure used to correct skin-friction coefficients determined by integral law, Preston tube and Clauser techniques for survey rig interference. However the corrections estimated are themselves small, (as has been indicated in Section 3.2, they amount to 4 per cent at most), so that errors in the corrections are unlikely to exceed 1 or 2 per cent of measured values.

for this is a three-dimensional flow effect with the neglected terms in equation (8) as a secondary reason. Thus a comparison of measured momentum thickness distribution with that obtained by integration of equation (8) provides some measure of the confidence with which the experimental data can be used.

Equation (8) has been solved by evaluating $d\delta_2/ds$ at each survey station using measured pressure distributions and H_{12}, with C_f derived from the Green (2) integral law. The momentum thickness distribution which satisfied equation (8) was then obtained by an iterative process, starting with the experimental distribution. Since errors incurred in this procedure are cumulative, integrations on the wing have been started at the first survey station aft of mid-chord; by not using the less-accurate data at forward stations more realistic comparisons can be made over the rear of each section. In the case of the wake measurements, integration was carried out in the upstream direction, starting at the survey station furthest removed from the wing: in this way, discrepancies are more clearly shown where they are most likely to occur, viz. near the trailing edge.

Because distributions of C_f and H_{12} have not been modified at each iteration and because errors are cumulative, the resulting comparisons give a very pessimistic estimate of errors in momentum thickness due to three-dimensional effects and terms omitted in using equation (8). Accordingly the comparisons shown in Fig. 14 are thought to be very encouraging. In all three cases the rate of growth of momentum thickness predicted by equation (8) near the trailing edge is lower than that indicated by the measurements on the upper surface and higher on the lower surface. In this region the terms omitted from equation (8) are as likely to be the source of this discrepancy as three-dimensional effects. Fig. 14c shows a significant difference in δ_2 over the part of the lower surface covered: this may be due to experimental error at the starting station or to a local three-dimensional effect. A similar, but smaller, effect is also seen in Fig. 14a, but no such effect is shown in Fig. 14b. Upper surface and wake measurements are seen to be quite consistent with the momentum integral equation calculations.

If the data just presented is used as a rough guide to the maximum possible experimental error in momentum thickness measurement, then the probable error is thought to be about $\pm 0{\cdot}00010$. Possible errors in other integral parameters are expected to be in proportion to this error in δ_2.

6. Comparisons of Boundary-Layer Estimates with Measurements

The present measurements have been compared with estimates made using two turbulent boundary-layer calculation methods, one Green's extension of Head's integral 'entrainment' method[8], and the other Bradshaw's method[22] which uses the turbulent energy equation. Both methods have been programmed in FORTRAN for the computers installed at R.A.E. The program of Bradshaw's method was also used to estimate the effects of streamwise surface curvature on the calculations. The flow was assumed to be precisely two-dimensional in all cases.

Turbulent boundary-layer calculations were started at the transition points with suitable 'starting' parameters, which were computed as follows. For each case the location of the stagnation point was estimated, and for each surface laminar boundary-layer development was calculated by the method of Rott and Crabtree[24]. The value of momentum thickness thus obtained at the transition point was assumed unchanged by the transition process, which itself was assumed to occur instantaneously. Other turbulent boundary-layer parameters at transition points were estimated using relations published by Nash and MacDonald[25] (i.e. assuming an equilibrium boundary layer). To start calculations by Bradshaw's method, these parameters were used to generate a 'Coles' profile by a procedure incorporated in the computer program.

Momentum thickness comparisons are shown in Figs. 15 to 17. In general terms, agreement between estimates and measurements is good except near the trailing edge on the upper surface. In each case, the rate of growth of momentum thickness at the trailing edge is over-estimated on the lower surface and under-estimated on the upper by either method. This is, partly at least, due to the discrepancy (already noted in Section 5) between the experimental results and those obtained by integration of the usual form of the two-dimensional momentum integral equation (equation (8)). Estimates by Bradshaw's method without curvature terms included, tend to lie below the experimental data; the effect of including curvature terms is to reduce estimated momentum thickness and therefore agreement is generally

worsened. Estimates made using Green's method are very similar to or greater than those using Bradshaw's method and these are seen to give better agreement with measurements at the trailing edge on the upper surface.

Shape parameter comparisons are made in Figs. 18 to 20, and again the general level of agreement is good. Curvature terms tend to improve estimates made by Bradshaw's method for the lower surface, but show no marked improvement or otherwise on the upper surface. In the case of Section 2815, the inclusion of these terms appears to have a large effect near the trailing edge. Estimates by Green's method show approximately the same level of agreement with upper surface measurements as do those by Bradshaw's method, but on the lower surface they tend to be inferior. At forward stations on the lower surface, Green's estimates are low while, near the trailing edge, they are greater than measurements, particularly in the case of Section 2814. The trailing edge discrepancy is in accord with Horton's conclusion[26] that Head's original entrainment method (on which Green's method is founded) over-estimates shape parameter and under-estimates skin friction in a region of increasing pressure gradient following an adverse pressure gradient. Developments of the entrainment method which take account of boundary-layer 'history' are expected to correct this deficiency.

Comparisons of skin friction results are shown in Figs. 21 to 27. The experimental results shown in these figures are those computed from integral parameters using the Green (1) skin-friction law (equation (5), Section 3.4). (It will be recalled that results using this law are typical of those obtained using other available 'integral' laws and by performing a 'Clauser' analysis on profile data.) On the upper surface, Green estimates tend to be in better agreement with the measurements than the Bradshaw estimates, particularly towards the trailing edge where skin friction is low: again the inclusion of curvature terms in Bradshaw estimates shows no obvious improvement and in fact results in the prediction of separation ahead of the trailing edge in two cases, though this does not occur in practice. On the lower surface, the opposite is again the case and Bradshaw's method gives better agreement with the data than does Green's. The low estimate of skin friction near the trailing edge by Green's method is associated with the high estimate of shape parameter mentioned above.

It is interesting to use the present results to check how far they satisfy some of the relations used in Green's computation procedure. The equations given by Green in Ref. 8 have been programmed by the present author in the following form for two-dimensional section work:

$$\frac{d\delta_2}{ds} = \frac{C_f}{2} - (H_{12} + 2 - M_1^2)\frac{\delta_2}{u_1}\frac{du_1}{ds}, \tag{9a}$$

$$\frac{\delta_2\, dH_1}{ds} = F - H_1\left[\frac{C_f}{2} - (H_{12} + 1)\frac{\delta_2}{u_1}\frac{du_1}{ds}\right], \tag{9b}$$

$$F = 0{\cdot}0299(H_1 - 3)^{-0{\cdot}6169}, \tag{9c}$$

$$\bar{H} = 1 + 1{\cdot}12(H_1 - 2 - \sqrt{(H_1 - 2)^2 - 3})^{0{\cdot}915}, \tag{9d}$$

$$H_{12} = (\bar{H} + 1)(1 + 0{\cdot}177M_1^2) - 1, \tag{9e}$$

and the skin-friction law quoted in Section 3.4, equation (7). $\bar{H}$ is defined as δ_1'/δ_2.

Originally F was defined as the entrainment parameter and H_1 as δ_0/δ_2: however it has been pointed out to the present author by Dr. Green that precise physical interpretations of F and H_1 are unnecessary, beyond the fact that they are both unique functions of H_{12} satisfying equation (9b). Thus Green's method gives generally close estimates of δ_2, H_{12} and C_f, in spite of the fact that δ_0/δ_2 is not particularly-well represented by H_1 as given by equation (9d): this comparison is shown in Fig. 27. Here the experimental data shown are for boundary-layer surveys made aft of mid-chord (to eliminate less-accurate information from this comparison) and for all wake data (since an extension of Green's method to wake calculations

is available which incorporates equation (9d) unmodified*). The experimental data is seen to lie below the line defined by Green's equation, and in fact the present results are well fitted by the equation:

$$\bar{H} = 1 + 1{\cdot}69(H_1 - 2{\cdot}5)^{-1{\cdot}103}.$$

This relation is applicable only within the Reynolds number range of the present tests, viz.

$$4 < \log_{10}(u_1\delta_2/\nu_1) < 5,$$

since Thompson has noted[27] that $\bar{H}$ is dependent on momentum thickness Reynolds number as well as on δ_0/δ_2.

The parameter F has been calculated using both equations (9b) and (9c), in each case using the auxiliary relations (9d) and (9e) to calculate H_1 and dH_1/ds in terms of experimental values of H_{12}. Other parameters used in the calculations were also obtained from the measurements. These two evaluations of F are shown for two survey conditions by the different symbols in Figs. 28 and 29. In comparing these results it should be remembered that evaluation of equation (9b) which provides the definition of F, requires numerical differentiation of experimental data and thus large errors are possible. The results suggest that equation (9c) gives a good representation of the parameter F (insofar as the two sets of symbols coincide) on the upper surface of each section, but a poor representation on the lower surface. Agreement is particularly poor on the lower surface of Section 2814 aft of about 80 per cent chord; this is to be expected in view of the discrepancies in estimates of H_{12} already noted. The full lines in Figs. 28 and 29 represent the value of F calculated in the course of the estimates of δ_2, etc., discussed above. The difference between the full line and the equation (9c) data is due only to the difference between estimated and measured H_{12} and, since this difference is much smaller than that between the full line and the equation (9b) data, the results show that the calculation method is not strongly dependent on the value of the parameter F.

7. Comparisons of Wake Estimates with Measurements

Measurements of momentum thickness and shape parameter in the wake are compared with estimates in Figs. 30 to 32. Fig. 30 includes estimates made using an extension of the well-known Squire and Young wake law[28], while all three figures show estimates made by Green's method[8], in a slightly modified form. All the estimates start from trailing edge values of δ_2 and H_{12}, which were obtained by extrapolation of experimental boundary layer data.

7.1. Extension of Squire and Young Wake Law

The momentum thickness of the wake far downstream of an aerofoil can be expressed in terms of measurements of δ_2, H_{12} at an upstream station by integrating the two-dimensional momentum integral equation to yield:

$$\frac{(\delta_2)_\infty}{\delta_2} = \left(\frac{M_1}{M_{1\infty}}\right)^{H_{12}+2}\left(\frac{1 + 0{\cdot}2M_{1\infty}^2}{1 + 0{\cdot}2M_1^2}\right)^{\frac{1}{2}(H_{12}+7)} \exp\left\{\int_{H_{12\infty}}^{H_{12}} \ln\left(\frac{u_{1\infty}}{u_1}\right) dH_{12}\right\}. \tag{10}$$

Suffix ∞ denotes a position far downstream of the aerofoil. It is easily shown that, far downstream, the shape parameter becomes

$$H_{12\infty} = 1 + 0{\cdot}4M_{1\infty}^2. \tag{11}$$

* See Ref. 8; the wake equations are also quoted here in Section 7.2.

Squire and Young assumed that $\ln(u_{1\infty}/u_1)$ varied linearly with H_{12} in the wake: this assumption simplifies (10) to:

$$\frac{(\delta_2)_\infty}{\delta_2} = \left(\frac{M_1}{M_{1\infty}}\right)^{\frac{1}{2}(H_{12}+H_{12\infty}+4)} \left(\frac{1 + 0{\cdot}2M_{1\infty}^2}{1 + 0{\cdot}2M_1^2}\right)^{\frac{1}{2}(H_{12}+H_{12\infty}+14)}. \tag{12}$$

Mach number and velocity far downstream have been calculated from 'empty' tunnel calibration data at the position of the model (wake 'blockage' effects were found to be negligible). $(\delta_2)_\infty$ was thus calculated in terms of trailing edge conditions, and H_{12} and δ_2 at intermediate stations were then readily obtained.

The results of this calculation for Section 2814 (Fig. 30) show that estimated H_{12} tends to its limiting value more rapidly than do the experimental results. This is a consequence of the Squire and Young assumption, which is not supported by the present data; Fig. 33 shows that $\ln(u_{1\infty}/u_1)$ is not a linear function of H_{12}. In the case of momentum thickness agreement is good, mainly because the precise assumptions made regarding shape factor distribution are not important. The Squire and Young assumption thus appears to give reasonably accurate predictions of momentum thickness, but less accurate predictions of shape factor and consequently of displacement surface.

7.2. Green's Method

The wake calculation procedure proposed by Green[8] is to continue separate upper and lower surface boundary-layer calculations beyond the trailing edge, with a different entrainment function in the wake and, of course, no skin friction. His equations for each 'surface' may be summarised as follows (cf. equations (9)):

$$\frac{d\delta_2}{dX} = -(H_{12} + 2 - M_1^2)\frac{\delta_2}{u_1}\frac{du_1}{dX}, \tag{13a}$$

$$\frac{\delta_2\, dH_1}{dX} = F + H_1(H_{12} + 1)\frac{\delta_2}{u_1}\frac{du_1}{dX}, \tag{13b}$$

$$F = \gamma F_w + (1 - \gamma)F_H, \tag{13c}$$

$$\overline{H} = 1 + 1{\cdot}12(H_1 - 2 - \sqrt{(H_1 - 2)^2 - 3})^{0{\cdot}915}, \tag{13d}$$

$$H_{12} = (\overline{H} + 1)(1 + 0{\cdot}2M_1^2) - 1, \tag{13e}$$

$$F_H = 0{\cdot}0299(H_1 - 3)^{-0{\cdot}6169}, \tag{13f}$$

$$F_w = 0{\cdot}435(\overline{H} - 1)^{0{\cdot}907} \text{ and} \tag{13g}$$

$$\gamma = 1 - \exp((1 - X)/N\delta_{TE}), \tag{13h}$$

N is a constant, chosen by Green as 5 on the basis of some experimental data available for symmetrical sections at zero incidence. F_w is the asymptotic value of F far downstream of the trailing edge.

In addition, the method was modified slightly by the present author to permit the calculation to give total wake parameters at each station*. It was assumed that the parameter F could be determined with

* Such a modification is desirable since, for asymmetric wakes, it is not practicable to differentiate between 'upper' and 'lower' surfaces, and any comparisons involving measurements must be made for the complete wake.

sufficient accuracy by assuming a symmetrical wake (which was found to develop within about 10 per cent chord of the trailing edge in the present cases). Thus the above equations were used with γ evaluated using total boundary-layer thickness at the trailing edge, and F_w and F_H in equation (13c) were replaced by $2F_w$ and $2F_H$ respectively.

Calculations using this simpler method are shown together with those using the full method in Figs. 30 to 32. Both methods give indistinguishable results for momentum thickness, while differences between estimates of H_{12} are not large. Neither calculation method is significantly superior to the other when compared with measured values of H_{12}.

Generally, agreement of estimates with measurements of both δ_2 and H_{12} is good, though estimates of δ_2 are lower than measurements for Section 2815, most noticeably within about 20 per cent chord of the trailing edge. This could be explained by low trailing edge 'starting' values for δ_2, but this seems unlikely on the basis of the boundary-layer comparisons presented earlier.

Again, the evaluation of the parameter F has been checked. Since it is not practicable to divide the experimental wake profiles into separate 'upper' and 'lower' surface components, the equations used are those relevant to the total wake. 'Experimental' values of F were obtained using equations (13b) and (13c) separately and, as in the case of the boundary layer, each was evaluated in terms of H_{12} using Green's auxiliary relations. These two results are shown in Fig. 34 by different symbols; if F is taken to be defined by equation (13b), then, on average, equation (13c) over-estimates F slightly but the general level of agreement is considerably better than that shown for boundary-layer data. As in the case of boundary-layer estimates, calculations of F (shown by the full lines) agree more closely with values obtained using equation (13c) than with those obtained using (13b), and again the inference is that estimates of δ_2 and H_{12} do not depend strongly on the precise value of F. Finally, Fig. 34 includes the asymptotic value of F (i.e. F_w), to which the calculation using equation (13c) tends when the proximity of the trailing edge is ignored, (F_w is denoted by a broken line). It is seen that F approaches this limit closely aft of about 40 per cent chord from the trailing edge, so that this is approximately the region within which entrainment changes from that applicable to a boundary layer to that of an isolated wake.

8. Conclusions

Boundary layer and wake surveys have been made on two aerofoil sections, R.A.E. 2814 and R.A.E. 2815, at Reynolds numbers of about 15×10^6 and at high subsonic speeds. Integral parameters have been derived from profile data after making allowances for:

(a) the omission from integrals of the boundary-layer region within a pitot tube radius of the wing surface;
(b) the upstream three-dimensional influence of the survey rig;
(c) pitot tube displacement effects;
(d) effects of local turbulence on pressure measurements.

Profile data and integral parameters are tabulated.

Skin-friction coefficients have been calculated using four alternative integral laws, all of which were found to give very similar results to each other and to values derived from comparisons of boundary-layer profile data with a suitable law of the wall. Skin friction was also determined by the Preston tube technique; differences between two alternative Preston tube calibrations used have been ascribed to differences in the compressibility transforms used, but skin-friction results are about 5 per cent to 8 per cent higher than those obtained using integral laws. Later wind-tunnel measurements suggest that this discrepancy is also due to uncertainties regarding compressibility corrections. Skin-friction measurements made using the razor-blade technique are approximately 5 per cent lower than integral law results.

The integral results generally satisfy the two-dimensional momentum integral equation well, though discrepancies in the rate of growth of momentum thickness exist in each case near the trailing edge.

Boundary-layer parameters have been compared with estimates made using (i) Green's extension to compressible flow of Head's entrainment procedure, and (ii) Bradshaw's turbulent energy method. In general, Green's method gives closer argeement with measurements on the upper surface than on the

lower surface, while the opposite is true in the case of Bradshaw's method. Calculations including surface curvature terms in Bradshaw's procedure show no consistent improvement in estimation accuracy. Both methods under-estimate momentum thickness at the trailing edge on the upper surface. Skin-friction comparisons suggest that Bradshaw's method is likely to predict separation prematurely. Green's entrainment parameter does not fit lower surface measurements closely, and his relation between $\bar{H}$ and H_1 tends to lie above the present results.

Wake results are compared firstly with some simple estimates for Section 2814, which make use of an extension to compressible flow of the Squire and Young wake law. These estimates agree well with measurements of momentum thickness. Comparisons with Green's wake entrainment technique show generally good agreement both for momentum thickness and for shape parameter, though momentum thickness for Section 2814 is under-estimated, particularly near the trailing edge.

Acknowledgements

The author is grateful to (i) Mr. P. Bradshaw, presently of Imperial College, London, for supplying details of his boundary-layer calculation method and for providing a copy of his computer program, (ii) Dr. J. E. Green, for providing details of his calculation methods for boundary layers and wakes in advance of publication, and (iii) Mr. A. W. Smith, formerly of R.A.E., Bedford, for considerable assistance with the experimental work and analysis.

LIST OF SYMBOLS

c	Wing chord, 762 mm (30 in), all other lengths are expressed in wing chord units
C_f	Local skin-friction coefficient, $\tau_w/\frac{1}{2}\rho_1 u_1^2$
C_L	Lift coefficient
F	Entrainment parameter
H	Boundary layer or wake shape parameter
H_1	δ_0/δ_2
H_{12}	δ_1/δ_2
$\bar{H}$	δ_1'/δ_2
M	Mach number
R	Reynolds number
s	Distance along wing surface
u	Velocity
T	Temperature (degrees Kelvin)
X	Chordwise distance, origin at leading edge
Y	Ordinate normal to wing surface or to free stream
x, y	Parameters used to describe calibrations of Preston tubes or razor-blades
δ	Boundary-layer or wake thickness (in wing chord units) δ_1, δ_2 etc. are defined in Section 3.1
μ	Viscosity
ν	Kinematic viscosity, μ/ρ
ρ	Density
τ	Shear stress

Suffices applied to ρ, u, etc.

1	Outer edge of boundary layer or wake
w	Wall value

REFERENCES

No.	Author(s)	Title, etc.
1	K. G. Smith L. Gaudet K. G. Winter	The use of surface pitot tubes as skin friction meters at supersonic speeds. A.R.C. R. & M. 3351 (1962)
2	L. F. East	Measurement of skin friction at low subsonic speeds by the razor-blade technique. A.R.C. R. & M. 3525 (1966)
3	D. Isaacs	Calibration of the 8 ft × 8 ft wind tunnel at subsonic speeds. A.R.C. R. & M. 3583 (1967)
4	S. Goldstein A. D. Young	The linear perturbation theory of compressible flow, with applications to wind-tunnel interference. A.R.C. R. & M. 1909 (1943)
5	G. J. Nothwang	An evaluation of four experimental methods for measuring mean properties of a supersonic turbulent boundary layer. N.A.C.A. Report 1320 (1957)
6	D. Coles	The turbulent boundary layer in a compressible fluid. U.S.A. Rand Report R-403-PR (1962)
7	J. P. Johnston	The turbulent boundary layer at a plane of symmetry in a three-dimensional flow. *Journal of Basic Engineering*, September 1960
8	J. E. Green	Application of Head's entrainment method to the prediction of turbulent boundary layers and wakes in compressible flow. R.A.E. Technical Report 72079 (1972)
9	K. G. Winter J. C. Rotta K. G. Smith	Studies of the turbulent boundary layer on a waisted body of revolution in subsonic and supersonic flow. A.R.C. R. & M. 3633 (1968)
10	J. E. Green	The prediction of turbulent boundary layer development in compressible flow. *J. Fluid Mech.*, Vol. 31, pp. 753–778 (1968)
11	F. A. MacMillan	Experiments on pitot-tubes in shear flow. A.R.C. R. & M. 3028 (1956)
12	M. G. Hall	Experimental measurements in a three-dimensional turbulent boundary layer in supersonic flow. AGARDograph 97 (Part 2) pp. 829–854 (1965)
13	L. Landweber	Re-analysis of boundary-layer data on a flat plate. U.S.A. Iowa State University, Inst. of Hydraulic Res. ACSIL/61/526 (1960)
14	D. F. Myring	The effects of normal pressure gradients on the boundary layer momentum integral equation. R.A.E. Technical Report 68214 A.R.C. 30858 (1968)
15	E. J. Hopkins E. R. Keener	Study of surface pitots for measuring turbulent skin friction at supersonic Mach numbers—adiabatic wall. N.A.S.A. T.N. D-3478 (1966)

No.	Author(s)	Title, etc.
16	V. C. Patel	Calibration of the Preston tube and limitations on its use in pressure gradients. *J. Fluid Mech.*, Vol. 23, pp. 185–208 (1965)
17	R. Shaw	The influence of hole dimensions on static pressure measurements. *J. Fluid Mech.*, Vol. 7 (1960)
18	K. G. Winter L. Gaudet	Turbulent boundary layer studies at high Reynolds numbers at Mach numbers between 0·2 and 2·8. R.A.E. Technical Report 70251 (1970)
19	H. Ludwieg W. Tillmann	Untersuchungen über die Wandschubspannung in turbulenten Reibungsschichten. Ing. Arch. 17, pp. 288–299 (1949) N.A.C.A. T.M. 1285 (English translation) (1950)
20	J. F. Nash A. G. J. MacDonald	A turbulent skin-friction law for use at subsonic and transonic speeds. A.R.C. C.P. 948 (1966)
21	B. G. J. Thompson	A critical review of existing methods of calculating the turbulent boundary layer. A.R.C. R. & M. 3479 (1964)
22	P. Bradshaw D. H. Ferriss	Calculation of boundary-layer development using the turbulent energy equation. II Compressible flow on adiabatic walls. N.P.L. Aero Report 1217 A.R.C. 28541 (1966)
23	D. H. Ferriss P. Bradshaw	A computer program for the calculation of boundary layer development using the turbulent energy equation. N.P.L. Aero Report 1269 and Addendum A.R.C. 30231 (1968)
24	N. Rott L. F. Crabtree	Simplified laminar boundary-layer calculations for bodies of revolution and for yawed wings. *J. Aero. Sciences*, Vol. 19 (8), pp. 553–565 (1952)
25	J. F. Nash A. G. J. MacDonald	The calculation of momentum thickness in a turbulent boundary layer at Mach numbers up to unity. A.R.C. C.P. 963 (1966)
26	H. P. Horton	Entrainment in equilibrium and non-equilibrium turbulent boundary layers. H.S.A./Hatfield/Research/1094/HPH (1969)
27	B. G. J. Thompson	A new two-parameter family of mean velocity profiles for incompressible turbulent boundary layers on smooth walls. A.R.C. R. & M. 3463 (1965)
28	H. B. Squire A. D. Young	The calculation of profile drag of aerofoils. A.R.C. R. & M. 1838 (1937)
29	A. L. Braslow E. C. Knox	Simplified method for determination of critical height of distributed roughness particles for boundary-layer transition at Mach numbers from 0 to 5. N.A.C.A. T.N. 4363 (1958)
30	L. Gaudet	Unpublished RAE work

TABLE 1

Section 2814: $C_L = 0{\cdot}42$

Section Geometry and Survey Condition

Max. thickness-chord ratio = 12 per cent
Mach number = 0·725: incidence = 1·44°

Upper Surface				Lower Surface and Wake			
X	Z	C_p	Survey†	X	Z	C_p	Survey†
0	0	0·966		0	0	0·966	
0·0007	0·0033	0·588		0·0006	0·0032	1·138	
0·0023	0·0064	0·070		0·0023	0·0064	1·050	
0·0093	0·0124	−0·451		0·0089	0·0122	0·681	
0·0229	0·0188	−0·599		0·0246	0·0201	0·346	
0·0712	0·0321	−0·730		0·0571	0·0300	0·115	
0·1079	0·0386	−0·707		0·1053	0·0399	−0·047	
0·1579	0·0453	−0·710		0·1667	0·0486	−0·179	
0·2166	0·0510	−0·698		0·2333	0·0551	−0·272	
0·2666	0·0546	−0·683		0·3000	0·0588	−0·367	
0·3167	0·0573	−0·690	Table 4	0·3500	0·0601	−0·452	Table 5
0·3665	0·0591	−0·688		0·4000	0·0595	−0·484	
0·4166	0·0599	−0·656	Table 4	0·4500	0·0566	−0·403	
0·4666	0·0601	−0·670		0·5000	0·0517	−0·269	Table 5
0·5166	0·0594	−0·708	Table 4	0·5666	0·0437	−0·133	
0·5666	0·0574	−0·646		0·6332	0·0347	−0·018	Table 5
0·6256	0·0524	−0·514	Table 4	0·6999	0·0253	0·091	
0·6942	0·0468	−0·388		0·7665	0·0165	0·166	Table 5
0·7499	0·0402	−0·282	Table 4	0·8332	0·0091	0·215	Table 5
0·8006	0·0333	−0·182		0·8998	0·0033	0·255	Table 5
0·8457	0·0267	−0·094	Table 4	0·9499	0·0007	0·276	Table 5
0·8885	0·0201	−0·019		0·9833	0·0001	0·260	Table 5
0·9305	0·0134	0·057	Table 4	0·9970	0	0·242*	Table 5
0·9682	0·0069	0·141	Table 4	1·0200		0·226	Table 6
0·9918	0·0020	0·208	Table 4	1·0500		0·199	Table 6
0·9970	0·0007	0·220*	Table 4	1·0877		0·166	Table 6
				1·1077		0·142	Table 6
				1·1277		0·135	Table 6
				1·1543		0·118	Table 6
				1·1877		0·107	Table 6
				1·2210		0·098	Table 6
				1·3877		0·066	Table 6
				1·5543		0·052	Table 6
				1·8877		0·038	Table 6

* Interpolated C_p.

† The making of a survey at a given station is indicated by reference to the table number where profile data for the survey is listed.

TABLE 2

Section 2815: $C_L = 0{\cdot}51$

Section Geometry and Survey Condition

Max. thickness-chord ratio = 14 per cent
Mach number = 0·661; incidence = 2·57°

Upper Surface				Lower Surface and Wake			
X	Z	C_p	Survey†	X	Z	C_p	Survey†
0	0	0·868		0	0	0·868	
0·0006	0·0036	0·486		0·0005	0·0030	1·097	
0·0020	0·0067	0·045		0·0053	0·0098	0·916	
0·0074	0·0128	−0·481		0·0258	0·0200	0·509	
0·0188	0·0200	−0·733		0·0595	0·0300	0·301	
0·0367	0·0280	−0·811		0·1029	0·0400	0·145	
0·0607	0·0360	−0·877		0·1582	0·0501	−0·016	
0·0923	0·0441	−0·932		0·2316	0·0599	−0·188	Table 8
0·1332	0·0521	−0·936		0·3197	0·0664	−0·315	Table 8
0·1888	0·0602	−0·930		0·3997	0·0676	−0·392	
0·2297	0·0645	−0·927		0·4797	0·0633	−0·328	Table 8
0·2716	0·0680	−0·920	Table 7	0·5644	0·0540	−0·178	
0·3117	0·0703	−0·919		0·6722	0·0390	−0·008	Table 8
0·3516	0·0716	−0·888	Table 7	0·7693	0·0249	0·102	Table 8
0·4007	0·0720	−0·820		0·8617	0·0130	0·176	Table 8
0·4496	0·0710	−0·739	Table 7	0·9380	0·0048	0·222*	Table 8
0·5179	0·0679	−0·626		0·9862	0·0009	0·251	Table 8
0·5854	0·0630	−0·515	Table 7	0·9970	0·0002	0·259*	Table 8
0·6608	0·0554	−0·398	Table 7	1·0417		0·206	Table 9
0·7218	0·0479	−0·293	Table 7	1·1000		0·159	Table 9
0·7750	0·0403	−0·193	Table 7	1.1700		0·121	Table 9
0·8238	0·0329	−0·111	Table 7	1·3000		0·083	Table 9
0·8696	0·0253	−0·031	Table 7	1·6000		0·046	Table 9
0·9119	0·0180	0·050	Table 7				
0·9518	0·0103	0·148	Table 7				
0·9878	0·0026	0·237	Table 7				
0·9970	0·0007	0·256*	Table 7				

* Interpolated C_p.
† See note on Table 1.

TABLE 3

Section 2815: $C_L = 0{\cdot}70$

Section Geometry and Survey Condition

Max. thickness-chord ratio = 14 per cent
Mach number = 0·664: incidence = 3·83°

Upper Surface				Lower Surface and Wake			
X	Z	C_p	Survey†	X	Z	C_p	Survey†
0	0	0·604		0	0	0·604	
0·0006	0·0036	0·133		0·0005	0·0030	1·000	
0·0020	0·0067	−0·388		0·0053	0·0098	1·042	
0·0074	0·0128	−0·940		0·0258	0·0200	0·664	
0·0188	0·0200	−1·167		0·0595	0·0300	0·436	
0·0367	0·0280	−1·204		0·1029	0·0400	0·269	
0·0607	0·0360	−1·274		0·1582	0·0501	0·099	
0·0923	0·0441	−1·256		0·2316	0·0599	−0·078	Table 11
0·1332	0·0521	−1·282		0·3197	0·0664	−0·218	Table 11
0·1888	0·0602	−1·295		0·3997	0·0676	−0·306	
0·2297	0·0645	−1·257		0·4797	0·0633	−0·262	Table 11
0·2716	0·0680	−1·001		0·5644	0·0540	−0·134	
0·3117	0·0703	−1·080		0·6722	0·0390	0·018	Table 11
0·3516	0·0716	−1·015		0·7693	0·0249	0·119	Table 11
0·4007	0·0720	−0·903		0·8617	0·0130	0·186	Table 11
0·4496	0·0710	−0·806	Table 10	0·9380	0·0048	0·220*	Table 11
0·5179	0·0679	−0·673		0·9862	0·0009	0·241	
0·5854	0·0630	−0·548	Table 10	0·9970	0·0002	0·246*	Table 11
0·6608	0·0554	−0·418	Table 10	1·1000		0·156	Table 12
0·7218	0·0479	−0·305	Table 10	1·3000		0·082	Table 12
0·7750	0·0403	−0·199	Table 10	1·6000		0·046	Table 12
0·8238	0·0329	−0·111	Table 10				
0·8696	0·0253	−0·028	Table 10				
0·9119	0·0180	0·054	Table 10				
0·9518	0·0103	0·146	Table 10				
0·9878	0·0026	0·223					
0·9970	0·0007	0·241*	Table 10				

* Interpolated C_p.
† See note on Table 1.

TABLE 4

Boundary Layer Profile Data; Section 2814, $C_L = 0{\cdot}42$, Upper Surface

X = 0.3107			X = 0.4166			X = 0.5166			X = 0.6256			X = 0.7499		
Y	u/u_1	ρ/ρ_1	Y	u/u_1	ρ/ρ_1	Y	u/u_1	ρ/ρ_1	Y	u/u_1	ρ/ρ_1	Y	u/u_1	ρ/ρ_1
0.00033	0.6814	0.9182	0.00033	0.6599	0.9138	0.00033	0.6845	0.9150	0.00033	0.5786	0.9074	0.00033	0.5405	0.9182
0.00040	0.6942	0.9206	0.00040	0.6759	0.9168	0.00040	0.6845	0.9150	0.00040	0.5851	0.9083	0.00040	0.5441	0.9187
0.00057	0.6977	0.9213	0.00057	0.6792	0.9174	0.00047	0.6891	0.9159	0.00047	0.5955	0.9099	0.00047	0.5541	0.9198
0.00073	0.7186	0.9255	0.00063	0.6958	0.9206	0.00057	0.7012	0.9184	0.00063	0.6094	0.9120	0.00063	0.5618	0.9207
0.00080	0.7283	0.9275	0.00080	0.7105	0.9236	0.00070	0.7142	0.9211	0.00080	0.6252	0.9145	0.00070	0.5656	0.9212
0.00090	0.7489	0.9319	0.00103	0.7311	0.9278	0.00100	0.7347	0.9255	0.00093	0.6435	0.9175	0.00093	0.5858	0.9237
0.00107	0.7685	0.9362	0.00133	0.7639	0.9349	0.00130	0.7526	0.9295	0.00127	0.6633	0.9209	0.00130	0.6069	0.9264
0.00130	0.7919	0.9416	0.00150	0.7802	0.9386	0.00170	0.7848	0.9371	0.00183	0.6922	0.9260	0.00167	0.6267	0.9291
0.00137	0.8113	0.9462	0.00180	0.7995	0.9432	0.00213	0.8083	0.9428	0.00210	0.7251	0.9322	0.00197	0.6520	0.9326
0.00187	0.8464	0.9549	0.00203	0.8229	0.9488	0.00250	0.8367	0.9502	0.00233	0.7417	0.9354	0.00240	0.6716	0.9354
0.00203	0.8629	0.9592	0.00250	0.8542	0.9568	0.00290	0.8618	0.9570	0.00267	0.7600	0.9391	0.00297	0.6917	0.9384
0.00210	0.8799	0.9638	0.00280	0.8727	0.9617	0.00337	0.8799	0.9620	0.00307	0.7812	0.9436	0.00330	0.7166	0.9423
0.00250	0.8986	0.9690	0.00297	0.8889	0.9661	0.00367	0.8985	0.9674	0.00337	0.8055	0.9489	0.00360	0.7349	0.9453
0.00283	0.9232	0.9760	0.00337	0.9059	0.9709	0.00407	0.9170	0.9729	0.00377	0.8292	0.9543	0.00390	0.7525	0.9483
0.00307	0.9470	0.9831	0.00367	0.9269	0.9770	0.00460	0.9419	0.9806	0.00430	0.8524	0.9597	0.00443	0.7847	0.9539
0.00357	0.9683	0.9897	0.00400	0.9458	0.9827	0.00530	0.9670	0.9888	0.00465	0.8713	0.9644	0.00507	0.8042	0.9575
0.00397	0.9846	0.9949	0.00447	0.9631	0.9881	0.00597	0.9837	0.9944	0.00493	0.8880	0.9686	0.00543	0.8280	0.9620
0.00480	0.9975	0.9992	0.00493	0.9791	0.9931	0.00683	0.9961	0.9986	0.00533	0.9085	0.9739	0.00580	0.8496	0.9662
0.00570	0.9980	0.9993	0.00590	0.9951	0.9984	0.00787	0.9987	0.9995	0.00590	0.9287	0.9793	0.00620	0.8664	0.9696
0.00653	0.9985	0.9995	0.00670	0.9976	0.9993	0.00880	0.9992	0.9997	0.00653	0.9507	0.9855	0.00657	0.8836	0.9732
0.00733	0.9997	0.9999	0.00797	0.9984	0.9995	0.01033	0.9997	0.9999	0.00717	0.9730	0.9919	0.00697	0.9038	0.9775
			0.00910	0.9990	0.9997	0.01120	1.0003	1.0001	0.00813	0.9904	0.9971	0.00767	0.9216	0.9814
			0.00997	0.9990	0.9997				0.00910	0.9976	0.9993	0.00813	0.9451	0.9868
			0.01047	1.0006	1.0002				0.01000	0.9994	0.9998	0.00877	0.9670	0.9919
									0.01023	1.0001	1.0000	0.00960	0.9824	0.9956
												0.01047	0.9922	0.9981
												0.01127	0.9981	0.9995
												0.01223	0.9996	0.9999
												0.01247	0.9996	0.9999

TABLE 4 (Concluded)

X = 0.8457			X = 0.9305			X = 0.9682			X = 0.9918			X = 0.9970		
Y	u/u_1	ρ/ρ_1	Y	u/u_1	ρ/ρ_1	Y	u/u_1	ρ/ρ_1	Y	u/u_1	ρ/ρ_1	Y	u/u_1	ρ/ρ_1
0.00033	0.5025	0.9226	~~0.00037~~	~~0.4314~~	~~0.9294~~	~~0.00033~~	~~0.3405~~	~~0.9305~~	0.00033	0.2589	0.9315	0.00033	0.2353	0.9321
0.00040	0.5093	0.9233	0.00043	0.4290	0.9293	0.00040	0.3370	0.9303	0.00040	0.2720	0.9319	0.00040	0.2386	0.9322
0.00047	0.5093	0.9233	0.00053	0.4373	0.9298	0.00047	0.3405	0.9305	0.00047	0.2720	0.9319	~~0.00047~~	~~0.2321~~	~~0.9320~~
0.00063	0.5203	0.9244	0.00060	0.4441	0.9303	0.00057	0.3598	0.9315	0.00053	0.2720	0.9319	0.00053	0.2449	0.9324
0.00070	0.5251	0.9248	0.00063	0.4464	0.9305	0.00080	0.3719	0.9321	0.00067	0.2914	0.9327	0.00060	0.2449	0.9324
0.00107	0.5463	0.9270	0.00103	0.4654	0.9319	0.00140	0.4017	0.9338	0.00127	0.3103	0.9335	0.00100	0.2704	0.9333
0.00160	0.5785	0.9305	0.00150	0.4865	0.9335	0.00220	0.4250	0.9352	0.00180	0.3347	0.9345	0.00147	0.2902	0.9340
0.00240	0.6048	0.9336	0.00190	0.5041	0.9349	0.00250	0.4418	0.9363	0.00240	0.3533	0.9354	0.00227	0.3198	0.9352
0.00297	0.6278	0.9363	0.00243	0.5211	0.9364	0.00310	0.4629	0.9377	0.00293	0.3740	0.9365	0.00230	0.3373	0.9360
0.00330	0.6480	0.9389	0.00297	0.5404	0.9380	0.00357	0.4824	0.9391	0.00337	0.3924	0.9374	0.00320	0.3553	0.9369
0.00370	0.6645	0.9410	0.00347	0.5636	0.9401	0.00420	0.5024	0.9406	0.00390	0.4105	0.9384	0.00377	0.3730	0.9377
0.00403	0.6835	0.9436	0.00403	0.5804	0.9417	0.00483	0.5235	0.9422	0.00443	0.4271	0.9394	0.00430	0.3955	0.9389
0.00457	0.7015	0.9461	0.00450	0.6040	0.9441	0.00530	0.5434	0.9438	0.00507	0.4441	0.9405	0.00493	0.4154	0.9400
0.00507	0.7232	0.9492	0.00510	0.6252	0.9462	0.00587	0.5662	0.9457	0.00540	0.4615	0.9416	0.00553	0.4333	0.9410
0.00543	0.7398	0.9517	0.00567	0.6458	0.9484	0.00657	0.5919	0.9480	0.00610	0.4830	0.9430	0.00637	0.4713	0.9434
0.00580	0.7586	0.9545	0.00617	0.6655	0.9506	0.00713	0.6090	0.9495	0.00667	0.5035	0.9444	0.00723	0.4999	0.9453
0.00627	0.7791	0.9578	0.00653	0.6823	0.9525	0.00777	0.6373	0.9522	0.00723	0.5226	0.9458	0.00767	0.5172	0.9465
0.00673	0.8063	0.9622	0.00700	0.6993	0.9545	0.00827	0.6542	0.9539	0.00780	0.5409	0.9472	0.00833	0.5395	0.9482
0.00750	0.8330	0.9668	0.00747	0.7168	0.9566	0.00883	0.6739	0.9559	0.00803	0.5573	0.9484	0.00890	0.5558	0.9494
0.00803	0.8530	0.9704	0.00763	0.7358	0.9590	0.00927	0.7000	0.9587	0.00867	0.5806	0.9503	0.00933	0.5796	0.9513
0.00840	0.8700	0.9735	0.00843	0.7560	0.9616	0.00977	0.7161	0.9605	0.00920	0.6017	0.9521	0.00983	0.5961	0.9526
0.00887	0.8866	0.9766	0.00887	0.7726	0.9638	0.01017	0.7333	0.9624	0.00977	0.6205	0.9537	0.01020	0.6158	0.9543
0.00940	0.9054	0.9802	0.00927	0.7917	0.9663	0.01083	0.7522	0.9646	0.01017	0.6382	0.9553	0.01100	0.6415	0.9566
0.00997	0.9276	0.9846	0.00990	0.8168	0.9699	0.01130	0.7737	0.9672	0.01070	0.6564	0.9570	0.01153	0.6632	0.9586
0.01060	0.9441	0.9879	0.01050	0.8389	0.9731	0.01190	0.7936	0.9697	0.01123	0.6752	0.9588	0.01203	0.6851	0.9607
0.01120	0.9645	0.9922	0.01093	0.8557	0.9756	0.01240	0.8112	0.9719	0.01177	0.6949	0.9608	0.01280	0.7122	0.9634
0.01200	0.9807	0.9957	0.01153	0.8788	0.9792	0.01287	0.8284	0.9742	0.01220	0.7124	0.9626	0.01333	0.7297	0.9652
0.01280	0.9891	0.9976	0.01220	0.8978	0.9822	0.01330	0.8471	0.9767	0.01277	0.7325	0.9647	0.01380	0.7505	0.9674
0.01367	0.9956	0.9990	0.01277	0.9187	0.9856	0.01387	0.8659	0.9793	0.01330	0.7564	0.9673	0.01427	0.7713	0.9697
0.01457	0.9989	0.9998	0.01340	0.9353	0.9885	0.01437	0.8843	0.9819	0.01390	0.7755	0.9695	0.01510	0.7945	0.9723
0.01520	1.0006	1.0001	0.01400	0.9553	0.9919	0.01493	0.9006	0.9843	0.01450	0.7976	0.9721	0.01557	0.8112	0.9743
			0.01480	0.9682	0.9942	0.01543	0.9194	0.9871	0.01517	0.8243	0.9753	0.01603	0.8294	0.9765
			0.01570	0.9836	0.9970	0.01620	0.9386	0.9900	0.01587	0.8455	0.9780	0.01647	0.8458	0.9785
			0.01680	0.9920	0.9985	0.01703	0.9570	0.9929	0.01647	0.8648	0.9805	0.01693	0.8634	0.9807
			0.01773	0.9970	0.9994	0.01787	0.9730	0.9955	0.01717	0.8892	0.9838	0.01747	0.8818	0.9831
			0.01887	0.9975	0.9995	0.01880	0.9847	0.9974	0.01803	0.9101	0.9866	0.01820	0.9047	0.9862
			0.01973	0.9993	0.9999	0.01963	0.9902	0.9984	0.01877	0.9339	0.9900	0.01860	0.9233	0.9888
						0.02047	0.9940	0.9990	0.01963	0.9526	0.9928	0.01970	0.9420	0.9914
						0.02133	0.9979	0.9996	0.02050	0.9681	0.9951	0.02067	0.9627	0.9944
						0.02217	0.9989	0.9998	0.02163	0.9845	0.9976	0.02157	0.9791	0.9968
						0.02260	0.9994	0.9999	0.02243	0.9886	0.9982	0.02240	0.9863	0.9979
									0.02363	0.9940	0.9990	0.02323	0.9901	0.9985
									0.02443	0.9969	0.9995	0.02437	0.9955	0.9993
									0.02523	0.9992	0.9999	0.02520	0.9985	0.9998
									0.02620	0.9981	0.9997	0.02620	0.9972	0.9996
									0.02690	0.9998	1.0000	0.02647	0.9996	0.9999

TABLE 5

Boundary Layer Profile Data; Section 2814, $C_L = 0{\cdot}42$, Lower Surface

X = 0.3500

Y	u/u_1	ρ/ρ_1
0.00033	0.7071	0.9353
0.00040	0.7197	0.9374
0.00050	0.7209	0.9376
0.00057	0.7245	0.9383
0.00067	0.7445	0.9419
0.00093	0.7668	0.9460
0.00100	0.7916	0.9508
0.00117	0.8097	0.9545
0.00143	0.8358	0.9599
0.00153	0.8543	0.9639
0.00170	0.8728	0.9681
0.00187	0.8915	0.9724
0.00220	0.9190	0.9789
0.00247	0.9350	0.9829
0.00273	0.9565	0.9883
0.00307	0.9741	0.9930
0.00357	0.9905	0.9974
0.00443	0.9997	0.9999
0.00470	1.0004	1.0001

X = 0.5000

Y	u/u_1	ρ/ρ_1
0.00033	0.6214	0.9292
0.00040	0.6147	0.9283
0.00040	0.6199	0.9290
0.00053	0.6298	0.9303
0.00053	0.6393	0.9316
0.00083	0.6639	0.9351
0.00097	0.6830	0.9379
0.00120	0.7028	0.9409
0.00127	0.7191	0.9434
0.00150	0.7360	0.9461
0.00170	0.7597	0.9501
0.00187	0.7778	0.9532
0.00207	0.7997	0.9571
0.00230	0.8194	0.9608
0.00260	0.8446	0.9656
0.00283	0.8667	0.9700
0.00303	0.8839	0.9736
0.00333	0.9042	0.9778
0.00357	0.9237	0.9821
0.00387	0.9431	0.9865
0.00423	0.9619	0.9908
0.00467	0.9792	0.9949
0.00543	0.9959	0.9990
0.00620	1.0002	1.0001

X = 0.6332

Y	u/u_1	ρ/ρ_1
0.00033	0.5144	0.9319
0.00040	0.5216	0.9325
0.00053	0.5265	0.9330
0.00053	0.5313	0.9334
0.00067	0.5335	0.9336
0.00067	0.5518	0.9353
0.00103	0.5711	0.9372
0.00123	0.5899	0.9391
0.00143	0.6098	0.9412
0.00180	0.6310	0.9435
0.00207	0.6512	0.9459
0.00227	0.6704	0.9481
0.00257	0.6888	0.9504
0.00283	0.7146	0.9536
0.00320	0.7318	0.9559
0.00340	0.7525	0.9587
0.00383	0.7782	0.9623
0.00410	0.7971	0.9650
0.00440	0.8156	0.9678
0.00460	0.8382	0.9713
0.00513	0.8671	0.9759
0.00540	0.8831	0.9786
0.00570	0.9031	0.9820
0.00627	0.9307	0.9869
0.00680	0.9549	0.9913
0.00743	0.9790	0.9959
0.00833	0.9939	0.9988
0.00980	1.0003	1.0001

X = 0.7665

Y	u/u_1	ρ/ρ_1
0.00033	0.4887	0.9425
0.00040	0.5009	0.9434
0.00047	0.5055	0.9437
0.00057	0.5082	0.9439
0.00057	0.5177	0.9446
0.00080	0.5364	0.9460
0.00123	0.5556	0.9475
0.00163	0.5736	0.9490
0.00210	0.6015	0.9513
0.00253	0.6211	0.9531
0.00277	0.6390	0.9547
0.00317	0.6585	0.9566
0.00363	0.6777	0.9585
0.00403	0.6955	0.9603
0.00433	0.7130	0.9621
0.00480	0.7360	0.9646
0.00527	0.7573	0.9669
0.00560	0.7745	0.9689
0.00590	0.7912	0.9709
0.00653	0.8174	0.9741
0.00683	0.8350	0.9763
0.00747	0.8651	0.9802
0.00810	0.8930	0.9840
0.00867	0.9178	0.9875
0.00927	0.9346	0.9900
0.00973	0.9507	0.9924
0.01033	0.9683	0.9950
0.01120	0.9832	0.9973
0.01217	0.9935	0.9990
0.01313	0.9980	0.9997
0.01413	0.9993	0.9999
0.01440	0.9998	1.0000

X = 0.8332

Y	u/u_1	ρ/ρ_1
0.00033	0.5041	0.9463
0.00047	0.5130	0.9469
0.00047	0.5163	0.9471
0.00057	0.5204	0.9474
0.00063	0.5250	0.9477
0.00083	0.5446	0.9492
0.00117	0.5638	0.9506
0.00153	0.5843	0.9522
0.00200	0.6008	0.9536
0.00237	0.6209	0.9553
0.00283	0.6384	0.9568
0.00330	0.6553	0.9584
0.00387	0.6737	0.9601
0.00433	0.6911	0.9618
0.00480	0.7096	0.9636
0.00527	0.7262	0.9653
0.00580	0.7440	0.9671
0.00613	0.7633	0.9692
0.00660	0.7817	0.9712
0.00710	0.7990	0.9732
0.00770	0.8213	0.9758
0.00820	0.8411	0.9782
0.00860	0.8603	0.9806
0.00923	0.8774	0.9828
0.00993	0.8992	0.9856
0.01050	0.9193	0.9883
0.01107	0.9361	0.9907
0.01157	0.9524	0.9930
0.01207	0.9676	0.9952
0.01323	0.9838	0.9976
0.01423	0.9923	0.9988
0.01510	0.9966	0.9995
0.01623	0.9989	0.9998
0.01737	0.9996	0.9999

TABLE 5 (Concluded)

X = 0.8998

Y	u/u_1	ρ/ρ_1
0.00033	0.5081	0.9499
0.00040	0.5131	0.9503
0.00047	0.5209	0.9508
0.00047	0.5329	0.9516
0.00063	0.5390	0.9520
0.00093	0.5590	0.9534
0.00127	0.5799	0.9550
0.00163	0.6025	0.9567
0.00233	0.6240	0.9584
0.00297	0.6469	0.9603
0.00370	0.6666	0.9620
0.00423	0.6857	0.9637
0.00493	0.7061	0.9656
0.00557	0.7228	0.9672
0.00607	0.7400	0.9689
0.00670	0.7597	0.9708
0.00723	0.7785	0.9728
0.00797	0.8039	0.9755
0.00860	0.8216	0.9774
0.00900	0.8376	0.9792
0.00977	0.8550	0.9813
0.01043	0.8781	0.9840
0.01110	0.8966	0.9863
0.01183	0.9144	0.9885
0.01233	0.9311	0.9906
0.01333	0.9524	0.9934
0.01413	0.9674	0.9955
0.01510	0.9833	0.9977
0.01603	0.9918	0.9988
0.01687	0.9956	0.9994
0.01813	0.9995	0.9999
0.01853	1.0001	1.0000

X = 0.9499

Y	u/u_1	ρ/ρ_1
0.00033	0.5460	0.9527
0.00047	0.5600	0.9537
0.00063	0.5754	0.9548
0.00080	0.5932	0.9561
0.00087	0.5957	0.9563
0.00123	0.6152	0.9578
0.00170	0.6324	0.9592
0.00217	0.6494	0.9607
0.00290	0.6666	0.9621
0.00343	0.6847	0.9637
0.00397	0.7021	0.9653
0.00500	0.7239	0.9674
0.00560	0.7433	0.9693
0.00633	0.7626	0.9712
0.00690	0.7807	0.9731
0.00783	0.8025	0.9754
0.00857	0.8219	0.9775
0.00920	0.8422	0.9798
0.00977	0.8587	0.9817
0.01050	0.8771	0.9839
0.01140	0.8987	0.9866
0.01220	0.9166	0.9888
0.01290	0.9339	0.9910
0.01397	0.9543	0.9937
0.01507	0.9725	0.9962
0.01587	0.9827	0.9976
0.01697	0.9910	0.9987
0.01787	0.9951	0.9993
0.01877	0.9975	0.9996
0.01963	0.9987	0.9998
0.02047	0.9993	0.9999
0.02130	0.9993	0.9999
0.02173	0.9999	1.0000

X = 0.9833

Y	u/u_1	ρ/ρ_1
0.00040	0.5841	0.9537
0.00050	0.5931	0.9544
0.00067	0.6121	0.9559
0.00090	0.6304	0.9575
0.00100	0.6407	0.9584
0.00147	0.6584	0.9599
0.00207	0.6775	0.9617
0.00263	0.6969	0.9635
0.00337	0.7144	0.9652
0.00407	0.7326	0.9670
0.00487	0.7504	0.9688
0.00563	0.7675	0.9706
0.00640	0.7854	0.9725
0.00707	0.8030	0.9745
0.00790	0.8188	0.9763
0.00840	0.8349	0.9782
0.00923	0.8524	0.9802
0.01000	0.8734	0.9828
0.01087	0.8904	0.9850
0.01143	0.9074	0.9872
0.01223	0.9178	0.9885
0.01280	0.9368	0.9911
0.01370	0.9483	0.9926
0.01453	0.9648	0.9949
0.01533	0.9740	0.9962
0.01620	0.9834	0.9976
0.01710	0.9910	0.9987
0.01790	0.9955	0.9993
0.01887	0.9984	0.9998
0.01967	0.9998	1.0000

X = 0.9970

Y	u/u_1	ρ/ρ_1
0.00033	0.6226	0.9560
0.00047	0.6340	0.9570
0.00063	0.6431	0.9578
0.00087	0.6495	0.9584
0.00093	0.6607	0.9594
0.00123	0.6781	0.9610
0.00187	0.6988	0.9630
0.00263	0.7190	0.9650
0.00343	0.7325	0.9663
0.00430	0.7513	0.9683
0.00483	0.7697	0.9703
0.00570	0.7787	0.9713
0.00623	0.7957	0.9732
0.00697	0.8145	0.9753
0.00773	0.8312	0.9773
0.00857	0.8448	0.9789
0.00940	0.8635	0.9812
0.01007	0.8808	0.9834
0.01080	0.8975	0.9856
0.01167	0.9118	0.9875
0.01250	0.9303	0.9900
0.01330	0.9469	0.9923
0.01423	0.9601	0.9942
0.01520	0.9733	0.9961
0.01620	0.9834	0.9975
0.01710	0.9902	0.9985
0.01793	0.9933	0.9990
0.01877	0.9963	0.9995
0.01960	0.9981	0.9997
0.02043	0.9986	0.9998
0.02137	0.9994	0.9999
0.02153	1.0000	1.0000

TABLE 6

Wake Profile Data; Section 2814, $C_L = 0{\cdot}42$

X = 1.0200			X = 1.0500			X = 1.0880			X = 1.1080			X = 1.1280		
Y	u/u_1	ρ/ρ_1	Y	u/u_1	ρ/ρ_1	Y	u/u_1	ρ/ρ_1	Y	u/u_1	ρ/ρ_1	Y	u/u_1	ρ/ρ_1
0.03820	0.9989	0.9998	0.03893	0.9968	0.9995	0.04087	0.9934	0.9989	0.04393	0.9989	0.9998	0.04390	0.9986	0.9997
0.03617	0.9954	0.9993	0.03650	0.9853	0.9977	0.03787	0.9824	0.9971	0.04150	0.9963	0.9994	0.04160	0.9954	0.9992
0.03413	0.9824	0.9973	0.03487	0.9689	0.9951	0.03610	0.9653	0.9944	0.03920	0.9896	0.9982	0.03937	0.9860	0.9976
0.03243	0.9626	0.9944	0.03333	0.9470	0.9918	0.03517	0.9442	0.9911	0.03660	0.9746	0.9956	0.03720	0.9705	0.9949
0.03127	0.9435	0.9916	0.03177	0.9190	0.9878	0.03290	0.9216	0.9876	0.03500	0.9537	0.9921	0.03537	0.9511	0.9917
0.03003	0.9266	0.9892	0.03060	0.8993	0.9850	0.03210	0.9019	0.9847	0.03323	0.9313	0.9885	0.03400	0.9318	0.9885
0.02917	0.9104	0.9870	0.02917	0.8789	0.9822	0.03027	0.8730	0.9806	0.03160	0.9087	0.9849	0.03217	0.9116	0.9854
0.02827	0.8893	0.9841	0.02783	0.8531	0.9788	0.02860	0.8439	0.9766	0.02977	0.8812	0.9807	0.03047	0.8830	0.9810
0.02693	0.8692	0.9815	0.02667	0.8306	0.9759	0.02767	0.8264	0.9743	0.02890	0.8644	0.9783	0.02937	0.8645	0.9783
0.02677	0.8528	0.9794	0.02567	0.8123	0.9736	0.02700	0.8068	0.9718	0.02780	0.8456	0.9756	0.02850	0.8476	0.9758
0.02540	0.8358	0.9773	0.02480	0.7946	0.9715	0.02523	0.7705	0.9673	0.02693	0.8282	0.9731	0.02720	0.8220	0.9723
0.02407	0.8071	0.9738	0.02337	0.7576	0.9672	0.02447	0.7537	0.9654	0.02607	0.8104	0.9707	0.02603	0.8009	0.9694
0.02330	0.7887	0.9717	0.02253	0.7309	0.9642	0.02360	0.7254	0.9621	0.02523	0.7910	0.9681	0.02447	0.7736	0.9659
0.02227	0.7716	0.9697	0.02160	0.6993	0.9609	0.02200	0.6913	0.9584	0.02420	0.7694	0.9654	0.02287	0.7417	0.9619
0.02097	0.7465	0.9670	0.02100	0.6796	0.9589	0.02090	0.6741	0.9566	0.02290	0.7454	0.9624	0.02163	0.7255	0.9600
0.01987	0.7184	0.9640	0.02053	0.6634	0.9573	0.02027	0.6580	0.9550	0.02187	0.7269	0.9602	0.01990	0.7055	0.9577
0.01893	0.6763	0.9598	0.01970	0.6263	0.9538	0.01773	0.6460	0.9538	0.02083	0.7042	0.9575	0.01757	0.6985	0.9569
0.01807	0.6305	0.9556	0.01890	0.6016	0.9516	0.01520	0.6660	0.9558	0.01953	0.6871	0.9556	0.01510	0.7119	0.9584
0.01757	0.6019	0.9531	0.01817	0.5751	0.9494	0.01387	0.6828	0.9575	0.01720	0.6786	0.9547	0.01373	0.7349	0.9611
0.01730	0.5563	0.9494	0.01660	0.5542	0.9477	0.01327	0.7008	0.9594	0.01487	0.6833	0.9552	0.01233	0.7561	0.9637
0.01720	0.5321	0.9476	0.01410	0.5672	0.9487	0.01153	0.7437	0.9642	0.01420	0.7008	0.9572	0.01077	0.7783	0.9665
0.01660	0.5004	0.9453	0.01370	0.5845	0.9501	0.00963	0.7833	0.9689	0.01297	0.7202	0.9594	0.00987	0.7972	0.9689
0.01643	0.4809	0.9440	0.01290	0.6034	0.9518	0.00813	0.8271	0.9744	0.01163	0.7412	0.9619	0.00910	0.8190	0.9719
0.01600	0.4482	0.9419	0.01130	0.6423	0.9553	0.00707	0.8439	0.9766	0.01057	0.7599	0.9642	0.00803	0.8381	0.9745
0.01550	0.4271	0.9407	0.00957	0.6916	0.9601	0.00630	0.8708	0.9803	0.00883	0.7941	0.9685	0.00707	0.8584	0.9774
0.01327	0.4378	0.9413	0.00863	0.7180	0.9628	0.00543	0.8885	0.9828	0.00797	0.8124	0.9710	0.00597	0.8862	0.9815
0.01277	0.4551	0.9424	0.00843	0.7349	0.9646	0.00437	0.9148	0.9866	0.00723	0.8359	0.9742	0.00510	0.9043	0.9842
0.01200	0.4713	0.9434	0.00780	0.7524	0.9666	0.00263	0.9544	0.9926	0.00627	0.8598	0.9776	0.00377	0.9229	0.9871
0.01127	0.4907	0.9447	0.00707	0.7712	0.9687	0.00103	0.9740	0.9957	0.00510	0.8818	0.9808	0.00190	0.9540	0.9921
0.01060	0.5145	0.9463	0.00597	0.8105	0.9734	-0.00117	0.9906	0.9985	0.00430	0.9013	0.9838	0.00030	0.9759	0.9958
0.00980	0.5348	0.9478	0.00430	0.8528	0.9787	-0.00350	0.9972	0.9995	0.00333	0.9189	0.9865	-0.00187	0.9928	0.9987
0.00933	0.5592	0.9497	0.00333	0.8815	0.9825	-0.00513	0.9990	0.9998	0.00257	0.9354	0.9891	-0.00407	0.9974	0.9995
0.00833	0.5946	0.9525	0.00247	0.9086	0.9863				0.00113	0.9514	0.9917			
0.00753	0.6236	0.9550	0.00080	0.9458	0.9917				0.00023	0.9709	0.9950			
0.00683	0.6419	0.9566	0.04070	0.9990	0.9998				-0.00160	0.9869	0.9977			
0.00623	0.6680	0.9590	-0.00083	0.9772	0.9964				-0.00413	0.9963	0.9994			
0.00570	0.6906	0.9612	-0.00277	0.9934	0.9989				-0.00677	0.9984	0.9997			
0.00517	0.7107	0.9632	-0.00513	0.9991	0.9999									
0.00430	0.7336	0.9656												
0.00397	0.7499	0.9674												
0.00350	0.7663	0.9691												
0.00283	0.7887	0.9717												
0.00230	0.8086	0.9740												
0.00167	0.8311	0.9767												
0.00087	0.8556	0.9798												
-0.00050	0.9021	0.9858												
-0.00153	0.9238	0.9888												
-0.00230	0.9462	0.9920												
-0.00340	0.9651	0.9947												
-0.00473	0.9835	0.9975												
-0.00737	0.9989	0.9998												
-0.00793	0.9989	0.9998												

TABLE 6 (Cont'd.)

X = 1.1540			X = 1.1880			X = 1.2210			X = 1.3880			X = 1.5540		
Y	u/u_1	ρ/ρ_1	Y	u/u_1	ρ/ρ_1	Y	u/u_1	ρ/ρ_1	Y	u/u_1	ρ/ρ_1	Y	u/u_1	ρ/ρ_1
0.04477	0.9985	0.9997	0.04750	0.9990	0.9998	0.05010	0.9997	0.9999	0.05973	1.0001	1.0000	0.06870	0.9999	1.0000
0.04207	0.9934	0.9988	0.04527	0.9960	0.9993	0.04773	0.9982	0.9997	0.05660	0.9987	0.9998	0.06590	0.9990	0.9998
0.03987	0.9820	0.9968	0.04307	0.9888	0.9980	0.04557	0.9936	0.9988	0.05447	0.9959	0.9992	0.06350	0.9976	0.9995
0.03787	0.9659	0.9940	0.04080	0.9760	0.9957	0.04330	0.9845	0.9972	0.05193	0.9906	0.9982	0.06053	0.9943	0.9989
0.03613	0.9463	0.9907	0.03870	0.9585	0.9927	0.04123	0.9712	0.9948	0.04977	0.9822	0.9967	0.05807	0.9891	0.9979
0.03437	0.9251	0.9873	0.03637	0.9336	0.9885	0.03900	0.9498	0.9911	0.04730	0.9719	0.9948	0.05600	0.9833	0.9968
0.03300	0.9064	0.9843	0.03487	0.9117	0.9849	0.03750	0.9316	0.9880	0.04503	0.9521	0.9912	0.05387	0.9761	0.9955
0.03157	0.8822	0.9805	0.03327	0.8908	0.9816	0.03583	0.9100	0.9845	~~0.04443~~	~~0.9912~~	~~0.9984~~	0.05177	0.9658	0.9935
0.03020	0.8613	0.9774	0.03200	0.8709	0.9785	0.03440	0.8934	0.9818	0.04413	0.9453	0.9900	0.04977	0.9546	0.9915
0.02900	0.8378	0.9740	0.03057	0.8501	0.9754	0.03313	0.8749	0.9789	0.04163	0.9277	0.9869	0.04717	0.9407	0.9890
0.02767	0.8199	0.9715	0.02903	0.8282	0.9723	0.03160	0.8482	0.9749	0.03993	0.9083	0.9836	0.04493	0.9260	0.9864
0.02620	0.7955	0.9681	0.02773	0.8086	0.9695	0.02990	0.8301	0.9723	0.03750	0.8922	0.9810	0.04287	0.9118	0.9840
0.02460	0.7666	0.9644	0.02643	0.7890	0.9669	0.02803	0.8057	0.9688	0.03577	0.8717	0.9777	0.04067	0.8989	0.9818
0.02280	0.7452	0.9617	0.02453	0.7655	0.9638	0.02547	0.7834	0.9658	0.03307	0.8532	0.9748	0.03837	0.8876	0.9799
0.02113	0.7278	0.9596	0.02180	0.7490	0.9617	0.02293	0.7676	0.9637	0.03087	0.8426	0.9732	0.03627	0.8759	0.9780
0.01850	0.7209	0.9587	0.01967	0.7468	0.9614	0.02083	0.7662	0.9635	0.02823	0.8310	0.9714	0.03400	0.8671	0.9766
0.01643	0.7351	0.9605	0.01757	0.7555	0.9625	0.01857	0.7728	0.9644	0.02530	0.8271	0.9708	0.03160	0.8609	0.9756
0.01477	0.7530	0.9627	0.01503	0.7778	0.9654	0.01650	0.7936	0.9672	0.02283	0.8310	0.9714	0.02950	0.8592	0.9754
0.01240	0.7787	0.9659	0.01373	0.7978	0.9681	0.01483	0.8115	0.9696	0.02050	0.8400	0.9728	0.02710	0.8604	0.9755
0.01073	0.8135	0.9706	0.01233	0.8177	0.9708	0.01247	0.8363	0.9732	0.01770	0.8583	0.9756	0.02473	0.8648	0.9762
0.00980	0.8303	0.9729	0.01130	0.8357	0.9733	0.01080	0.8622	0.9770	0.01537	0.8741	0.9780	0.02263	0.8695	0.9770
0.00877	0.8499	0.9757	0.00963	0.8561	0.9763	0.00960	0.8799	0.9797	0.01323	0.8935	0.9812	0.02030	0.8794	0.9786
0.00763	0.8696	0.9786	0.00797	0.8821	0.9803	0.00817	0.9016	0.9831	0.01090	0.9140	0.9846	0.01770	0.8905	0.9804
0.00683	0.8867	0.9812	0.00707	0.8999	0.9830	0.00633	0.9185	0.9859	0.00830	0.9308	0.9874	0.01517	0.9080	0.9833
0.00533	0.9050	0.9841	0.00597	0.9170	0.9858	0.00460	0.9422	0.9898	0.00627	0.9473	0.9903	0.01247	0.9222	0.9858
0.00363	0.9395	0.9896	0.00460	0.9375	0.9891	0.00350	0.9584	0.9926	0.00373	0.9654	0.9936	0.00993	0.9366	0.9883
0.00247	0.9562	0.9924	0.00280	0.9568	0.9924	0.00107	0.9784	0.9961	0.00150	0.9779	0.9959	0.00777	0.9506	0.9908
0.00073	0.9767	0.9959	0.00090	0.9743	0.9954	-0.00160	0.9901	0.9982	-0.00063	0.9866	0.9975	0.00547	0.9602	0.9925
-0.00157	0.9897	0.9982	-0.00160	0.9914	0.9984	-0.00410	0.9966	0.9994	-0.00323	0.9924	0.9986	0.00340	0.9706	0.9944
-0.00423	0.9974	0.9995	-0.00360	0.9974	0.9995	-0.00607	0.9991	0.9998	-0.00553	0.9957	0.9992	0.00107	0.9799	0.9962
-0.00500	0.9984	0.9997	-0.00590	0.9990	0.9998				-0.00757	0.9981	0.9996	-0.00237	0.9857	0.9973
			-0.00677	1.0000	1.0000				-0.01017	0.9981	0.9996	-0.00520	0.9928	0.9986
									-0.01110	0.9996	0.9999	-0.00757	0.9976	0.9995
												-0.01017	0.9985	0.9997
												-0.01103	0.9996	0.9999

TABLE 6 (Concluded)

X = 1.8880

Y	u/u_1	ρ/ρ_1
0.08120	0.9996	0.9999
0.07917	0.9990	0.9998
0.07663	0.9981	0.9996
0.07393	0.9962	0.9993
0.07130	0.9940	0.9988
0.06870	0.9896	0.9980
0.06657	0.9854	0.9972
0.06400	0.9796	0.9961
0.06157	0.9737	0.9950
0.05943	0.9668	0.9937
0.05693	0.9585	0.9922
0.05473	0.9488	0.9904
0.05177	0.9394	0.9888
0.04917	0.9294	0.9870
0.04710	0.9220	0.9857
0.04443	0.9128	0.9841
0.04200	0.9044	0.9827
0.03893	0.8989	0.9818
0.03617	0.8950	0.9811
0.03390	0.8932	0.9808
0.03187	0.8926	0.9807
0.02933	0.8955	0.9812
0.02703	0.8977	0.9816
0.02500	0.9018	0.9822
0.02273	0.9072	0.9832
0.02020	0.9139	0.9843
0.01797	0.9209	0.9855
0.01463	0.9331	0.9876
0.01140	0.9426	0.9893
0.00853	0.9538	0.9913
0.00627	0.9599	0.9925
0.00403	0.9698	0.9943
0.00167	0.9753	0.9953
-0.00063	0.9796	0.9961
-0.00297	0.9858	0.9973
-0.00530	0.9896	0.9980
-0.00773	0.9920	0.9985
-0.00983	0.9949	0.9990
-0.01227	0.9966	0.9994
-0.01460	0.9981	0.9996
-0.01687	0.9990	0.9998
-0.01900	0.9995	0.9999
-0.02060	1.0000	1.0000

TABLE 7

Boundary Layer Profile Data; Section 2815, C_L = 0·51, Upper Surface

X = 0.2716

Y	u/u_1	ρ/ρ_1
0.00033	0.6565	0.9128
0.00057	0.6850	0.9182
0.00063	0.7006	0.9213
0.00077	0.7185	0.9249
0.00093	0.7374	0.9289
0.00110	0.7554	0.9328
0.00117	0.7760	0.9379
0.00147	0.8111	0.9457
0.00163	0.8322	0.9509
0.00193	0.8670	0.9600
0.00217	0.8869	0.9654
0.00240	0.9138	0.9731
0.00277	0.9431	0.9818
0.00300	0.9592	0.9868
0.00333	0.9793	0.9932
0.00387	0.9955	0.9985
0.00467	1.0000	1.0000

X = 0.3516

Y	u/u_1	ρ/ρ_1
0.00033	0.6323	0.9103
0.00040	0.6346	0.9107
0.00047	0.6453	0.9126
0.00057	0.6536	0.9140
0.00063	0.6640	0.9159
0.00093	0.7065	0.9240
0.00117	0.7360	0.9300
0.00130	0.7618	0.9355
0.00160	0.7869	0.9412
0.00190	0.8131	0.9473
0.00215	0.8374	0.9532
0.00243	0.8664	0.9607
~~0.00275~~	~~0.9998~~	~~0.9999~~
0.00280	0.8940	0.9681
0.00310	0.9248	0.9768
0.00333	0.9431	0.9822
0.00377	0.9684	0.9899
0.00417	0.9864	0.9956
0.00507	0.9982	0.9994
0.00553	0.9998	0.9999

X = 0.4496

Y	u/u_1	ρ/ρ_1
0.00033	0.5768	0.9073
0.00047	0.5870	0.9088
0.00053	0.5855	0.9086
0.00067	0.6009	0.9109
0.00073	0.6037	0.9113
0.00087	0.6286	0.9152
0.00103	0.6461	0.9181
0.00123	0.6627	0.9209
0.00137	0.6822	0.9243
0.00157	0.6987	0.9273
0.00180	0.7149	0.9303
0.00193	0.7322	0.9337
0.00220	0.7547	0.9382
0.00250	0.7776	0.9429
0.00270	0.7978	0.9473
0.00307	0.8146	0.9510
0.00320	0.8318	0.9549
0.00337	0.8542	0.9603
0.00370	0.8792	0.9664
0.00407	0.8966	0.9709
0.00427	0.9141	0.9754
0.00463	0.9359	0.9814
0.00507	0.9549	0.9867
0.00563	0.9759	0.9927
0.00633	0.9941	0.9982
0.00713	0.9985	0.9996
0.00747	0.9996	0.9999

X = 0.5854

Y	u/u_1	ρ/ρ_1
0.00033	0.5520	0.9160
0.00040	0.5578	0.9167
0.00053	0.5669	0.9179
0.00053	0.5747	0.9189
0.00060	0.5813	0.9197
0.00090	0.6140	0.9241
0.00117	0.6363	0.9272
0.00143	0.6550	0.9300
0.00170	0.6743	0.9329
0.00197	0.6914	0.9356
0.00223	0.7136	0.9392
0.00263	0.7397	0.9436
0.00293	0.7598	0.9472
0.00327	0.7794	0.9508
0.00360	0.7958	0.9539
0.00387	0.8140	0.9574
0.00413	0.8302	0.9606
0.00453	0.8515	0.9650
0.00483	0.8704	0.9690
0.00523	0.8914	0.9736
0.00567	0.9112	0.9781
0.00620	0.9353	0.9838
0.00663	0.9523	0.9879
0.00720	0.9706	0.9924
0.00790	0.9891	0.9971
0.00870	0.9968	0.9991
0.00957	0.9993	0.9998
0.01000	0.9999	1.0000

X = 0.6608

Y	u/u_1	ρ/ρ_1
0.00033	0.5396	0.9219
0.00047	0.5519	0.9233
0.00047	0.5593	0.9241
0.00063	0.5737	0.9258
0.00077	0.5807	0.9266
0.00093	0.6011	0.9291
0.00117	0.6190	0.9313
0.00153	0.6416	0.9343
0.00187	0.6623	0.9371
0.00223	0.6827	0.9400
0.00253	0.6993	0.9424
0.00277	0.7157	0.9449
0.00317	0.7386	0.9485
0.00363	0.7625	0.9524
0.00407	0.7837	0.9559
0.00443	0.8042	0.9595
0.00490	0.8284	0.9639
0.00530	0.8453	0.9670
0.00570	0.8663	0.9710
0.00610	0.8863	0.9750
0.00657	0.9060	0.9790
0.00707	0.9251	0.9831
0.00753	0.9444	0.9872
0.00817	0.9631	0.9914
0.00887	0.9807	0.9954
0.00987	0.9938	0.9985
0.01067	0.9983	0.9996
0.01140	0.9994	0.9998

TABLE 7 (Cont'd)

X = 0.7218

Y	u/u_1	ρ/ρ_1
0.00053	0.5015	0.9239
0.00060	0.5066	0.9243
0.00067	0.5117	0.9248
0.00073	0.5252	0.9261
0.00083	0.5352	0.9271
0.00103	0.5542	0.9291
0.00130	0.5752	0.9314
0.00163	0.5949	0.9336
0.00203	0.6184	0.9363
0.00243	0.6374	0.9386
0.00283	0.6602	0.9415
0.00313	0.6786	0.9439
0.00340	0.6969	0.9464
0.00383	0.7151	0.9489
0.00423	0.7316	0.9513
0.00463	0.7493	0.9539
0.00500	0.7682	0.9568
~~0.00543~~	~~0.8629~~	~~0.9418~~
0.00543	0.7901	0.9603
0.00580	0.8076	0.9631
0.00617	0.8248	0.9660
0.00667	0.8430	0.9691
0.00703	0.8592	0.9720
0.00737	0.8783	0.9754
0.00793	0.8947	0.9785
0.00847	0.9187	0.9831
0.00893	0.9364	0.9866
0.00953	0.9544	0.9903
0.01020	0.9706	0.9937
0.01100	0.9871	0.9972
0.01187	0.9946	0.9988
0.01273	0.9984	0.9997
0.01340	1.0000	1.0000

X = 0.7758

Y	u/u_1	ρ/ρ_1
0.00033	0.5046	0.9303
0.00053	0.5150	0.9312
0.00067	0.5222	0.9319
0.00067	0.5226	0.9319
0.00080	0.5289	0.9325
0.00100	0.5469	0.9342
0.00150	0.5689	0.9363
0.00183	0.5925	0.9388
0.00227	0.6088	0.9405
0.00260	0.6281	0.9426
0.00290	0.6446	0.9445
0.00353	0.6680	0.9473
0.00390	0.6874	0.9496
0.00427	0.7063	0.9520
0.00467	0.7246	0.9544
0.00503	0.7410	0.9566
0.00547	0.7603	0.9593
0.00590	0.7769	0.9617
0.00637	0.8001	0.9651
0.00690	0.8226	0.9685
0.00743	0.8448	0.9720
0.00810	0.8696	0.9761
0.00863	0.8888	0.9793
0.00920	0.9076	0.9826
0.00957	0.9241	0.9855
0.01020	0.9428	0.9890
0.01087	0.9609	0.9923
0.01157	0.9775	0.9955
0.01243	0.9885	0.9977
0.01337	0.9955	0.9991
0.01417	0.9993	0.9999
0.01443	0.9997	0.9999

X = 0.8238

Y	u/u_1	ρ/ρ_1
0.00033	0.5162	0.9358
0.00053	0.5261	0.9366
0.00070	0.5353	0.9374
0.00077	0.5391	0.9378
0.00077	0.5414	0.9380
0.00123	0.5598	0.9396
0.00163	0.5778	0.9413
0.00200	0.5972	0.9432
0.00253	0.6189	0.9454
0.00303	0.6425	0.9479
0.00350	0.6611	0.9500
0.00383	0.6777	0.9518
0.00430	0.6968	0.9541
0.00483	0.7182	0.9567
0.00533	0.7373	0.9590
0.00577	0.7564	0.9615
0.00613	0.7730	0.9637
0.00657	0.7911	0.9662
0.00720	0.8123	0.9692
0.00757	0.8285	0.9715
0.00807	0.8501	0.9747
0.00870	0.8702	0.9778
0.00923	0.8876	0.9805
0.00963	0.9053	0.9834
0.01027	0.9218	0.9861
0.01077	0.9400	0.9892
0.01147	0.9570	0.9922
0.01227	0.9720	0.9949
0.01307	0.9858	0.9974
0.01400	0.9923	0.9986
0.01487	0.9969	0.9994
0.01577	0.9981	0.9997
0.01667	0.9986	0.9997
0.01753	0.9992	0.9999
0.01823	0.9991	0.9998

X = 0.8696

Y	u/u_1	ρ/ρ_1
0.00033	0.4730	0.9374
0.00053	0.4828	0.9381
0.00060	0.4887	0.9385
0.00067	0.4959	0.9391
0.00087	0.5046	0.9397
0.00130	0.5213	0.9410
0.00170	0.5393	0.9425
0.00220	0.5624	0.9444
0.00283	0.5851	0.9464
0.00320	0.6033	0.9481
0.00370	0.6198	0.9497
0.00417	0.6400	0.9516
0.00473	0.6634	0.9540
0.00540	0.6864	0.9565
0.00595	0.7059	0.9589
0.00643	0.7270	0.9610
0.00680	0.7450	0.9631
0.00737	0.7637	0.9654
0.00777	0.7812	0.9675
0.00833	0.7977	0.9696
0.00890	0.8174	0.9722
0.00923	0.8355	0.9747
0.00983	0.8529	0.9771
0.01030	0.8712	0.9797
0.01100	0.8909	0.9825
0.01147	0.9076	0.9850
0.01210	0.9294	0.9884
0.01280	0.9456	0.9910
0.01360	0.9629	0.9938
0.01460	0.9782	0.9963
0.01543	0.9892	0.9982
0.01637	0.9956	0.9992
0.01717	0.9972	0.9995
0.01810	0.9987	0.9998
0.01893	0.9994	0.9999
0.01987	0.9997	1.0000

X = 0.9119

Y	u/u_1	ρ/ρ_1
0.00033	0.4186	0.9391
0.00043	0.4221	0.9393
0.00057	0.4316	0.9399
0.00080	0.4474	0.9408
0.00097	0.4580	0.9415
0.00147	0.4803	0.9430
0.00187	0.4981	0.9442
0.00223	0.5144	0.9453
0.00267	0.5309	0.9466
0.00317	0.5523	0.9482
0.00383	0.5723	0.9498
0.00427	0.5889	0.9511
0.00490	0.6141	0.9533
0.00540	0.6314	0.9549
0.00583	0.6512	0.9567
0.00633	0.6673	0.9582
0.00670	0.6835	0.9598
0.00713	0.7018	0.9616
0.00763	0.7188	0.9634
0.00810	0.7370	0.9653
0.00860	0.7549	0.9673
0.00913	0.7731	0.9693
0.00960	0.7914	0.9715
0.01020	0.8105	0.9737
0.01073	0.8296	0.9761
0.01127	0.8472	0.9783
0.01173	0.8676	0.9809
0.01247	0.8867	0.9835
0.01307	0.9084	0.9864
0.01363	0.9260	0.9889
0.01440	0.9447	0.9916
0.01520	0.9603	0.9939
0.01610	0.9756	0.9962
0.01693	0.9865	0.9979
0.01793	0.9941	0.9991
0.01873	0.9976	0.9996
0.01970	0.9992	0.9999
0.01993	0.9997	1.0000

TABLE 7 (Concluded)

X = 0.9518			X = 0.9878			X = 0.9970		
Y	u/u_1	ρ/ρ_1	Y	u/u_1	ρ/ρ_1	Y	u/u_1	ρ/ρ_1
0.00033	0.3323	0.9413	0.00033	0.1958	0.9423	0.00033	0.2505	0.9435
0.00043	0.3387	0.9416	0.00047	0.2017	0.9425	0.00047	0.2562	0.9437
0.00057	0.3510	0.9421	0.00063	0.2143	0.9428	0.00053	0.2629	0.9439
0.00077	0.3600	0.9425	0.00077	0.2224	0.9430	0.00073	0.2651	0.9440
0.00083	0.3615	0.9426	0.00093	0.2314	0.9432	0.00087	0.2651	0.9440
0.00127	0.3856	0.9437	0.00123	0.2496	0.9437	0.00140	0.2831	0.9445
0.00193	0.4121	0.9450	0.00200	0.2772	0.9445	0.00200	0.3000	0.9451
0.00240	0.4307	0.9460	0.00260	0.3012	0.9453	0.00290	0.3266	0.9460
0.00290	0.4474	0.9469	0.00320	0.3216	0.9460	0.00370	0.3470	0.9468
0.00340	0.4656	0.9480	0.00383	0.3390	0.9467	0.00440	0.3631	0.9475
0.00393	0.4831	0.9490	0.00407	0.3580	0.9474	0.00507	0.3867	0.9485
0.00430	0.5008	0.9501	0.00490	0.3804	0.9484	0.00573	0.4039	0.9493
0.00463	0.5169	0.9511	0.00550	0.4022	0.9494	0.00630	0.4243	0.9503
0.00530	0.5381	0.9526	0.00613	0.4221	0.9503	0.00693	0.4406	0.9511
0.00587	0.5607	0.9541	0.00663	0.4398	0.9512	0.00760	0.4647	0.9523
0.00657	0.5860	0.9560	0.00727	0.4609	0.9523	0.00827	0.4829	0.9533
0.00720	0.6101	0.9579	0.00760	0.4788	0.9533	0.00873	0.4992	0.9543
0.00790	0.6288	0.9593	0.00820	0.4953	0.9542	0.00930	0.5171	0.9553
0.00837	0.6472	0.9609	0.00883	0.5198	0.9556	0.00980	0.5333	0.9563
0.00867	0.6636	0.9623	0.00947	0.5385	0.9568	0.01023	0.5495	0.9573
0.00917	0.6836	0.9640	0.00973	0.5560	0.9579	0.01073	0.5670	0.9585
0.00980	0.7043	0.9659	0.01030	0.5766	0.9593	0.01130	0.5885	0.9599
0.01037	0.7223	0.9676	0.01110	0.5991	0.9608	0.01203	0.6104	0.9615
0.01087	0.7397	0.9692	0.01153	0.6163	0.9620	0.01263	0.6289	0.9628
0.01127	0.7578	0.9710	0.01213	0.6342	0.9634	0.01323	0.6487	0.9643
0.01167	0.7753	0.9728	0.01263	0.6506	0.9646	0.01383	0.6675	0.9658
0.01233	0.7920	0.9745	0.01310	0.6682	0.9660	0.01437	0.6860	0.9673
0.01287	0.8099	0.9765	0.01363	0.6890	0.9677	0.01480	0.7024	0.9687
0.01340	0.8262	0.9782	0.01400	0.7105	0.9695	0.01547	0.7230	0.9704
0.01400	0.8492	0.9808	0.01457	0.7315	0.9713	0.01607	0.7418	0.9721
0.01457	0.8667	0.9829	0.01527	0.7484	0.9728	0.01667	0.7633	0.9740
0.01510	0.8845	0.9850	0.01583	0.7691	0.9747	0.01740	0.7841	0.9760
0.01583	0.9022	0.9871	0.01630	0.7906	0.9767	0.01767	0.8010	0.9776
0.01647	0.9236	0.9898	0.01697	0.8078	0.9784	0.01837	0.8211	0.9796
0.01717	0.9407	0.9920	0.01763	0.8288	0.9805	0.01897	0.8399	0.9815
0.01800	0.9547	0.9938	0.01837	0.8543	0.9831	0.01987	0.8571	0.9833
0.01883	0.9686	0.9957	0.01893	0.8753	0.9853	0.02033	0.8778	0.9856
0.01980	0.9815	0.9974	0.01970	0.8926	0.9872	0.02117	0.8950	0.9875
0.02077	0.9905	0.9987	0.02037	0.9107	0.9893	0.02183	0.9112	0.9893
0.02177	0.9946	0.9993	0.02110	0.9270	0.9911	0.02237	0.9325	0.9917
0.02283	0.9969	0.9996	0.02187	0.9437	0.9931	0.02330	0.9446	0.9932
0.02397	0.9989	0.9999	0.02270	0.9590	0.9949	0.02423	0.9619	0.9953
0.02447	0.9996	0.9999	0.02350	0.9692	0.9962	0.02520	0.9742	0.9968
			0.02447	0.9827	0.9978	0.02613	0.9839	0.9980
			0.02540	0.9919	0.9990	0.02720	0.9930	0.9991
			0.02623	0.9939	0.9992	0.02813	0.9962	0.9995
			0.02713	0.9953	0.9994	0.02897	0.9978	0.9997
			0.02823	0.9971	0.9996	0.03000	0.9969	0.9996
			0.02907	0.9987	0.9998	0.03100	0.9975	0.9997
			0.02993	0.9971	0.9996	0.03147	0.9978	0.9997
			0.03040	0.9987	0.9998			

TABLE 8

Boundary Layer Profile Data; Section 2815, $C_L = 0{\cdot}51$, Lower Surface

X = 0.2316			X = 0.3197			X = 0.4797			X = 0.6722			X = 0.7693		
Y	u/u_1	ρ/ρ_1	Y	u/u_1	ρ/ρ_1	Y	u/u_1	ρ/ρ_1	Y	u/u_1	ρ/ρ_1	Y	u/u_1	ρ/ρ_1
0.00040	0.7862	0.9645	0.00047	0.7313	0.9517	0.00047	0.6498	0.9376	0.00040	0.5453	0.9438	0.00047	0.5251	0.9493
0.00050	0.7998	0.9665	0.00070	0.7608	0.9560	0.00060	0.6658	0.9397	0.00057	0.5642	0.9454	0.00063	0.5411	0.9505
0.00057	0.8202	0.9694	0.00087	0.7866	0.9600	0.00073	0.6849	0.9424	0.00070	0.5797	0.9467	0.00077	0.5527	0.9513
0.00067	0.8350	0.9717	0.00093	0.7951	0.9614	0.00087	0.7039	0.9451	0.00090	0.5944	0.9480	0.00097	0.5674	0.9524
0.00073	0.8597	0.9741	0.00110	0.8234	0.9660	0.00100	0.7167	0.9469	0.00107	0.6124	0.9497	0.00113	0.5845	0.9537
0.00090	0.8767	0.9782	0.00127	0.8499	0.9706	0.00113	0.7372	0.9500	0.00140	0.6355	0.9519	0.00147	0.6078	0.9556
0.00107	0.9014	0.9823	0.00157	0.8879	0.9774	0.00140	0.7662	0.9546	0.00167	0.6562	0.9540	0.00190	0.6288	0.9573
0.00113	0.9179	0.9851	0.00187	0.9186	0.9832	0.00167	0.7998	0.9601	0.00197	0.6758	0.9560	0.00220	0.6462	0.9588
0.00140	0.9432	0.9895	0.00220	0.9443	0.9883	0.00180	0.8164	0.9630	0.00223	0.6956	0.9581	0.00260	0.6682	0.9608
0.00153	0.9601	0.9925	0.00250	0.9676	0.9931	0.00207	0.8367	0.9666	0.00253	0.7220	0.9610	0.00297	0.6896	0.9628
0.00180	0.9768	0.9956	0.00297	0.9882	0.9974	0.00240	0.8636	0.9715	0.00293	0.7411	0.9632	0.00330	0.7093	0.9647
0.00220	0.9931	0.9987	0.00387	0.9993	0.9999	0.00273	0.8895	0.9765	0.00313	0.7573	0.9651	0.00370	0.7282	0.9665
0.00287	0.9994	0.9999				0.00300	0.9098	0.9805	0.00347	0.7756	0.9673	0.00337	0.7086	0.9646
						0.00323	0.9333	0.9854	0.00370	0.7934	0.9696	0.00383	0.7328	0.9670
						0.00350	0.9504	0.9890	0.00397	0.8095	0.9716	0.00427	0.7572	0.9695
						0.00393	0.9680	0.9928	0.00423	0.8266	0.9739	0.00480	0.7808	0.9720
						0.00433	0.9848	0.9965	0.00457	0.8462	0.9765	0.00520	0.7997	0.9741
						0.00517	0.9980	0.9995	0.00483	0.8637	0.9789	0.00547	0.8177	0.9762
						0.00570	0.9999	1.0000	0.00517	0.8850	0.9820	0.00597	0.8392	0.9787
									0.00557	0.9015	0.9844	0.00633	0.8578	0.9809
									0.00580	0.9179	0.9868	0.00680	0.8774	0.9833
									0.00620	0.9340	0.9893	0.00730	0.8973	0.9858
									0.00660	0.9532	0.9923	0.00770	0.9141	0.9880
									0.00707	0.9705	0.9951	0.00810	0.9305	0.9902
									0.00767	0.9868	0.9978	0.00850	0.9474	0.9925
									0.00850	0.9967	0.9994	0.00913	0.9646	0.9949
									0.00933	0.9991	0.9998	0.00983	0.9812	0.9973
												0.01067	0.9939	0.9991
												0.01167	0.9995	0.9999
												0.01217	0.9995	0.9999

TABLE 8 (Concluded)

X = 0.8617			X = 0.9380			X = 0.9862			X = 0.9970		
Y	u/u_1	ρ/ρ_1	Y	u/u_1	ρ/ρ_1	Y	u/u_1	ρ/ρ_1	Y	u/u_1	ρ/ρ_1
0.00033	0.5598	0.9553	0.00043	0.5674	0.9575	0.00033	0.5738	0.9595	0.00033	0.5690	0.9588
0.00050	0.5738	0.9562	0.00053	0.5767	0.9582	0.00047	0.5790	0.9598	0.00053	0.5780	0.9594
0.00057	0.5848	0.9570	0.00063	0.5835	0.9586	0.00063	0.5938	0.9608	0.00057	0.5877	0.9600
0.00070	0.5896	0.9574	0.00080	0.5952	0.9595	0.00070	0.6024	0.9614	0.00070	0.5959	0.9606
0.00083	0.6016	0.9583	0.00083	0.5991	0.9597	0.00083	0.6118	0.9621	0.00083	0.6088	0.9615
0.00127	0.6206	0.9597	0.00107	0.6155	0.9609	0.00120	0.6334	0.9637	0.00110	0.6342	0.9634
0.00157	0.6366	0.9610	0.00137	0.6322	0.9622	0.00160	0.6517	0.9651	0.00160	0.6551	0.9650
0.00203	0.6566	0.9626	0.00170	0.6488	0.9635	0.00210	0.6678	0.9663	0.00213	0.6760	0.9666
0.00260	0.6796	0.9646	0.00223	0.6672	0.9650	0.00267	0.6861	0.9678	0.00293	0.6976	0.9684
0.00303	0.6991	0.9663	0.00263	0.6842	0.9664	0.00320	0.7028	0.9691	0.00357	0.7159	0.9699
0.00357	0.7163	0.9679	0.00327	0.7003	0.9677	0.00377	0.7193	0.9705	0.00423	0.7340	0.9715
0.00400	0.7376	0.9698	0.00377	0.7170	0.9692	0.00453	0.7398	0.9723	0.00497	0.7532	0.9732
0.00460	0.7552	0.9715	0.00437	0.7370	0.9710	0.00527	0.7590	0.9740	0.00567	0.7701	0.9748
0.00507	0.7733	0.9733	0.00493	0.7537	0.9725	0.00583	0.7769	0.9757	0.00610	0.7862	0.9763
0.00540	0.7895	0.9750	0.00557	0.7724	0.9743	0.00640	0.7930	0.9772	0.00690	0.8059	0.9782
0.00587	0.8062	0.9767	0.00610	0.7899	0.9760	0.00703	0.8111	0.9789	0.00760	0.8220	0.9798
0.00647	0.8247	0.9786	0.00670	0.8078	0.9778	0.00773	0.8290	0.9807	0.00823	0.8406	0.9817
0.00697	0.8423	0.9806	0.00730	0.8241	0.9794	0.00833	0.8458	0.9824	0.00893	0.8575	0.9834
0.00733	0.8587	0.9824	0.00787	0.8418	0.9813	0.00903	0.8642	0.9843	0.00963	0.8758	0.9854
0.00783	0.8769	0.9845	0.00850	0.8588	0.9831	0.00963	0.8806	0.9861	0.01027	0.8918	0.9871
0.00837	0.8953	0.9866	0.00900	0.8748	0.9849	0.01030	0.8971	0.9879	0.01103	0.9091	0.9891
0.00893	0.9125	0.9887	0.00960	0.8917	0.9868	0.01097	0.9137	0.9897	0.01173	0.9288	0.9913
0.00947	0.9291	0.9908	0.01023	0.9088	0.9887	0.01167	0.9302	0.9916	0.01260	0.9449	0.9932
0.01010	0.9474	0.9931	0.01087	0.9258	0.9907	0.01257	0.9479	0.9937	0.01347	0.9609	0.9951
0.01070	0.9649	0.9953	0.01157	0.9430	0.9928	0.01337	0.9652	0.9957	0.01447	0.9762	0.9970
0.01160	0.9796	0.9973	0.01240	0.9600	0.9949	0.01427	0.9777	0.9972	0.01540	0.9857	0.9982
0.01247	0.9903	0.9987	0.01337	0.9768	0.9970	0.01527	0.9880	0.9985	0.01630	0.9925	0.9991
0.01333	0.9952	0.9993	0.01420	0.9873	0.9984	0.01613	0.9947	0.9993	0.01720	0.9966	0.9996
0.01417	0.9984	0.9998	0.01520	1.0010	1.0001	0.01703	0.9974	0.9997	0.01810	0.9987	0.9998
0.01520	0.9996	0.9999	0.01580	0.9964	0.9995	0.01777	0.9992	0.9999	0.01903	0.9993	0.9999
0.01660	1.0003	1.0000							0.01920	0.9993	0.9999

TABLE 9

Wake Profile Data; Section 2815, $C_L = 0{\cdot}51$

X = 1.0420

Y	u/u_1	ρ/ρ_1
0.00207	1.0000	1.0000
0.00533	0.9936	0.9991
0.00793	0.9685	0.9959
0.00973	0.9367	0.9919
0.01053	0.9180	0.9896
0.01157	0.9005	0.9875
0.01237	0.8814	0.9853
0.01330	0.8648	0.9834
0.01380	0.8473	0.9815
0.01483	0.8295	0.9795
0.01563	0.8094	0.9774
0.01660	0.7838	0.9748
0.01747	0.7655	0.9730
0.01833	0.7364	0.9703
0.01910	0.7109	0.9679
0.01997	0.6842	0.9656
0.02083	0.6448	0.9623
0.02193	0.5996	0.9589
0.02280	0.5691	0.9567
0.02357	0.5432	0.9549
0.02423	0.5250	0.9537
0.02683	0.5214	0.9535
0.02797	0.5379	0.9546
0.02970	0.5718	0.9569
0.03037	0.5932	0.9584
0.03120	0.6157	0.9601
0.03207	0.6417	0.9621
0.03293	0.6611	0.9637
0.03400	0.6914	0.9662
0.03483	0.7195	0.9687
0.03577	0.7430	0.9709
0.03633	0.7683	0.9733
0.03717	0.7874	0.9752
0.03803	0.8147	0.9780
0.03897	0.8385	0.9805
0.03993	0.8587	0.9827
0.04077	0.8827	0.9854
0.04160	0.9052	0.9880
0.04307	0.9405	0.9923
0.04473	0.9692	0.9959
0.04743	0.9890	0.9985
0.04987	0.9959	0.9995
0.05230	0.9978	0.9997
0.05533	1.0000	1.0000

X = 1.1000

Y	u/u_1	ρ/ρ_1
0.01260	1.0001	1.0000
0.01517	0.9989	0.9998
0.01777	0.9926	0.9990
0.02027	0.9761	0.9967
0.02220	0.9505	0.9932
0.02480	0.9088	0.9878
0.02750	0.8593	0.9817
0.03010	0.7960	0.9746
0.03237	0.7410	0.9689
0.03337	0.7174	0.9666
0.03533	0.6806	0.9632
0.03803	0.6522	0.9608
0.04043	0.6540	0.9609
0.04313	0.6809	0.9633
0.04570	0.7280	0.9677
0.04803	0.7726	0.9721
0.04893	0.8005	0.9751
0.05087	0.8386	0.9793
0.05333	0.8946	0.9860
0.05403	0.9155	0.9886
0.05593	0.9446	0.9924
0.05837	0.9772	0.9968
0.06103	0.9928	0.9990
0.06310	0.9981	0.9997
0.06617	0.9999	1.0000

X = 1.1700

Y	u/u_1	ρ/ρ_1
0.00847	1.0000	1.0000
0.01093	0.9983	0.9997
0.01367	0.9945	0.9992
0.01623	0.9833	0.9975
0.01883	0.9606	0.9943
0.02143	0.9258	0.9895
0.02257	0.9081	0.9871
0.02410	0.8823	0.9838
0.02517	0.8654	0.9816
0.02663	0.8380	0.9783
0.02777	0.8169	0.9758
0.02933	0.7917	0.9730
0.03047	0.7745	0.9711
0.03183	0.7526	0.9687
0.03463	0.7288	0.9663
0.03713	0.7242	0.9658
0.03977	0.7367	0.9671
0.04227	0.7662	0.9702
0.04493	0.8004	0.9739
0.04733	0.8395	0.9785
0.05010	0.8841	0.9840
0.05123	0.9011	0.9862
0.05263	0.9258	0.9895
0.05517	0.9581	0.9939
0.05770	0.9829	0.9975
0.06020	0.9921	0.9988
0.06260	0.9972	0.9996
0.06500	0.9983	0.9997
0.06627	1.0000	1.0000

X = 1.3000

Y	u/u_1	ρ/ρ_1
0.01457	0.9999	1.0000
0.01707	0.9988	0.9998
0.01950	0.9977	0.9996
0.02157	0.9929	0.9989
0.02403	0.9807	0.9970
0.02643	0.9649	0.9947
0.02900	0.9421	0.9913
0.03030	0.9250	0.9889
0.03223	0.9038	0.9859
0.03427	0.8765	0.9823
0.03687	0.8484	0.9786
0.03957	0.8203	0.9752
0.04217	0.8043	0.9732
0.04470	0.7955	0.9722
0.04730	0.7937	0.9720
0.04990	0.8054	0.9734
0.05243	0.8238	0.9756
0.05510	0.8463	0.9784
0.05770	0.8725	0.9817
0.06027	0.9023	0.9857
0.06293	0.9250	0.9889
0.06547	0.9515	0.9927
0.06810	0.9711	0.9956
0.07030	0.9829	0.9974
0.07303	0.9923	0.9988
0.07537	0.9971	0.9996
0.07843	0.9993	0.9999
0.07910	0.9999	1.0000

X = 1.6000

Y	u/u_1	ρ/ρ_1
0.00277	1.0000	1.0000
0.00577	0.9971	0.9995
0.00810	0.9955	0.9993
0.01053	0.9927	0.9988
0.01300	0.9867	0.9979
0.01547	0.9792	0.9967
0.01830	0.9685	0.9950
0.02057	0.9572	0.9933
0.02320	0.9443	0.9913
0.02557	0.9309	0.9893
0.02830	0.9130	0.9867
0.03073	0.9001	0.9849
0.03330	0.8869	0.9831
0.03600	0.8767	0.9817
0.03877	0.8683	0.9805
0.04127	0.8643	0.9800
0.04370	0.8629	0.9798
0.04640	0.8670	0.9803
0.04910	0.8741	0.9813
0.05163	0.8824	0.9824
0.05450	0.8970	0.9845
0.05683	0.9068	0.9859
0.05933	0.9212	0.9879
0.06200	0.9366	0.9902
0.06457	0.9480	0.9919
0.06713	0.9595	0.9936
0.06957	0.9711	0.9954
0.07227	0.9803	0.9969
0.07477	0.9873	0.9980
0.07710	0.9910	0.9986
0.07973	0.9948	0.9992
0.08207	0.9968	0.9995
0.08457	0.9978	0.9997
0.08753	0.9989	0.9998
0.09040	1.0000	1.0000

TABLE 10

Boundary Layer Profile Data; Section 2815, $C_L = 0{\cdot}70$, Upper Surface

X = 0.4496			X = 0.5854			X = 0.6608			X = 0.7218			X = 0.7750		
Y	u/u_1	ρ/ρ_1	Y	u/u_1	ρ/ρ_1	Y	u/u_1	ρ/ρ_1	Y	u/u_1	ρ/ρ_1	Y	u/u_1	ρ/ρ_1
0.00033	0.6243	0.9082	0.00033	0.5632	0.9155	0.00033	0.5401	0.9195	0.00033	0.4860	0.9209	0.00033	0.4933	0.9282
0.00047	0.6267	0.9086	0.00063	0.5804	0.9178	0.00050	0.5454	0.9201	0.00050	0.5013	0.9223	0.00050	0.5058	0.9293
0.00050	0.6313	0.9094	0.00077	0.5921	0.9193	0.00060	0.5588	0.9217	0.00060	0.5034	0.9225	0.00073	0.5179	0.9304
0.00053	0.6373	0.9105	0.00100	0.6069	0.9214	0.00070	0.5656	0.9225	0.00067	0.5149	0.9236	0.00090	0.5308	0.9316
0.00067	0.6513	0.9129	0.00113	0.6164	0.9227	0.00080	0.5749	0.9236	0.00077	0.5229	0.9244	0.00107	0.5380	0.9323
0.00093	0.6759	0.9175	0.00143	0.6378	0.9258	0.00103	0.5951	0.9261	0.00090	0.5405	0.9262	0.00133	0.5547	0.9339
0.00117	0.6952	0.9212	0.00173	0.6584	0.9289	0.00140	0.6184	0.9291	0.00123	0.5593	0.9282	0.00177	0.5738	0.9358
0.00143	0.7174	0.9256	0.00203	0.6781	0.9320	0.00173	0.6375	0.9317	0.00143	0.5825	0.9308	0.00210	0.5925	0.9378
0.00177	0.7412	0.9306	0.00233	0.6963	0.9349	0.00207	0.6546	0.9340	0.00187	0.6002	0.9329	0.00250	0.6092	0.9396
0.00207	0.7621	0.9351	0.00260	0.7142	0.9379	0.00240	0.6732	0.9367	0.00220	0.6228	0.9356	0.00300	0.6314	0.9421
0.00230	0.7784	0.9387	0.00300	0.7328	0.9411	0.00280	0.6908	0.9393	0.00280	0.6446	0.9383	0.00343	0.6512	0.9444
0.00253	0.8008	0.9439	0.00330	0.7564	0.9453	0.00320	0.7083	0.9420	0.00313	0.6611	0.9404	0.00393	0.6692	0.9466
0.00280	0.8211	0.9488	0.00373	0.7821	0.9501	0.00353	0.7267	0.9449	0.00350	0.6794	0.9429	0.00433	0.6875	0.9488
0.00307	0.8392	0.9533	0.00410	0.7987	0.9533	0.00387	0.7470	0.9482	0.00390	0.6983	0.9455	0.00483	0.7057	0.9512
0.00333	0.8572	0.9579	0.00440	0.8159	0.9568	0.00427	0.7632	0.9509	0.00430	0.7164	0.9481	0.00533	0.7268	0.9540
0.00367	0.8778	0.9634	0.00483	0.8426	0.9623	0.00467	0.7864	0.9550	0.00470	0.7337	0.9506	0.00577	0.7443	0.9564
0.00400	0.8974	0.9688	0.00530	0.8620	0.9664	0.00513	0.8040	0.9581	0.00513	0.7516	0.9533	0.00630	0.7637	0.9591
0.00423	0.9149	0.9737	0.00560	0.8803	0.9705	0.00550	0.8203	0.9611	0.00550	0.7713	0.9564	0.00673	0.7838	0.9621
0.00460	0.9334	0.9791	0.00613	0.9033	0.9757	0.00590	0.8409	0.9651	0.00597	0.7885	0.9592	0.00723	0.8038	0.9651
0.00493	0.9507	0.9843	0.00660	0.9257	0.9810	0.00627	0.8569	0.9682	0.00633	0.8061	0.9621	0.00770	0.8200	0.9676
0.00543	0.9715	0.9908	0.00703	0.9424	0.9851	0.00660	0.8730	0.9715	0.00677	0.8227	0.9649	0.00803	0.8375	0.9704
0.00613	0.9887	0.9963	0.00753	0.9644	0.9906	0.00703	0.8909	0.9752	0.00720	0.8393	0.9678	0.00857	0.8538	0.9730
0.00693	0.9973	0.9991	0.00837	0.9826	0.9954	0.00757	0.9104	0.9793	0.00757	0.8578	0.9711	0.00907	0.8722	0.9761
0.00760	0.9993	0.9998	0.00923	0.9933	0.9982	0.00793	0.9264	0.9828	0.00807	0.8740	0.9741	0.00947	0.8889	0.9790
			0.01013	0.9979	0.9994	0.00847	0.9440	0.9867	0.00860	0.8915	0.9774	0.01010	0.9067	0.9821
			0.01093	0.9989	0.9997	0.00897	0.9600	0.9904	0.00910	0.9095	0.9809	0.01063	0.9229	0.9851
			0.01193	0.9992	0.9998	0.00970	0.9768	0.9944	0.00953	0.9255	0.9841	0.01120	0.9399	0.9882
			0.01227	0.9992	0.9998	0.01050	0.9901	0.9976	0.01010	0.9432	0.9877	0.01193	0.9594	0.9919
						0.01130	0.9962	0.9991	0.01080	0.9619	0.9917	0.01267	0.9758	0.9951
						0.01230	0.9992	0.9998	0.01153	0.9786	0.9953	0.01367	0.9868	0.9973
						0.01283	0.9999	1.0000	0.01247	0.9896	0.9977	0.01450	0.9938	0.9987
									0.01367	0.9975	0.9994	0.01530	0.9978	0.9996
									0.01450	0.9994	0.9999	0.01617	0.9987	0.9997
									0.01487	0.9998	0.9999	0.01697	0.9990	0.9998
												0.01783	0.9990	0.9998
												0.01923	0.9990	0.9998
												0.02550	0.9990	0.9998

TABLE 10 (Concluded)

X = 0.8238			X = 0.8696			X = 0.9119			X = 0.9518			X = 0.9970		
Y	u/u_1	ρ/ρ_1	Y	u/u_1	ρ/ρ_1	Y	u/u_1	ρ/ρ_1	Y	u/u_1	ρ/ρ_1	Y	u/u_1	ρ/ρ_1
0.00033	0.4564	0.9310	0.00033	0.4242	0.9339	0.00033	0.3673	0.9363	0.00033	0.2945	0.9393	0.00033	0.1518	0.9415
0.00040	0.4629	0.9315	0.00043	0.4336	0.9345	0.00053	0.3823	0.9371	0.00043	0.2999	0.9395	0.00043	0.1594	0.9416
0.00067	0.4793	0.9328	0.00063	0.4408	0.9350	0.00063	0.3892	0.9375	0.00053	0.3052	0.9397	0.00050	0.1575	0.9416
0.00087	0.4896	0.9336	0.00073	0.4479	0.9354	0.00073	0.3967	0.9379	0.00063	0.3121	0.9399	0.00060	0.1594	0.9416
0.00100	0.4993	0.9344	0.00087	0.4538	0.9358	0.00087	0.4039	0.9383	0.00073	0.3172	0.9401	0.00070	0.1630	0.9417
0.00133	0.5188	0.9360	0.00113	0.4730	0.9372	0.00117	0.4209	0.9392	0.00100	0.3335	0.9408	0.00107	0.1834	0.9421
0.00183	0.5412	0.9379	0.00157	0.4913	0.9385	0.00160	0.4399	0.9404	0.00157	0.3543	0.9417	0.00150	0.2002	0.9424
0.00230	0.5614	0.9398	0.00203	0.5123	0.9401	0.00203	0.4585	0.9415	0.00213	0.3711	0.9425	0.00220	0.2171	0.9428
0.00270	0.5801	0.9415	0.00253	0.5302	0.9416	0.00253	0.4748	0.9426	0.00267	0.3884	0.9433	0.00273	0.2339	0.9433
0.00320	0.5977	0.9433	0.00293	0.5463	0.9429	0.00300	0.4958	0.9440	0.00313	0.4094	0.9443	0.00333	0.2531	0.9438
0.00367	0.6147	0.9450	0.00343	0.5626	0.9443	0.00367	0.5144	0.9453	0.00387	0.4256	0.9452	0.00400	0.2698	0.9443
0.00413	0.6323	0.9468	0.00410	0.5867	0.9464	0.00410	0.5313	0.9466	0.00430	0.4429	0.9462	0.00437	0.2875	0.9449
0.00467	0.6543	0.9492	0.00460	0.6044	0.9481	0.00453	0.5477	0.9478	0.00480	0.4590	0.9471	0.00500	0.3060	0.9455
0.00517	0.6720	0.9512	0.00497	0.6218	0.9497	0.00513	0.5655	0.9492	0.00533	0.4782	0.9482	0.00560	0.3225	0.9461
0.00563	0.6923	0.9535	0.00560	0.6393	0.9514	0.00570	0.5846	0.9508	0.00590	0.4945	0.9492	0.00623	0.3407	0.9468
0.00620	0.7109	0.9558	0.00610	0.6587	0.9534	0.00620	0.6026	0.9523	0.00637	0.5107	0.9503	0.00670	0.3572	0.9474
0.00657	0.7300	0.9581	0.00657	0.6794	0.9556	0.00660	0.6207	0.9539	0.00687	0.5306	0.9516	0.00740	0.3744	0.9481
0.00720	0.7494	0.9606	0.00717	0.6965	0.9574	0.00713	0.6370	0.9554	0.00753	0.5479	0.9528	0.00790	0.3915	0.9489
0.00757	0.7655	0.9627	0.00743	0.7127	0.9592	0.00760	0.6539	0.9569	0.00813	0.5698	0.9544	0.00840	0.4119	0.9498
0.00813	0.7866	0.9656	0.00797	0.7289	0.9611	0.00810	0.6709	0.9586	0.00850	0.5874	0.9557	0.00890	0.4294	0.9507
0.00860	0.8034	0.9679	0.00850	0.7457	0.9631	0.00870	0.6905	0.9605	0.00917	0.6035	0.9569	0.00950	0.4474	0.9516
0.00903	0.8203	0.9703	0.00890	0.7620	0.9651	0.00913	0.7067	0.9621	0.00977	0.6211	0.9583	0.01033	0.4682	0.9527
0.00967	0.8381	0.9729	0.00947	0.7786	0.9671	0.00977	0.7309	0.9647	0.01010	0.6416	0.9600	0.01087	0.4851	0.9536
0.01020	0.8559	0.9756	0.00983	0.7959	0.9693	0.01023	0.7473	0.9665	0.01090	0.6645	0.9620	0.01127	0.5058	0.9548
0.01057	0.8736	0.9783	0.01047	0.8142	0.9717	0.01073	0.7633	0.9682	0.01140	0.6857	0.9638	0.01180	0.5251	0.9560
0.01117	0.8924	0.9813	0.01100	0.8337	0.9744	0.01130	0.7814	0.9703	0.01203	0.7022	0.9653	0.01263	0.5425	0.9570
0.01190	0.9137	0.9848	0.01153	0.8509	0.9767	0.01187	0.7995	0.9724	0.01253	0.7223	0.9672	0.01300	0.5618	0.9583
0.01253	0.9307	0.9876	0.01210	0.8702	0.9795	0.01233	0.8162	0.9744	0.01310	0.7399	0.9690	0.01360	0.5822	0.9596
0.01320	0.9471	0.9904	0.01263	0.8885	0.9821	0.01293	0.8340	0.9766	0.01373	0.7569	0.9706	0.01417	0.6026	0.9611
0.01390	0.9635	0.9933	0.01333	0.9071	0.9849	0.01360	0.8526	0.9790	0.01433	0.7743	0.9724	0.01480	0.6283	0.9629
0.01470	0.9758	0.9955	0.01400	0.9241	0.9875	0.01407	0.8692	0.9811	0.01490	0.7941	0.9745	0.01543	0.6478	0.9644
0.01560	0.9882	0.9978	0.01467	0.9421	0.9904	0.01463	0.8854	0.9833	0.01543	0.8167	0.9770	0.01607	0.6643	0.9657
0.01640	0.9940	0.9989	0.01567	0.9632	0.9938	0.01513	0.9018	0.9855	0.01610	0.8332	0.9788	0.01657	0.6810	0.9670
0.01733	0.9972	0.9995	0.01657	0.9761	0.9959	0.01560	0.9194	0.9880	0.01670	0.8526	0.9810	0.01727	0.7002	0.9686
0.01827	0.9989	0.9998	0.01820	0.9926	0.9987	0.01657	0.9366	0.9904	0.01743	0.8732	0.9835	0.01757	0.7166	0.9700
0.01913	0.9993	0.9999	0.01900	0.9955	0.9992	0.01740	0.9526	0.9928	0.01800	0.8908	0.9856	0.01803	0.7381	0.9719
			0.02177	0.9993	0.9999	0.01810	0.9689	0.9952	0.01870	0.9080	0.9877	0.01870	0.7568	0.9735
			0.02230	0.9993	0.9999	0.01900	0.9798	0.9969	0.01940	0.9247	0.9898	0.01933	0.7753	0.9752
						0.01983	0.9889	0.9983	0.02010	0.9409	0.9919	0.01977	0.7919	0.9768
						0.02067	0.9937	0.9990	0.02087	0.9574	0.9941	0.02043	0.8099	0.9786
						0.02150	0.9970	0.9995	0.02177	0.9702	0.9959	0.02100	0.8280	0.9804
						0.02237	0.9996	0.9999	0.02263	0.9795	0.9971	0.02167	0.8492	0.9826
						0.02263	0.9996	0.9999	0.02347	0.9890	0.9985	0.02233	0.8681	0.9846
									0.02430	0.9943	0.9992	0.02297	0.8842	0.9863
									0.02547	0.9965	0.9995	0.02370	0.9052	0.9886
									0.02633	0.9990	0.9999	0.02453	0.9194	0.9903
									0.02720	0.9996	0.9999	0.02557	0.9390	0.9925
												0.02633	0.9566	0.9946
												0.02747	0.9718	0.9965
												0.02833	0.9820	0.9977
												0.02917	0.9848	0.9981
												0.02997	0.9907	0.9988
												0.03097	0.9921	0.9990
												0.03213	0.9955	0.9994
												0.03317	0.9941	0.9993
												0.03427	0.9973	0.9997
												0.03543	0.9948	0.9993

TABLE 11

Boundary Layer Profile Data; Section 2815, $C_L = 0{\cdot}70$, Lower Surface

X = 0.2316			X = 0.3197			X = 0.4797			X = 0.6722			X = 0.7693		
Y	u/u_1	ρ/ρ_1	Y	u/u_1	ρ/ρ_1	Y	u/u_1	ρ/ρ_1	Y	u/u_1	ρ/ρ_1	Y	u/u_1	ρ/ρ_1
0.00033	0.8170	0.9721	0.00033	0.7505	0.9592	0.00033	0.6702	0.9440	0.00033	0.6012	0.9507	0.00033	0.5548	0.9518
0.00040	0.8256	0.9730	0.00047	0.7619	0.9607	0.00043	0.6766	0.9448	0.00043	0.6081	0.9513	0.00040	0.5613	0.9523
0.00057	0.8476	0.9763	0.00070	0.7938	0.9652	0.00047	0.6788	0.9451	0.00050	0.6150	0.9520	0.00050	0.5699	0.9529
0.00073	0.8723	0.9798	0.00083	0.7982	0.9658	0.00057	0.6890	0.9464	0.00060	0.6263	0.9530	0.00050	0.5750	0.9533
0.00087	0.8931	0.9828	0.00097	0.8165	0.9685	0.00067	0.7005	0.9480	0.00070	0.6332	0.9536	0.00060	0.5762	0.9534
0.00103	0.9158	0.9863	0.00120	0.8414	0.9723	0.00087	0.7283	0.9518	0.00097	0.6547	0.9557	0.00073	0.5923	0.9546
0.00137	0.9483	0.9914	0.00133	0.8589	0.9751	0.00107	0.7523	0.9553	0.00127	0.6805	0.9582	0.00100	0.6110	0.9561
0.00167	0.9766	0.9960	0.00147	0.8818	0.9788	0.00127	0.7743	0.9586	0.00163	0.7049	0.9608	0.00127	0.6279	0.9575
0.00217	0.9955	0.9992	0.00183	0.9113	0.9838	0.00147	0.7962	0.9620	0.00183	0.7226	0.9627	0.00157	0.6505	0.9595
0.00310	0.9998	1.0000	0.00203	0.9327	0.9875	0.00167	0.8196	0.9656	0.00213	0.7427	0.9649	0.00203	0.6693	0.9612
			0.00220	0.9522	0.9910	0.00187	0.8360	0.9686	0.00253	0.7603	0.9669	0.00233	0.6864	0.9627
			0.00257	0.9701	0.9943	0.00213	0.8599	0.9727	0.00270	0.7772	0.9689	0.00260	0.7030	0.9643
			0.00293	0.9878	0.9976	0.00237	0.8813	0.9765	0.00310	0.8002	0.9716	0.00290	0.7198	0.9659
			0.00367	1.0000	1.0000	0.00270	0.9042	0.9807	0.00330	0.8180	0.9738	0.00317	0.7363	0.9676
						0.00290	0.9203	0.9838	0.00360	0.8349	0.9760	0.00363	0.7529	0.9693
						0.00310	0.9371	0.9870	0.00390	0.8555	0.9787	0.00397	0.7700	0.9711
						0.00343	0.9575	0.9911	0.00420	0.8727	0.9810	0.00433	0.7862	0.9728
						0.00393	0.9778	0.9953	0.00457	0.8889	0.9833	0.00460	0.8031	0.9747
						0.00467	0.9953	0.9990	0.00490	0.9132	0.9867	0.00503	0.8219	0.9768
						0.00553	0.9998	1.0000	0.00540	0.9333	0.9896	0.00537	0.8388	0.9788
									0.00573	0.9502	0.9922	~~0.00557 0.9985 0.9998~~		
									0.00627	0.9684	0.9950	0.00560	0.8505	0.9801
									0.00683	0.9869	0.9979	0.00593	0.8673	0.9822
									0.00770	0.9974	0.9996	0.00630	0.8860	0.9845
									0.00847	0.9999	1.0000	0.00680	0.9076	0.9873
												~~0.00740 0.6332 0.9580~~		
												0.00700	0.9099	0.9876
												0.00737	0.9275	0.9899
												0.00777	0.9451	0.9922
												0.00840	0.9620	0.9946
												0.00903	0.9782	0.9968
												0.00987	0.9916	0.9988
												0.01067	0.9975	0.9996
												0.01150	0.9996	0.9999

TABLE 11 (Concluded)

X = 0.8617			X = 0.9380			X = 0.9970		
Y	u/u_1	ρ/ρ_1	Y	u/u_1	ρ/ρ_1	Y	u/u_1	ρ/ρ_1
0.00043	0.5527	0.9562	0.00033	0.5974	0.9600	0.00033	0.5852	0.9601
0.00053	0.5617	0.9568	0.00053	0.6062	0.9607	0.00047	0.6007	0.9612
0.00067	0.5724	0.9576	0.00067	0.6221	0.9618	~~0.00050 0.7197 0.9704~~		
0.00077	0.5765	0.9579	0.00083	0.6233	0.9619	0.00067	0.6253	0.9630
0.00090	0.5869	0.9586	0.00103	0.6329	0.9626	0.00087	0.6413	0.9641
0.00110	0.6079	0.9601	0.00140	0.6508	0.9640	0.00137	0.6625	0.9658
0.00143	0.6289	0.9617	0.00173	0.6701	0.9655	0.00190	0.6829	0.9674
0.00180	0.6455	0.9630	0.00223	0.6875	0.9670	~~0.00213 0.5976 0.9610~~		
0.00223	0.6638	0.9645	0.00273	0.7044	0.9684	0.00220	0.6928	0.9682
0.00270	0.6860	0.9663	0.00333	0.7240	0.9701	0.00273	0.7125	0.9698
0.00320	0.7065	0.9680	0.00397	0.7428	0.9718	0.00330	0.7293	0.9713
0.00373	0.7269	0.9699	0.00457	0.7621	0.9736	0.00397	0.7481	0.9729
0.00433	0.7507	0.9720	0.00507	0.7788	0.9752	0.00463	0.7669	0.9746
0.00477	0.7690	0.9738	0.00560	0.7960	0.9768	0.00513	0.7829	0.9761
0.00527	0.7855	0.9754	0.00613	0.8136	0.9786	0.00580	0.8013	0.9779
0.00567	0.8018	0.9770	0.00683	0.8330	0.9806	0.00653	0.8192	0.9796
0.00603	0.8178	0.9786	0.00740	0.8504	0.9824	0.00710	0.8356	0.9813
0.00660	0.8373	0.9807	0.00800	0.8679	0.9843	0.00783	0.8533	0.9831
0.00700	0.8535	0.9824	0.00853	0.8919	0.9869	0.00840	0.8699	0.9849
0.00747	0.8697	0.9842	0.00933	0.9054	0.9885	0.00893	0.8872	0.9867
0.00797	0.8874	0.9862	0.00990	0.9236	0.9906	0.00973	0.9051	0.9887
0.00840	0.9043	0.9881	0.01057	0.9406	0.9926	0.01043	0.9225	0.9907
~~0.00877 0.9985 0.9998~~			0.01133	0.9573	0.9946	0.01117	0.9394	0.9926
0.00887	0.9161	0.9895	0.01210	0.9734	0.9966	0.01197	0.9559	0.9946
0.00933	0.9340	0.9917	0.01293	0.9828	0.9978	0.01283	0.9683	0.9961
0.01003	0.9555	0.9943	0.01373	0.9918	0.9989	0.01373	0.9827	0.9978
0.01083	0.9718	0.9964	0.01467	0.9962	0.9995	0.01467	0.9894	0.9987
0.01163	0.9844	0.9980	0.01583	0.9989	0.9999	0.01547	0.9946	0.9993
0.01247	0.9937	0.9992	0.01673	0.9996	0.9999	0.01643	0.9974	0.9997
0.01340	0.9974	0.9997	0.01677	0.9996	0.9999	0.01730	0.9987	0.9998
0.01440	0.9993	0.9999				0.01813	0.9994	0.9999
0.01440	1.0000	1.0000				0.01950	0.9999	1.0000

TABLE 12

Wake Profile Data; Section 2815, $C_L = 0{\cdot}70$

X = 1.1000			X = 1.3000			X = 1.6000		
Y	u/u_1	ρ/ρ_1	Y	u/u_1	ρ/ρ_1	Y	u/u_1	ρ/ρ_1
0.00657	0.9999	1.0000	0.00033	0.9999	1.0000	0.00727	1.0000	1.0000
0.00950	0.9965	0.9995	0.00333	0.9994	0.9999	0.01097	0.9992	0.9999
0.01203	0.9895	0.9985	0.00607	0.9955	0.9993	0.01333	0.9976	0.9996
0.01523	0.9592	0.9943	0.00890	0.9888	0.9983	0.01543	0.9961	0.9994
0.01653	0.9396	0.9917	0.01153	0.9742	0.9961	0.01813	0.9945	0.9991
0.01823	0.9065	0.9874	0.01393	0.9546	0.9931	0.02070	0.9893	0.9983
0.01973	0.8736	0.9834	0.01643	0.9289	0.9894	0.02410	0.9810	0.9970
0.02280	0.8000	0.9749	0.01893	0.8987	0.9852	0.02640	0.9744	0.9959
0.02353	0.7765	0.9724	0.02113	0.8710	0.9815	0.02853	0.9650	0.9945
0.02493	0.7419	0.9689	0.02257	0.8548	0.9794	0.03107	0.9544	0.9929
0.02660	0.6999	0.9648	0.02433	0.8361	0.9771	0.03337	0.9401	0.9907
0.02820	0.6642	0.9616	0.02633	0.8155	0.9746	0.03570	0.9282	0.9889
0.02947	0.6448	0.9599	0.02900	0.7997	0.9727	0.03803	0.9138	0.9868
0.03273	0.6289	0.9586	0.03210	0.7875	0.9712	0.04040	0.9015	0.9851
0.03580	0.6478	0.9602	0.03480	0.7905	0.9716	0.04303	0.8881	0.9832
0.03673	0.6688	0.9620	0.03800	0.8041	0.9732	0.04563	0.8773	0.9817
0.03983	0.7210	0.9668	0.04053	0.8258	0.9758	0.04807	0.8702	0.9808
0.04067	0.7413	0.9688	0.04380	0.8543	0.9794	0.05087	0.8629	0.9798
0.04310	0.7912	0.9740	0.04670	0.8864	0.9836	0.05323	0.8617	0.9796
0.04393	0.8174	0.9768	0.04913	0.9082	0.9865	0.05590	0.8644	0.9800
0.04587	0.8507	0.9806	0.05157	0.9334	0.9901	0.05863	0.8698	0.9807
0.04637	0.8689	0.9828	0.05477	0.9611	0.9941	0.06147	0.8777	0.9818
0.04830	0.9055	0.9873	0.05780	0.9792	0.9966	0.06443	0.8911	0.9836
0.04947	0.9249	0.9898	0.06100	0.9925	0.9988	0.06710	0.9036	0.9854
0.05063	0.9482	0.9928	0.06370	0.9966	0.9995	0.06980	0.9162	0.9872
0.05220	0.9652	0.9951	0.06663	0.9992	0.9999	0.07233	0.9286	0.9890
0.05383	0.9850	0.9979	0.06730	0.9999	1.0000	0.07530	0.9444	0.9913
0.05677	0.9959	0.9994				0.07857	0.9618	0.9940
0.05980	0.9971	0.9996				0.08120	0.9693	0.9951
0.06493	0.9999	1.0000				0.08337	0.9769	0.9963
						0.08620	0.9857	0.9977
						0.08887	0.9901	0.9984
						0.09210	0.9953	0.9992
						0.09493	0.9974	0.9996
						0.09813	0.9990	0.9998
						0.10113	1.0000	1.0000

TABLE 13

Boundary-Layer Integral Results

Section 2814: $C_L = 0{\cdot}42$, $M = 0{\cdot}725$, $R = 15 \times 10^6$

(a) Upper Surface

X		δ_0	δ_1	δ_2	δ_3	δ_0^i	δ_1^i	δ_2^i	δ_3^i	δ_1^i
0·3167	1*	0·0037	0·00080	0·00047	0·00084	0·0038	0·00066	0·00050	0·00088	0·00062
	2	0·0037	0·00075	0·00044	0·00079	0·0038	0·00061	0·00047	0·00083	0·00057
	3	0·0038	0·00079	0·00047	0·00083	0·0039	0·00064	0·00050	0·00087	0·00060
0·4166	1	0·0049	0·00104	0·00061	0·00108	0·0050	0·00086	0·00065	0·00115	0·00081
	2	0·0048	0·00097	0·00057	0·00101	0·0049	0·00079	0·00061	0·00108	0·00074
	3	0·0049	0·00102	0·00059	0·00105	0·0050	0·00083	0·00064	0·00113	0·00078
0·5166	1	0·0056	0·00117	0·00069	0·00123	0·0058	0·00096	0·00073	0·00130	0·00090
	2	0·0056	0·00109	0·00064	0·00116	0·0058	0·00088	0·00068	0·00123	0·00083
	3	0·0056	0·00114	0·00066	0·00120	0·0058	0·00092	0·00071	0·00127	0·00086
0·6256	1	0·0068	0·00175	0·00100	0·00175	0·0071	0·00149	0·00107	0·00186	0·00139
	2	0·0067	0·00166	0·00095	0·00167	0·0070	0·00139	0·00102	0·00178	0·00130
	3	0·0067	0·00172	0·00098	0·00171	0·0070	0·00145	0·00105	0·00183	0·00135
0·7499	1	0·0084	0·00243	0·00139	0·00239	0·0087	0·00214	0·00147	0·00252	0·00201
	2	0·0083	0·00227	0·00131	0·00227	0·0086	0·00197	0·00138	0·00239	0·00185
	3	0·0083	0·00234	0·00134	0·00221	0·0085	0·00203	0·00142	0·00244	0·00191
0·8457	1	0·0102	0·00330	0·00186	0·00315	0·0105	0·00295	0·00196	0·00332	0·00279
	2	0·0100	0·00311	0·00178	0·00303	0·0103	0·00276	0·00187	0·00319	0·00262
	3	0·0099	0·00319	0·00181	0·00307	0·0102	0·00283	0·00190	0·00324	0·00268
0·9305	1	0·0127	0·00473	0·00254	0·00421	0·0130	0·00434	0·00267	0·00442	0·00412
	2	0·0125	0·00450	0·00245	0·00407	0·0127	0·00411	0·00258	0·00428	0·00390
	3	0·0124	0·00448	0·00249	0·00411	0·0126	0·00419	0·00261	0·00431	0·00398
0·9682	1	0·0142	0·00627	0·00314	0·00509	0·0147	0·00584	0·00330	0·00533	0·00554
	2	0·0138	0·00594	0·00303	0·00492	0·0143	0·00551	0·00319	0·00516	0·00522
	3	0·0137	0·00604	0·00306	0·00495	0·0142	0·00561	0·00322	0·00519	0·00532
0·9918	1	0·0157	0·00804	0·00371	0·00587	0·0161	0·00758	0·00389	0·00614	0·00718
	2	0·0154	0·00774	0·00362	0·00574	0·0158	0·00729	0·00381	0·00601	0·00690
	3	0·0153	0·00787	0·00365	0·00576	0·0157	0·00741	0·00384	0·00603	0·00701
0·9970	1	0·0156	0·00852	0·00379	0·00594	0·0160	0·00806	0·00397	0·00622	0·00764
	2	0·0151	0·00802	0·00367	0·00576	0·0155	0·00756	0·00384	0·00604	0·00715
	3	0·0150	0·00814	0·00369	0·00578	0·0154	0·00767	0·00387	0·00606	0·00726

* For each survey, row 1 of results lists uncorrected integrals;
row 2 of results lists integrals corrected for survey rig interference;
row 3 of results lists integrals corrected for survey rig interference, pitot displacement and fluctuating velocity effects.

TABLE 13 (Cont'd.)

(b) Lower Surface

X		δ_0	δ_1	δ_2	δ_3	δ_0^i	δ_1^i	δ_2^i	δ_3^i	δ_1^r
0·3500	1*	0·0033	0·00063	0·00039	0·00069	0·0034	0·00054	0·00040	0·00072	0·00051
	2	0·0033	0·00059	0·00036	0·00065	0·0034	0·00050	0·00037	0·00067	0·00046
	3	0·0034	0·00063	0·00039	0·00069	0·0035	0·00053	0·00040	0·00071	0·00050
0·5000	1	0·0042	0·00107	0·00063	0·00110	0·0043	0·00094	0·00067	0·00116	0·00089
	2	0·0041	0·00100	0·00059	0·00104	0·0042	0·00087	0·00063	0·00110	0·00083
	3	0·0042	0·00105	0·00062	0·00108	0·0043	0·00092	0·00066	0·00115	0·00087
0·6332	1	0·0065	0·00201	0·00115	0·00196	0·0067	0·00182	0·00121	0·00205	0·00173
	2	0·0064	0·00190	0·00110	0·00188	0·0066	0·00170	0·00116	0·00196	0·00162
	3	0·0064	0·00197	0·00113	0·00192	0·0065	0·00177	0·00119	0·00201	0·00169
0·7665	1	0·0094	0·00292	0·00171	0·00290	0·0096	0·00269	0·00178	0·00302	0·00258
	2	0·0092	0·00271	0·00162	0·00277	0·0094	0·00249	0·00168	0·00288	0·00238
	3	0·0091	0·00279	0·00166	0·00281	0·0093	0·00255	0·00172	0·00293	0·00245
0·8332	1	0·0114	0·00333	0·00201	0·00342	0·0116	0·00307	0·00208	0·00354	0·00295
	2	0·0112	0·00314	0·00192	0·00329	0·0114	0·00288	0·00200	0·00340	0·00277
	3	0·0112	0·00321	0·00195	0·00333	0·0113	0·00295	0·00203	0·00345	0·00283
0·8998	1	0·0132	0·00365	0·00226	0·00388	0·0134	0·00337	0·00233	0·00400	0·00326
	2	0·0128	0·00335	0·00213	0·00367	0·0130	0·00307	0·00219	0·00379	0·00295
	3	0·0128	0·00342	0·00216	0·00371	0·0129	0·00314	0·00223	0·00383	0·00304
0·9499	1	0·0136	0·00354	0·00227	0·00395	0·0138	0·00326	0·00234	0·00407	0·00316
	2	0·0132	0·00334	0·00218	0·00381	0·0124	0·00306	0·00224	0·00392	0·00296
	3	0·0132	0·00341	0·00221	0·00384	0·0134	0·00313	0·00227	0·00396	0·00302
0·9833	1	0·0148	0·00328	0·00216	0·00381	0·0151	0·00300	0·00222	0·00392	0·00291
	2	0·0144	0·00317	0·00211	0·00371	0·0147	0·00289	0·00217	0·00383	0·00280
	3	0·0144	0·00323	0·00214	0·00374	0·0147	0·00294	0·00220	0·00386	0·00286
0·9970	1	0·0151	0·00310	0·00208	0·00370	0·0153	0·00283	0·00214	0·00380	0·00274
	2	0·0146	0·00292	0·00199	0·00354	0·0148	0·00265	0·00205	0·00365	0·00257
	3	0·0146	0·00298	0·00201	0·00358	0·0148	0·00271	0·00208	0·00368	0·00262

* See footnote to Table 13(a).

TABLE 14

Boundary-Layer Integral Results

Section 2815: $C_L = 0{\cdot}51$, $M = 0{\cdot}661$, $R = 15{\cdot}6 \times 10^6$

(a) Upper Surface

X		δ_0	δ_1	δ_2	δ_3	δ_0^i	δ_1^i	δ_2^i	δ_3^i	δ_1^i
0·2716	1*	0·0031	0·00077	0·00043	0·00076	0·0032	0·00064	0·00046	0·00080	0·00060
	2	0·0030	0·00072	0·00040	0·00071	0·0032	0·00059	0·00043	0·00076	0·00055
	3	0·0031	0·00077	0·00043	0·00075	0·0032	0·00063	0·00046	0·00081	0·00059
0·3516	1	0·0038	0·00094	0·00053	0·00093	0·0039	0·00079	0·00057	0·00099	0·00074
	2	0·0038	0·00089	0·00050	0·00088	0·0039	0·00074	0·00054	0·00094	0·00069
	3	0·0038	0·00094	0·00053	0·00092	0·0039	0·00078	0·00056	0·00099	0·00073
0·4496	1	0·0051	0·00144	0·00080	0·00138	0·0053	0·00123	0·00085	0·00147	0·00115
	2	0·0050	0·00137	0·00076	0·00132	0·0052	0·00116	0·00081	0·00141	0·00108
	3	0·0050	0·00143	0·00079	0·00136	0·0052	0·00121	0·00085	0·00146	0·00112
0·5854	1	0·0066	0·00184	0·00106	0·00183	0·0069	0·00160	0·00112	0·00193	0·00151
	2	0·0066	0·00176	0·00102	0·00176	0·0068	0·00152	0·00108	0·00187	0·00143
	3	0·0066	0·00183	0·00105	0·00181	0·0068	0·00158	0·00111	0·00192	0·00149
0·6608	1	0·0079	0·00218	0·00126	0·00218	0·0081	0·00192	0·00133	0·00230	0·00181
	2	0·0078	0·00207	0·00121	0·00210	0·0080	0·00181	0·00221	0·00171	0·00171
	3	0·0078	0·00214	0·00124	0·00215	0·0080	0·00187	0·00131	0·00226	0·00177
0·7218	1	0·0091	0·00281	0·00159	0·00272	0·0094	0·00251	0·00168	0·00285	0·00238
	2	0·0090	0·00269	0·00154	0·00263	0·0093	0·00239	0·00163	0·00276	0·00226
	3	0·0090	0·00277	0·00158	0·00267	0·0093	0·00246	0·00166	0·00281	0·00233
0·7750	1	0·0101	0·00312	0·00179	0·00305	0·0104	0·00281	0·00188	0·00319	0·00267
	2	0·0100	0·00298	0·00172	0·00295	0·0103	0·00267	0·00181	0·00309	0·00254
	3	0·0099	0·00305	0·00176	0·00299	0·0102	0·00274	0·00184	0·00314	0·00260
0·8238	1	0·0111	0·00331	0·00193	0·00329	0·0114	0·00300	0·00201	0·00343	0·00286
	2	0·0110	0·00316	0·00186	0·00319	0·0113	0·00286	0·00195	0·00333	0·00272
	3	0·0110	0·00324	0·00190	0·00323	0·0113	0·00293	0·00198	0·00337	0·00279
0·8696	1	0·0122	0·00404	0·00231	0·00389	0·0125	0·00370	0·00241	0·00405	0·00354
	2	0·0121	0·00385	0·00223	0·00377	0·0124	0·00352	0·00233	0·00393	0·00336
	3	0·0121	0·00393	0·00226	0·00381	0·0124	0·00359	0·00236	0·00398	0·00343
0·9119	1	0·0132	0·00486	0·00269	0·00446	0·0136	0·00451	0·00280	0·00464	0·00432
	2	0·0130	0·00460	0·00259	0·00431	0·0134	0·00425	0·00270	0·00449	0·00406
	3	0·0130	0·00469	0·00262	0·00435	0·0133	0·00433	0·00273	0·00453	0·00414

* See footnote to Table 13(a).

TABLE 14 (Cont'd.)

X		δ_0	δ_1	δ_2	δ_3	δ_0^i	δ_1^i	δ_2^i	δ_3^i	δ_1'
0·9518	1	0·0152	0·00650	0·00333	0·00540	0·0156	0·00612	0·00347	0·00561	0·00586
	2	0·0150	0·00605	0·00320	0·00521	0·0154	0·00568	0·00332	0·00542	0·00542
	3	0·0149	0·00616	0·00323	0·00525	0·0153	0·00578	0·00336	0·00546	0·00552
0·9878	1	0·0172	0·00954	0·00418	0·00654	0·0176	0·00912	0·00436	0·00680	0·00872
	2	0·0169	0·00886	0·00404	0·00636	0·0173	0·00845	0·00421	0·00661	0·00807
	3	0·0169	0·00899	0·00406	0·00638	0·0173	0·00857	0·00423	0·00663	0·00819
0·9970	1	0·0177	0·01001	0·00447	0·00700	0·0181	0·00956	0·00465	0·00727	0·00914
	2	0·0175	0·00980	0·00443	0·00692	0·0180	0·00934	0·00462	0·00719	0·00893
	3	0·0174	0·00993	0·00446	0·00694	0·0179	0·00947	0·00465	0·00721	0·00905

TABLE 14 (Cont'd)

(b) Lower Surface

X		δ_0	δ_1	δ_2	δ_3	δ_0^i	δ_1^i	δ_2^i	δ_3^i	δ_1^t
0·2316	1*	0·0019	0·00034	0·00021	0·00038	0·0020	0·00030	0·00022	0·00039	0·00029
	2	0·0019	0·00033	0·00021	0·00037	0·0019	0·00029	0·00021	0·00038	0·00028
	3	0·0020	0·00036	0·00023	0·00040	0·0020	0·00032	0·00023	0·00041	0·00031
0·3197	1	0·0027	0·00053	0·00033	0·00059	0·0028	0·00047	0·00035	0·00061	0·00045
	2	0·0027	0·00052	0·00032	0·00057	0·0028	0·00045	0·00034	0·00060	0·00043
	3	0·0027	0·00055	0·00034	0·00061	0·0028	0·00048	0·00036	0·00064	0·00046
0·4797	1	0·0039	0·00091	0·00055	0·00096	0·0040	0·00080	0·00058	0·00101	0·00076
	2	0·0039	0·00090	0·00054	0·00095	0·0040	0·00079	0·00057	0·00099	0·00075
	3	0·0039	0·00094	0·00057	0·00099	0·0040	0·00083	0·00059	0·00104	0·00079
0·6722	1	0·0064	0·00182	0·00110	0·00188	0·0065	0·00167	0·00114	0·00195	0·00160
	2	0·0063	0·00179	0·00108	0·00185	0·0065	0·00163	0·00112	0·00192	0·00156
	3	0·0063	0·00185	0·00111	0·00189	0·0065	0·00169	0·00115	0·00197	0·00162
0·7693	1	0·0084	0·00243	0·00147	0·00252	0·0086	0·00225	0·00153	0·00261	0·00217
	2	0·0083	0·00233	0·00143	0·00244	0·0085	0·00214	0·00148	0·00252	0·00206
	3	0·0083	0·00239	0·00146	0·00248	0·0085	0·00220	0·00151	0·00257	0·00212
0·8617	1	0·0105	0·00266	0·00169	0·00293	0·0107	0·00246	0·00174	0·00302	0·00238
	2	0·0104	0·00256	0·00164	0·00285	0·0106	0·00235	0·00169	0·00294	0·00229
	3	0·0104	0·00263	0·00167	0·00289	0·0106	0·00242	0·00172	0·00298	0·00234
0·9380	1	0·0124	0·00300	0·00194	0·00337	0·0126	0·00278	0·00199	0·00347	0·00270
	2	0·0124	0·00297	0·00192	0·00335	0·0126	0·00275	0·00198	0·00343	0·00267
	3	0·0124	0·00304	0·00195	0·00339	0·0126	0·00281	0·00201	0·00347	0·00273
0·9862	1	0·0132	0·00309	0·00203	0·00355	0·0134	0·00287	0·00208	0·00364	0·00279
	2	0·0131	0·00306	0·00201	0·00352	0·0133	0·00283	0·00206	0·00360	0·00276
	3	0·0131	0·00313	0·00203	0·00356	0·0133	0·00289	0·00209	0·00364	0·00282
0·9970	1	0·0136	0·00305	0·00199	0·00347	0·0138	0·00283	0·00204	0·00356	0·00275
	2	0·0135	0·00305	0·00199	0·00347	0·0137	0·00281	0·00203	0·00355	0·00275
	3	0·0135	0·00311	0·00200	0·00350	0·0137	0·00287	0·00206	0·00359	0·00281

* See footnote to Table 13(a).

TABLE 15

Boundary-Layer Integral Results

Section 2815: $C_L = 0{\cdot}70$, $M = 0{\cdot}664$, $R = 15{\cdot}6 \times 10^6$

(a) Upper Surface

X		δ_0	δ_1	δ_2	δ_3	δ_0^i	δ_1^i	δ_2^i	δ_3^i	δ_1^t
0·4496	1*	0·0053	0·00135	0·00076	0·00133	0·0055	0·00114	0·00081	0·00142	0·00106
	2	0·0053	0·00130	0·00073	0·00128	0·0055	0·00108	0·00078	0·00137	0·00100
	3	0·0053	0·00135	0·00076	0·00133	0·0055	0·00133	0·00081	0·00142	0·00105
0·5854	1	0·0073	0·00207	0·00118	0·00204	0·0076	0·00180	0·00125	0·00216	0·00169
	2	0·0073	0·00196	0·00113	0·00196	0·0075	0·00169	0·00120	0·00207	0·00158
	3	0·0072	0·00203	0·00116	0·00200	0·0075	0·00175	0·00123	0·00213	0·00164
0·6608	1	0·0086	0·00249	0·00143	0·00246	0·0089	0·00218	0·00151	0·00259	0·00206
	2	0·0085	0·00238	0·00137	0·00238	0·0088	0·00208	0·00145	0·00251	0·00196
	3	0·0085	0·00245	0·00140	0·00242	0·0088	0·00214	0·00148	0·00256	0·00201
0·7218	1	0·0100	0·00309	0·00175	0·00298	0·0103	0·00275	0·00184	0·00213	0·00260
	2	0·0099	0·00296	0·00169	0·00289	0·0103	0·00263	0·00179	0·00305	0·00248
	3	0·0099	0·00304	0·00173	0·00294	0·0102	0·00270	0·00182	0·00310	0·00255
0·7750	1	0·0112	0·00351	0·00200	0·00341	0·0115	0·00316	0·00210	0·00357	0·00300
	2	0·0111	0·00333	0·00193	0·00330	0·0114	0·00298	0·00202	0·00345	0·00284
	3	0·0111	0·00340	0·00196	0·00335	0·0114	0·00305	0·00206	0·00350	0·00290
0·8238	1	0·0124	0·00418	0·00235	0·00395	0·012	0·00381	0·00246	0·00413	0·00362
	2	0·0123	0·00397	0·00226	0·00383	0·0126	0·00360	0·00237	0·00401	0·00342
	3	0·0122	0·00406	0·00230	0·00387	0·0126	0·00368	0·00241	0·00405	0·00350
0·8696	1	0·0138	0·00494	0·00272	0·00453	0·0142	0·00455	0·00285	0·00473	0·00433
	2	0·0136	0·00472	0·00264	0·00441	0·0140	0·00434	0·00277	0·00461	0·00413
	3	0·0136	0·00481	0·00268	0·00445	0·0140	0·00442	0·00280	0·00466	0·00421
0·9119	1	0·0149	0·00601	0·00318	0·00521	0·0153	0·00560	0·00332	0·00543	0·00534
	2	0·0147	0·00564	0·00306	0·00504	0·0151	0·00523	0·00320	0·00526	0·00499
	3	0·0146	0·00574	0·00309	0·00507	0·0150	0·00533	0·00327	0·00529	0·00508
0·9518	1	0·0166	0·00800	0·00390	0·00623	0·0171	0·00756	0·00407	0·00648	0·00722
	2	0·0164	0·00750	0·00377	0·00606	0·0168	0·00707	0·00393	0·00631	0·00675
	3	0·0163	0·00762	0·00380	0·00609	0·0168	0·00718	0·00397	0·00635	0·00686
0·9970	1	0·0193	0·01211	0·00483	0·00743	0·0198	0·01164	0·00503	0·00772	0·01110
	2	0·0189	0·01154	0·00470	0·00728	0·0194	0·01107	0·00490	0·00757	0·01057
	3	0·0188	0·01168	0·00472	0·00729	0·0193	0·01121	0·00492	0·00759	0·01070

* See footnote to Table 13(a).

TABLE 15 (Cont'd.)

(b) Lower Surface

X		δ_0	δ_1	δ_2	δ_3	δ_0^i	δ_1^i	δ_2^i	δ_3^i	δ_1^i
0·2316	1*	0·0019	0·00030	0·00019	0·00034	0·0019	0·00027	0·00020	0·00035	0·00026
	2	0·0019	0·00029	0·00018	0·00033	0·0019	0·00026	0·00019	0·00034	0·00025
	3	0·0019	0·00031	0·00020	0·00036	0·0020	0·00028	0·00021	0·00037	0·00027
0·3197	1	0·0027	0·00050	0·00032	0·00057	0·0028	0·00044	0·00033	0·00059	0·00043
	2	0·0027	0·00049	0·00031	0·00056	0·0028	0·00043	0·00032	0·00058	0·00041
	3	0·0027	0·00052	0·00033	0·00060	0·0028	0·00046	0·00035	0·00062	0·00044
0·4797	1	0·0039	0·00082	0·00050	0·00089	0·0039	0·00072	0·00053	0·00093	0·00069
	2	0·0038	0·00079	0·00049	0·00087	0·0039	0·00070	0·00051	0·00090	0·00067
	3	0·0038	0·00084	0·00052	0·00091	0·0039	0·00074	0·00054	0·00095	0·00071
0·6722	1	0·0060	0·00148	0·00093	0·00161	0·0061	0·00135	0·00096	0·00167	0·00130
	2	0·0059	0·00142	0·00090	0·00156	0·0061	0·00129	0·00092	0·00161	0·00124
	3	0·0059	0·00147	0·00093	0·00160	0·0061	0·00134	0·00095	0·00166	0·00129
0·7693	1	0·0081	0·00214	0·00133	0·00230	0·0083	0·00197	0·00138	0·00238	0·00190
	2	0·0081	0·00206	0·00129	0·00224	0·0082	0·00189	0·00133	0·00232	0·00183
	3	0·0081	0·00212	0·00132	0·00229	0·0082	0·00195	0·00137	0·00236	0·00188
0·8617	1	0·0101	0·00260	0·00165	0·00285	0·0103	0·00241	0·00169	0·00293	0·00234
	2	0·0100	0·00248	0·00158	0·00275	0·0102	0·00229	0·00163	0·00283	0·00222
	3	0·0100	0·00254	0·00161	0·00280	0·0101	0·00235	0·00166	0·00288	0·00228
0·9380	1	0·0116	0·00268	0·00176	0·00308	0·0118	0·00248	0·00181	0·00316	0·00241
	2	0·0116	0·00271	0·00177	0·00310	0·0118	0·00251	0·00182	0·00319	0·00244
	3	0·0116	0·00277	0·00180	0·00314	0·0118	0·00257	0·00185	0·00323	0·00249
0·9970	1	0·0128	0·00276	0·00184	0·00325	0·0130	0·00256	0·00189	0·00333	0·00249
	2	0·0128	0·00278	0·00184	0·00325	0·0130	0·00257	0·00189	0·00334	0·00251
	3	0·0128	0·00284	0·00187	0·00329	0·0130	0·00263	0·00192	0·00337	0·00256

* See footnote to Table 13(a).

TABLE 16

Section 2814: $M = 0{\cdot}725$, $C_L = 0{\cdot}42$, $R = 15 \times 10^6$

Wake Survey Data

X (chords aft of leading edge)	Uncorrected data			Data corrected for survey rig interference			Data corrected for survey rig interference and pitot displacement		
	$\delta^{(0\cdot995)}$	δ_1	δ_2	$\delta^{(0\cdot995)}$	δ_1	δ_2	$\delta^{(0\cdot995)}$	δ_1	δ_2
1·020	0·0423	0·01068	0·00596	0·0414	0·01017	0·00576	0·0416	0·01029	0·00581
1·050	0·0417	0·00910	0·00558	0·0410	0·00874	0·00540	0·0412	0·00884	0·00545
1·088	0·0433	0·00798	0·00522	0·0425	0·00767	0·00505	0·0427	0·00775	0·00509
1·108	0·0443	0·00766	0·00510	0·0439	0·00748	0·00499	0·0441	0·00755	0·00503
1·128	0·0445	0·00733	0·00497	0·0440	0·00717	0·00486	0·0442	0·00724	0·00490
1·154	0·0457	0·00711	0·00489	0·0452	0·00696	0·00479	0·0454	0·00702	0·00483
1·188	0·0472	0·00686	0·00481	0·0467	0·00672	0·00471	0·0469	0·00678	0·00475
1·221	0·0490	0·00665	0·00472	0·0485	0·00652	0·00463	0·0487	0·00657	0·00466
1·388	0·0580	0·00594	0·00445	0·0574	0·00582	0·00436	0·0576	0·00586	0·00439
1·554	0·0666	0·00576	0·00437	0·0658	0·00564	0·00427	0·0660	0·00567	0·00429
1·888	0·0828	0·00558	0·00434	0·0817	0·00542	0·00421	0·0819	0·00544	0·00423

TABLE 17

Section 2815: $M = 0{\cdot}66$, $R = 15{\cdot}6 \times 10^6$

Wake Survey Data

C_L	X (chords aft of leading edge)	Uncorrected data			Data corrected for survey rig interference			Data corrected for survey rig interference and pitot displacement		
		$\delta^{(0\cdot995)}$	δ_1	δ_2	$\delta^{(0\cdot995)}$	δ_1	δ_2	$\delta^{(0\cdot995)}$	δ_1	δ_2
0·51	1·042	0·0443	0·01029	0·00617	0·0437	0·01007	0·00609	0·0439	0·01017	0·00614
	1·100	0·0448	0·00832	0·00552	0·0440	0·00811	0·00543	0·0442	0·00819	0·00547
	1·170	0·0476	0·00728	0·00512	0·0466	0·00710	0·00503	0·0468	0·00716	0·00507
	1·300	0·0537	0·00640	0·00475	0·0526	0·00625	0·00466	0·0528	0·00630	0·00469
	1·600	0·0720	0·00576	0·00450	0·0699	0·00559	0·00440	0·0701	0·00562	0·00442
0·70	1·100	0·0465	0·00908	0·00590	0·0451	0·00878	0·00580	0·0453	0·00886	0·00585
	1·300	0·0563	0·00683	0·00504	0·0555	0·00673	0·00496	0·0557	0·00687	0·00499
	1·600	0·0758	0·00609	0·00475	0·0746	0·00598	0·00465	0·0748	0·00601	0·00467

Note: $\delta^{(0\cdot995)}$ is the width of wake between points at which $u/u_1 = 0{\cdot}995$.

TABLE 18

Section 2814: $M = 0{\cdot}725$, $R = 15 \times 10^6$, $C_L = 0{\cdot}42$

Skin Friction Coefficients

X	M_1	$\frac{\mu_1}{\nu_1} \times 10^{-6}$	C_f Preston tube			C_f Clauser method	C_f using integral parameters				C_f razor-blade	C_f flat-plate law
			Hopkins and Keener calib.	Re-analysed Hopkins and Keener data	Patel calib.		Winter Rotta Smith	(Green (1) (Spence transform)	Nash MacDonald	Green (2)		
Upper surface												
0·3167	1·0065	17·29	0·00263	0·00272	0·00273	0·00264	0·00264	0·00264	0·00264	0·00259	0·00248	0·00250
0·4166	0·9920	17·22	0·00247	0·00256	0·00255	0·00245	0·00241	0·00241	0·00244	0·00236	0·00233	0·00240
0·5166	1·0139	17·32	0·00262	0·00262	0·00272	0·00242	0·00238	0·00240	0·00245	0·00236	0·00231	0·00233
0·6256	0·9326	16·89	0·00195	0·00201	0·00198	0·00189	0·00183	0·00188	0·00188	0·00183	0·00161	
0·7499	0·8384	16·18	0·00176	0·00183	0·00179	0·00175	0·00161	0·00165	0·00169	0·00161	0·00147	
0·8457	0·7631	15·44	0·00155	0·00161	0·00157	0·00143	0·00137	0·00142	0·00146	0·00139	0·00123	
0·9305	0·7024	14·72	0·00114	0·00120	0·00116	0·00112	0·00107	0·00111	0·00114	0·00108	0·00110	
0·9682	0·6683	14·27	0·00079	0·00086	0·00082	0·00087	0·00080	0·00083	0·00085	0·00079	0·00076	
0·9918	0·6408	13·89	0·00047	0·00052	0·00050	0·00065	0·00056	0·00059	0·00055	0·00054	0·00054	
0·9970	0·6340	13·78	0·00041	0·00046	0·00044	0·00063	0·00052	0·00055	0·00049	0·00049	0·00051*	
Lower surface												
0·3500	0·9087	16·73	0·00285	0·00295	0·00296	0·00280	0·00289	0·00281	0·00286	0·00275	0·00273	
0·5000	0·8339	16·14	0·00226	0·00233	0·00231	0·00220	0·00209	0·00214	0·00210	0·00205	0·00177	
0·6332	0·7331	15·10	0·00165	0·00172	0·00168	0·00160	0·00161	0·00165	0·00165	0·00158	0·00158	
0·7665	0·6584	14·14	0·00155	0·00163	0·00158	0·00160	0·00155	0·00158	0·00160	0·00154	0·00159	
0·8332	0·6382	13·85	0·00161	0·00170	0·00165	0·00155	0·00153	0·00157	0·00160	0·00155	0·00156	
0·8998	0·6216	13·61	0·00167	0·00176	0·00171	0·00171	0·00164	0·00166	0·00171	0·00167	0·00165	
0·9499	0·6128	13·47	0·00185	0·00194	0·00189	0·00173	0·00171	0·00174	0·00177	0·00177	0·00174	
0·9833	0·6196	13·58	0·00198	0·00208	0·00203	0·00185	0·00182	0·00182	0·00190	0·00187	0·00186	
0·9970	0·6277	13·70	0·00227	0·00237	0·00233	0·00193	0·00196	0·00197	0·00203	0·00205	0·00192*	

* No razor-blade at this station: C_f obtained by interpolation.

TABLE 19

Section 2815: $M = 0{\cdot}661$, $R = 15{\cdot}6 \times 10^6$, $C_L = 0{\cdot}51$

Skin Friction Coefficients

X	M_1	$\frac{\mu_1}{\nu_1} \times 10^{-6}$	C_f Preston tube: Hopkins and Keener calib.	C_f Preston tube: Re-analysed Hopkins and Keener data	C_f Preston tube: Patel calib.	C_f Clauser method	C_f using integral parameters: Winter Rotta Smith	C_f using integral parameters: Green (1) (Spence transform)	C_f using integral parameters: Nash MacDonald	C_f using integral parameters: Green (2)	C_f razor-blade	C_f flat-plate law
Upper surface												
0·2716	0·9919	18·95	0·00240	0·00245	0·00247	0·00248	0·00233	0·00236	0·00237	0·00226	0·00218	0·00250
0·3516	0·9780	18·88	0·00223	0·00228	0·00228	0·00224	0·00219	0·00222	0·00218	0·00213	0·00212	
0·4496	0·9246	18·53	0·00190	0·00194	0·00193	0·00191	0·00180	0·00190	0·00191	0·00183	0·00190	
0·5854	0·8425	17·85	0·00175	0·00180	0·00178	0·00181	0·00176	0·00181	0·00183	0·00177	0·00178	
0·6608	0·8012	17·42	0·00170	0·00175	0·00173	0·00175	0·00165	0·00169	0·00176	0·00166	0·00167	
0·7218	0·7638	17·00	0·00150	0·00155	0·00152	0·00152	0·00144	0·00150	0·00152	0·00147	0·00144	
0·7750	0·7278	16·55	0·00153	0·00159	0·00155	0·00148	0·00142	0·00148	0·00149	0·00146	0·00145	
0·8238	0·6976	16·14	0·00160	0·00165	0·00162	0·00151	0·00140	0·00146	0·00149	0·00144	0·00130	
0·8696	0·6682	15·71	0·00138	0·00144	0·00141	0·00135	0·00123	0·00128	0·00133	0·00126	0·00128	
0·9119	0·6374	15·23	0·00113	0·00119	0·00115	0·00113	0·00107	0·00110	0·00115	0·00108	0·00115	
0·9518	0·5995	14·61	0·00076	0·00082	0·00078	0·00085	0·00079	0·00083	0·00084	0·00080	0·00087*	
0·9878	0·5667	14·03	0·00031	0·00035	0·00031	0·00052	0·00043	0·00046	0·00037	0·00039	0·00041	
0·9970	0·5618	13·94	0·00026	0·00030	0·00026		0·00035	0·00037	0·00026	0·00029	0·00025*	
Lower surface												
0·2316	0·7320	16·60	0·00335	0·00344	0·00351	0·00324	0·00313	0·00313		0·00305	0·00287	
0·3197	0·7765	17·15	0·00289	0·00297	0·00301	0·00274	0·00273	0·00275	0·00279	0·00267	0·00272	
0·4797	0·7783	17·17	0·00228	0·00234	0·00235	0·00220	0·00222	0·00227	0·00218	0·00220	0·00218	
0·6722	0·6637	15·64	0·00174	0·00180	0·00177	0·00175	0·00171	0·00177	0·00175	0·00171	0·00175	
0·7693	0·6214	14·97	0·00166	0·00173	0·00169	0·00167	0·00162	0·00166	0·00166	0·00162	0·00166	
0·8617	0·5936	14·50	0·00190	0·00198	0·00194	0·00180	0·00173	0·00177	0·00178	0·00176	0·00168	
0·9380	0·5743	14·16	0·00190	0·00197	0·00194	0·00175	0·00167	0·00170	0·00173	0·00171	0·00165*	
0·9862	0·5633	13·97	0·00196	0·00205	0·00201	0·00178	0·00168	0·00171	0·00176	0·00173	0·00164	
0·9970	0·5610	13·92	0·00184	0·00192	0·00188	0·00178	0·00168	0·00175	0·00175	0·00172	0·00162*	

* No razor-blade at this station; C_f obtained by interpolation.

TABLE 20

Section 2815: $M = 0{\cdot}664$, $R = 15{\cdot}6 \times 10^6$, $C_L = 0{\cdot}70$

Skin Friction Coefficients

X	M_1	$\frac{\mu_1}{\nu_1} \times 10^{-6}$	C_f Preston tube			C_f Clauser method	C_f using integral parameters				C_f razor-blade
			Hopkins and Keener calib.	Re-analysed Hopkins and Keener data	Patel calib.		Winter Rotta Smith	Green (1) (Spence transform)	Nash MacDonald	Green (2)	
Upper surface											
0·4496	0·9511	18·63	0·00214	0·00219	0·00219	0·00205	0·00194	0·00202	0·00200	0·00196	0·00181
0·5854	0·8573	17·91	0·00182	0·00187	0·00185	0·00176	0·00168	0·00177	0·00177	0·00174	0·00169
0·6608	0·8106	17·45	0·00169	0·00173	0·00171	0·00168	0·00156	0·00163	0·00165	0·00160	0·00155
0·7218	0·7691	16·99	0·00141	0·00146	0·00142	0·00146	0·00138	0·00144	0·00147	0·00142	0·00133
0·7750	0·7320	16·53	0·00146	0·00151	0·00148	0·00143	0·00136	0·00141	0·00147	0·00140	0·00132
0·8238	0·6990	16·09	0·00129	0·00134	0·00131	0·00130	0·00121	0·00126	0·00131	0·00124	0·00119
0·8696	0·6687	15·65	0·00113	0·00119	0·00115	0·00112	0·00107	0·00112	0·00116	0·00111	0·00113
0·9119	0·6365	15·15	0·00089	0·00095	0·00091	0·00096	0·00089	0·00094	0·00096	0·00091	0·00100
0·9518	0·6012	14·57	0·00061	0·00066	0·00063	0·00077	0·00064	0·00067	0·00066	0·00063	0·00072*
0·9970	0·5672	13·98	0·00018	0·00022	0·00018	0·00040	0·00028	0·00030	0·00017	0·00020	0·00018*
Lower surface											
0·2316	0·6938	16·01	0·00368	0·00379	0·00387	0·00350	0·00325	0·00328	0·00331	0·00322	0·00300
0·3197	0·7429	16·67	0·00312	0·00320	0·00325	0·00294	0·00284	0·00290	0·00293	0·00283	0·00277
0·4797	0·7580	16·85	0·00250	0·00257	0·00258	0·00240	0·00240	0·00243	0·00238	0·00236	0·00224
0·6722	0·6548	15·44	0·00213	0·00220	0·00218	0·00205	0·00200	0·00205	0·00201	0·00201	0·00187
0·7693	0·6175	14·84	0·00185	0·00193	0·00189	0·00183	0·00176	0·00180	0·00181	0·00177	0·00176
0·8617	0·5923	14·42	0·00185	0·00194	0·00189	0·00181	0·00174	0·00177	0·00179	0·00176	0·00176
0·9380	0·5764	14·14	0·00209	0·00218	0·00215	0·00182	0·00178	0·00181	0·00183	0·00183	0·00175*
0·9970	0·5666	13·96	0·00203	0·00212	0·00208	0·00188	0·00181	0·00183	0·00186	0·00185	0·00173*

* No razor-blade at these stations: C_f obtained by interpolation, using additional measurements at $X \simeq 0{\cdot}987$.

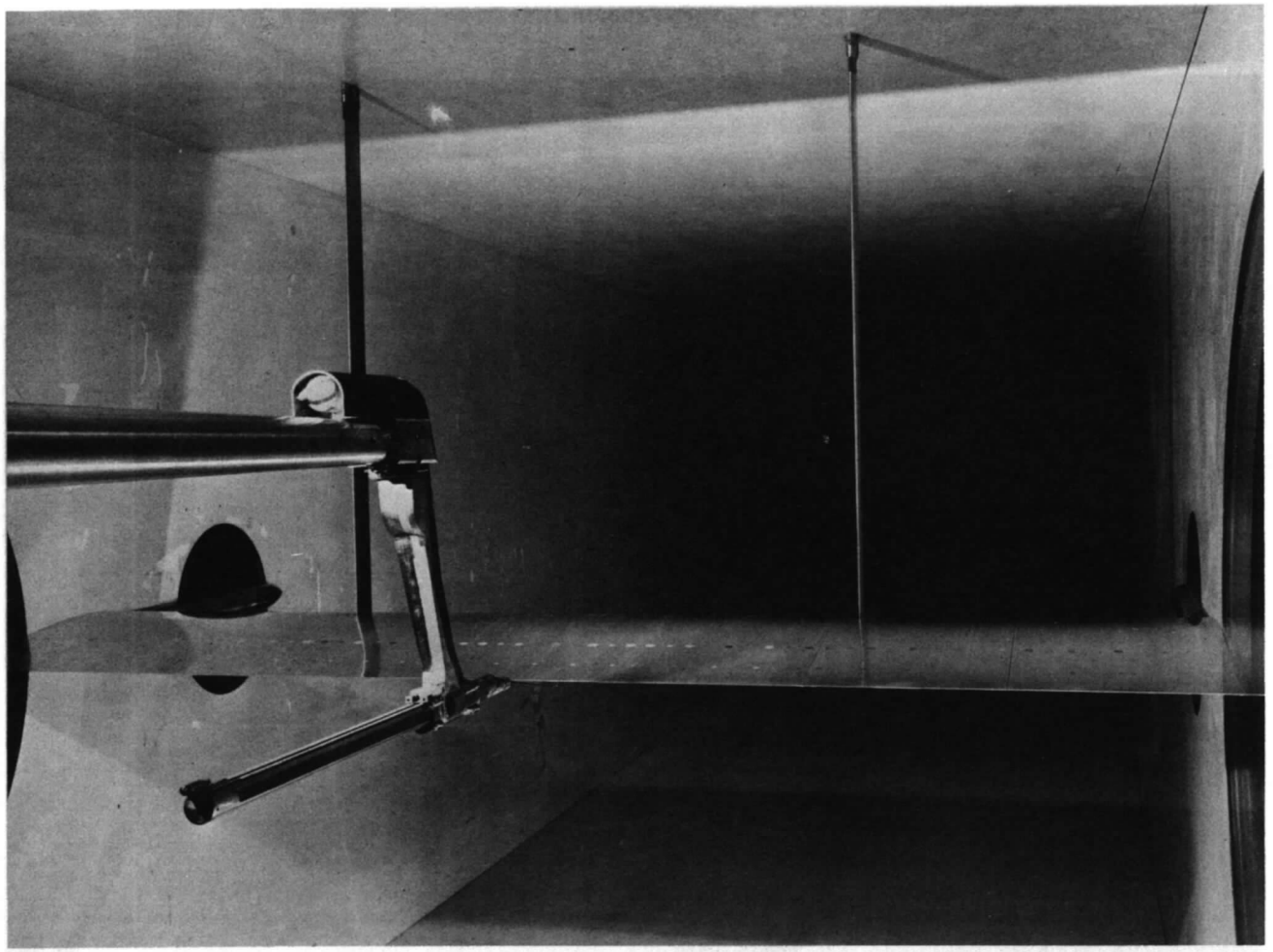

FIG. 1. Rear view of model and survey rig in tunnel.

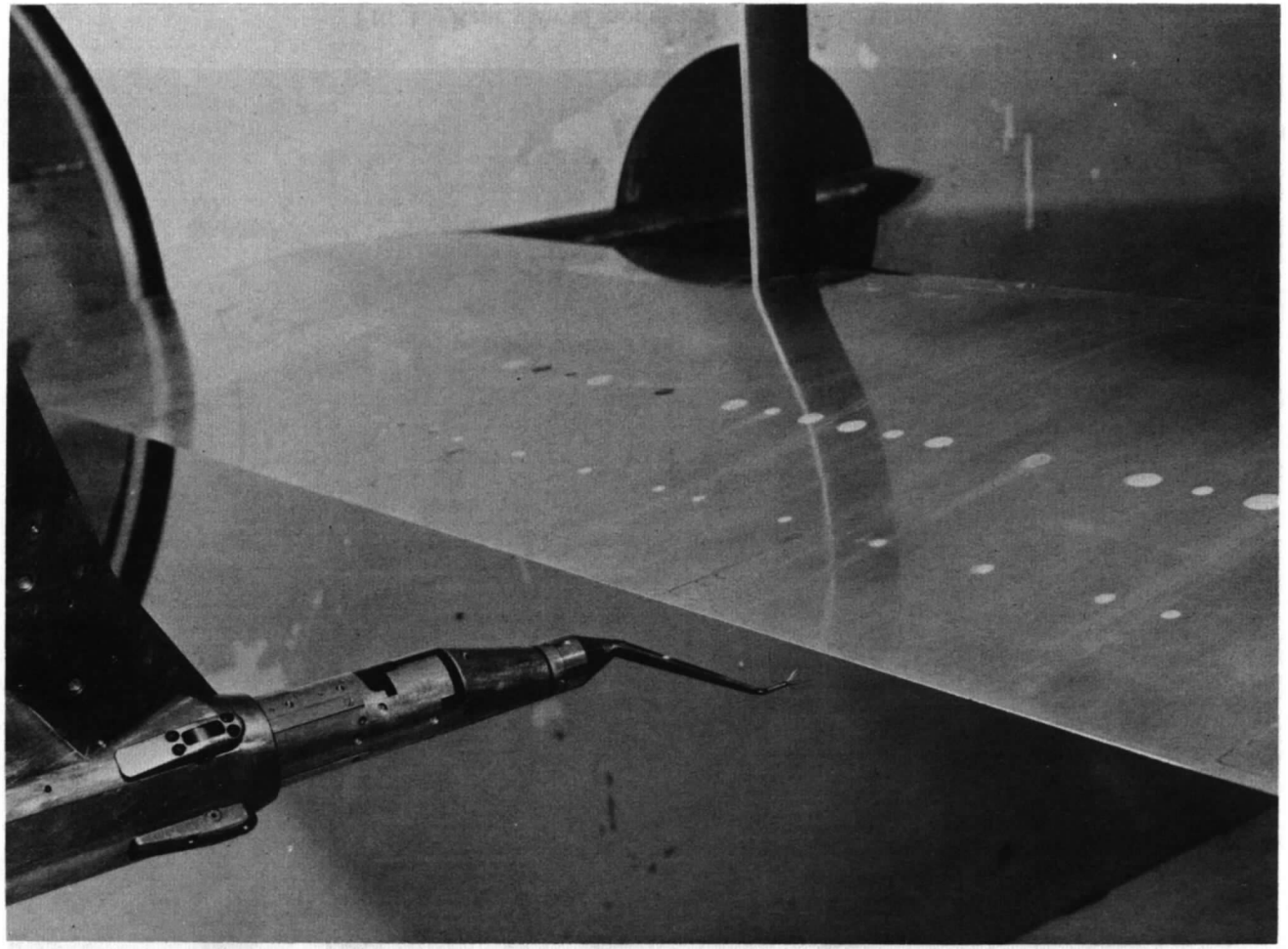

FIG. 2. Survey rig near trailing edge of R.A.E. 2815 section.

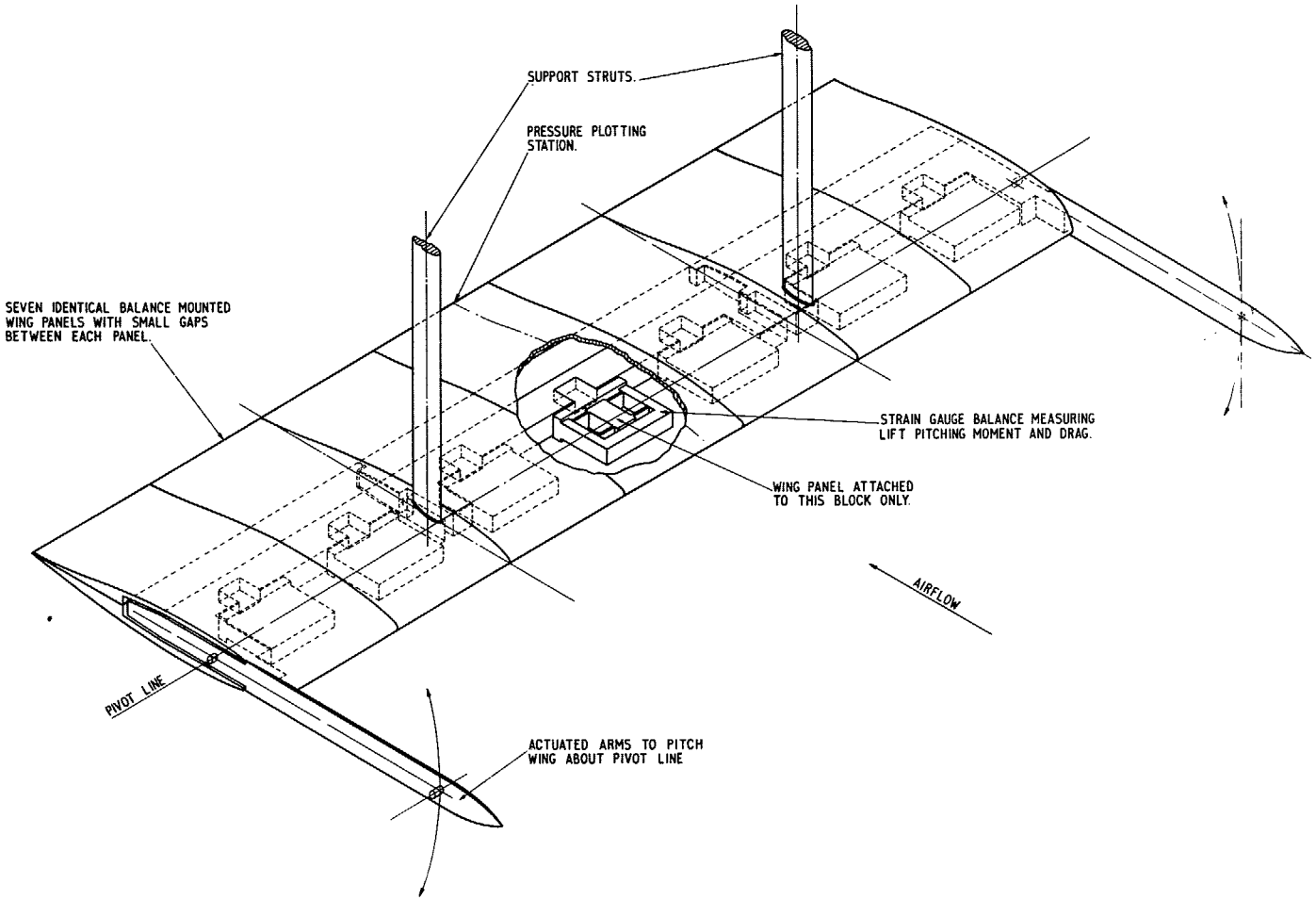

FIG. 3. Isometric sketch of wing and support system.

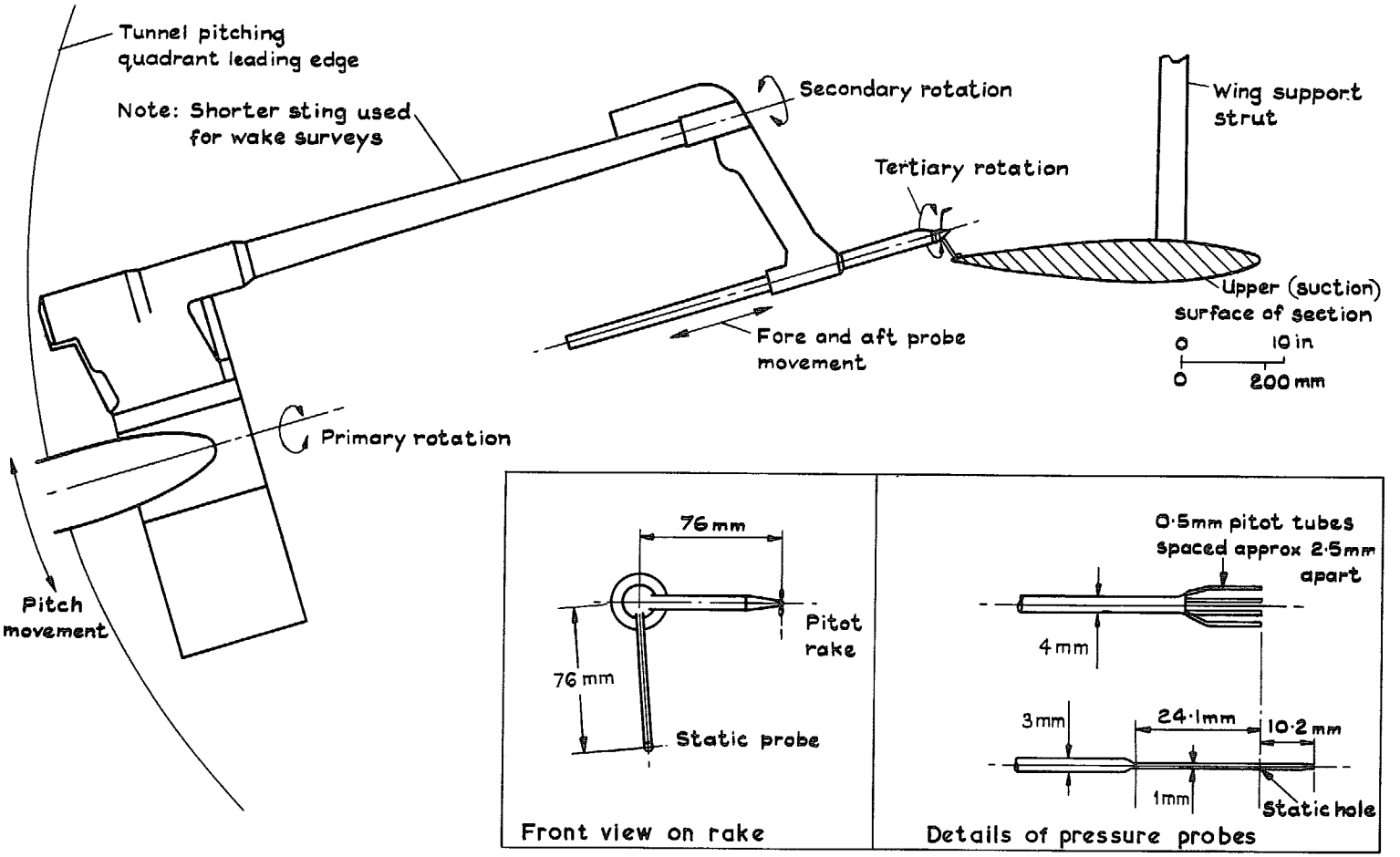

FIG. 4. Sketch of survey apparatus.

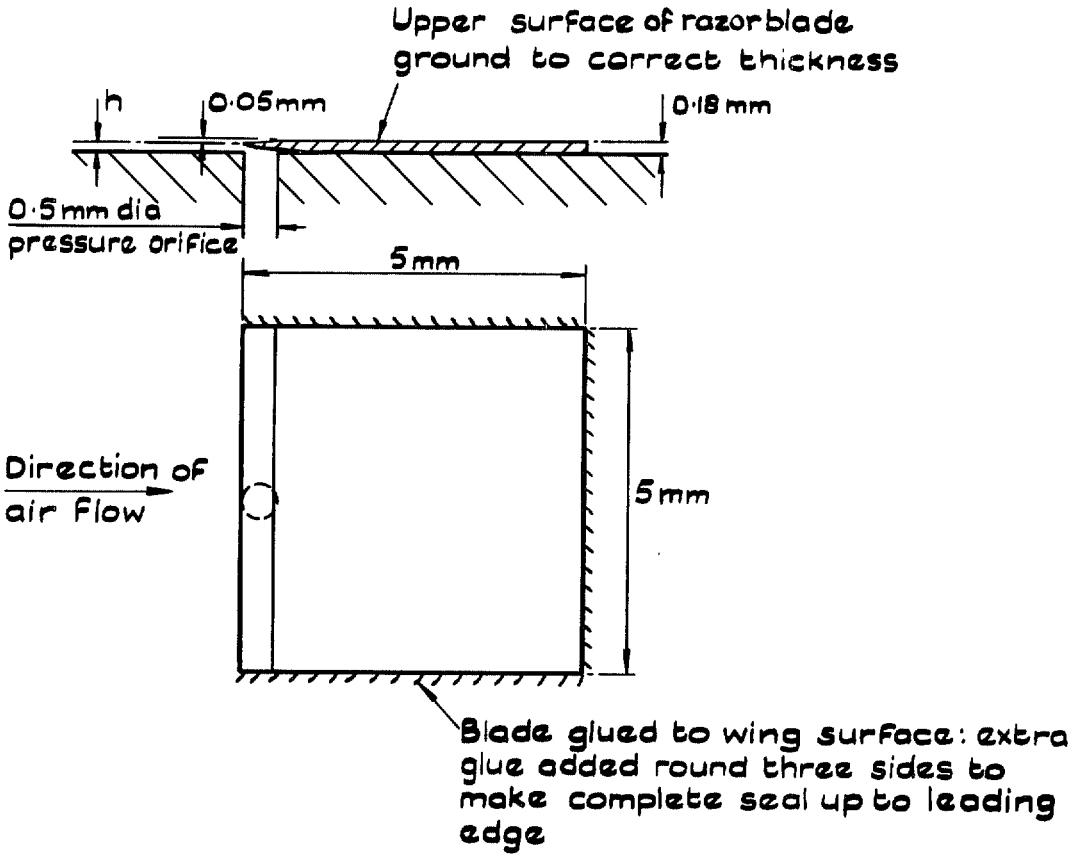

FIG. 5. Razor blade configuration.

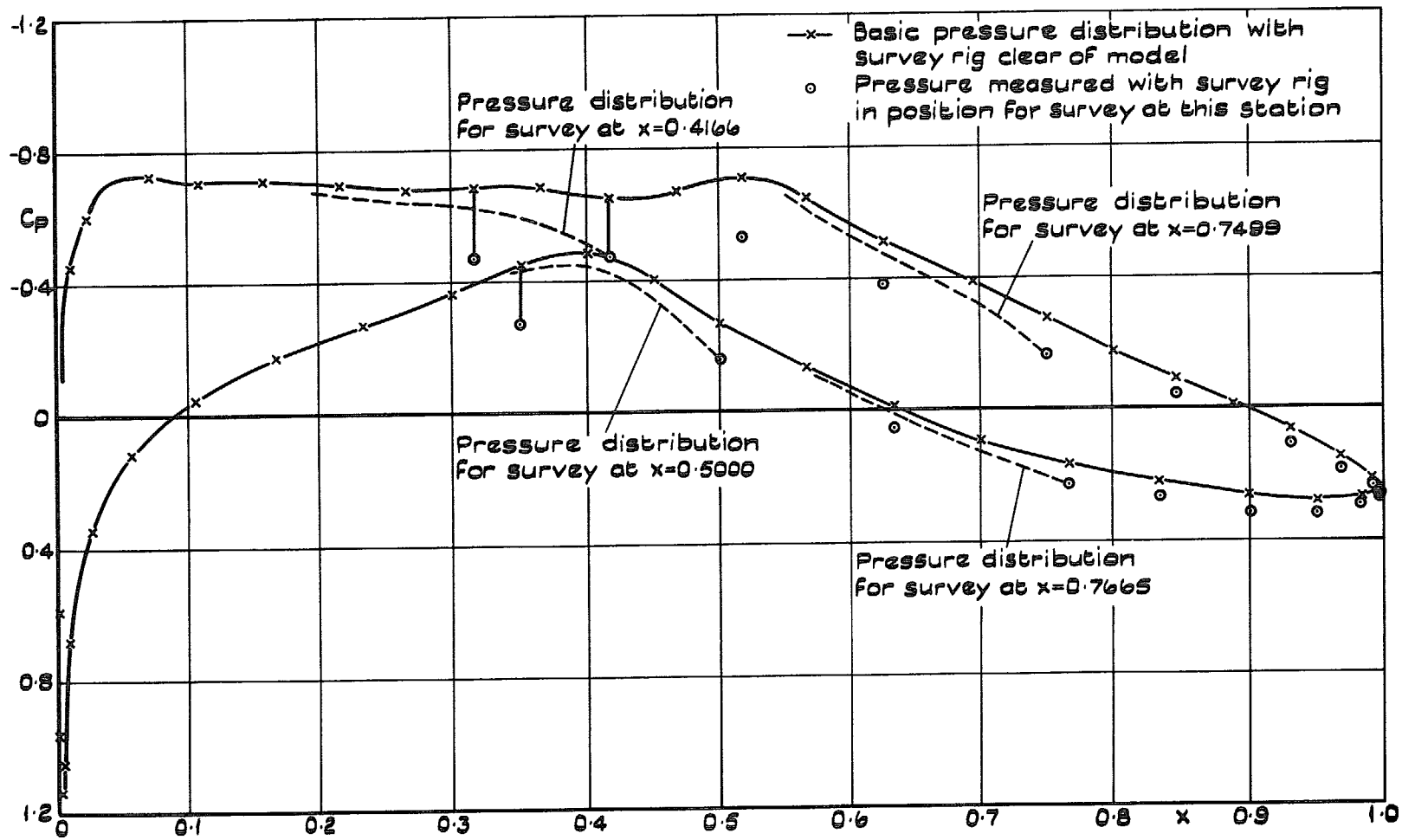

FIG. 6. Pressure distribution on section 2814: $M = 0{\cdot}725$, $C_L = 0{\cdot}42$, $R = 15 \times 10^6$.

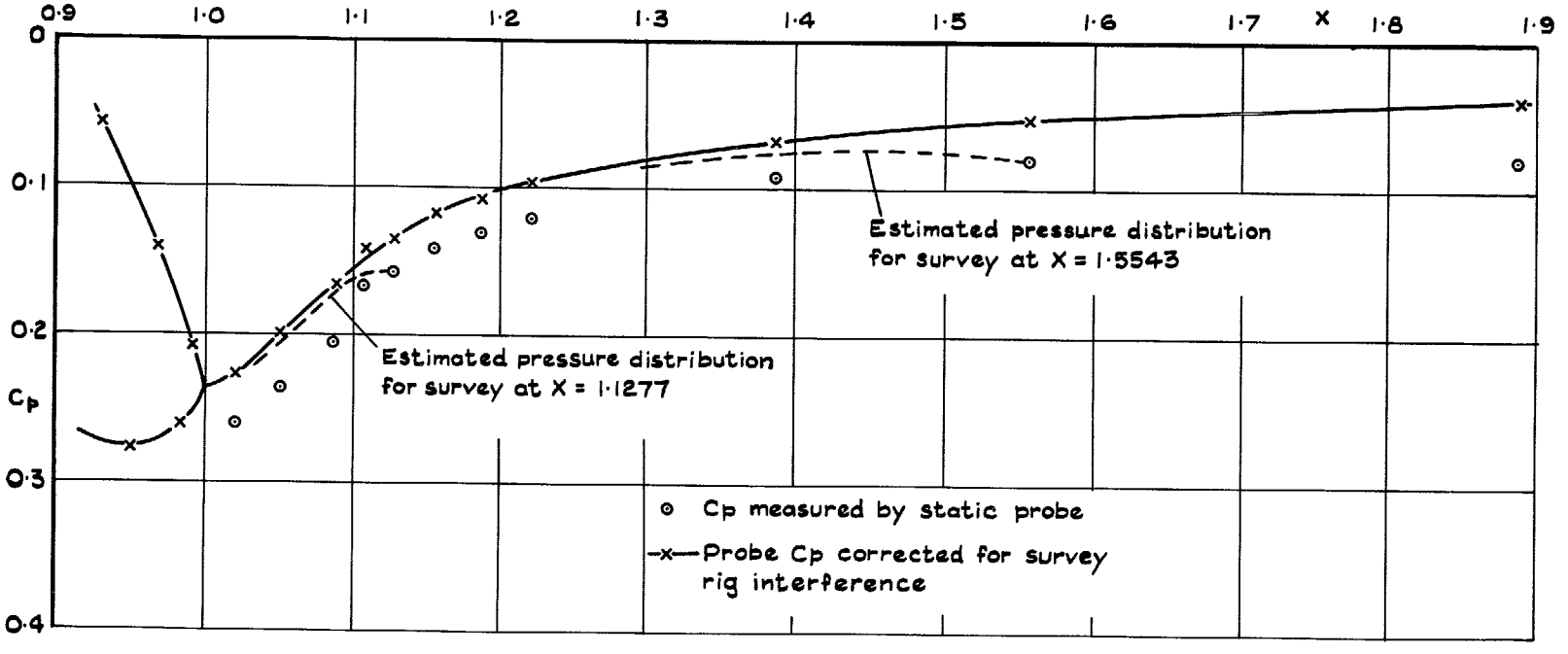

FIG. 7. Wake pressure distribution for section 2814: $M = 0{\cdot}725$, $C_L = 0{\cdot}42$, $R = 15 \times 10^6$.

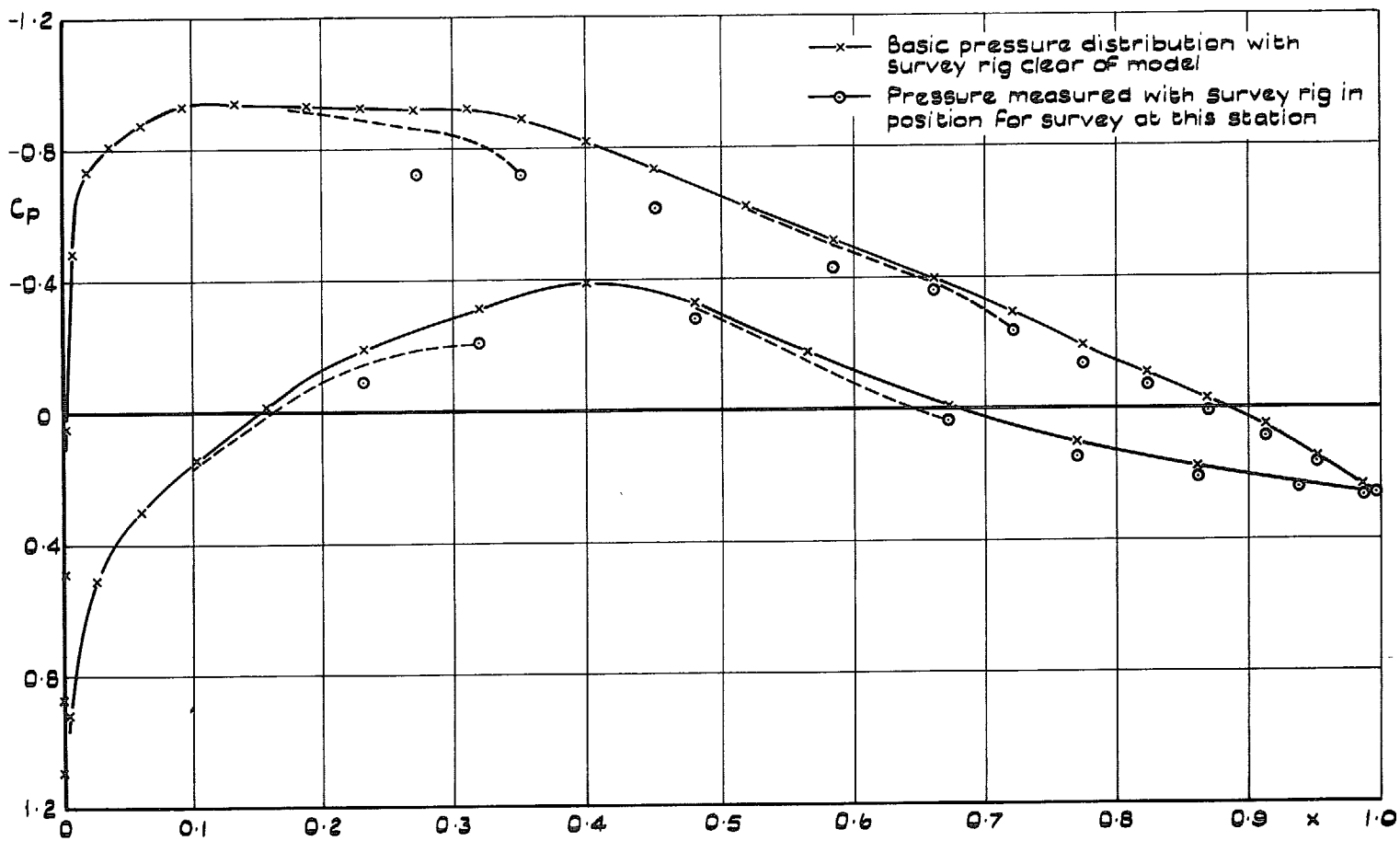

FIG. 8. Pressure distribution on section 2815; $C_L = 0{\cdot}51$, $M = 0{\cdot}661$, $R = 15{\cdot}6 \times 10^6$.

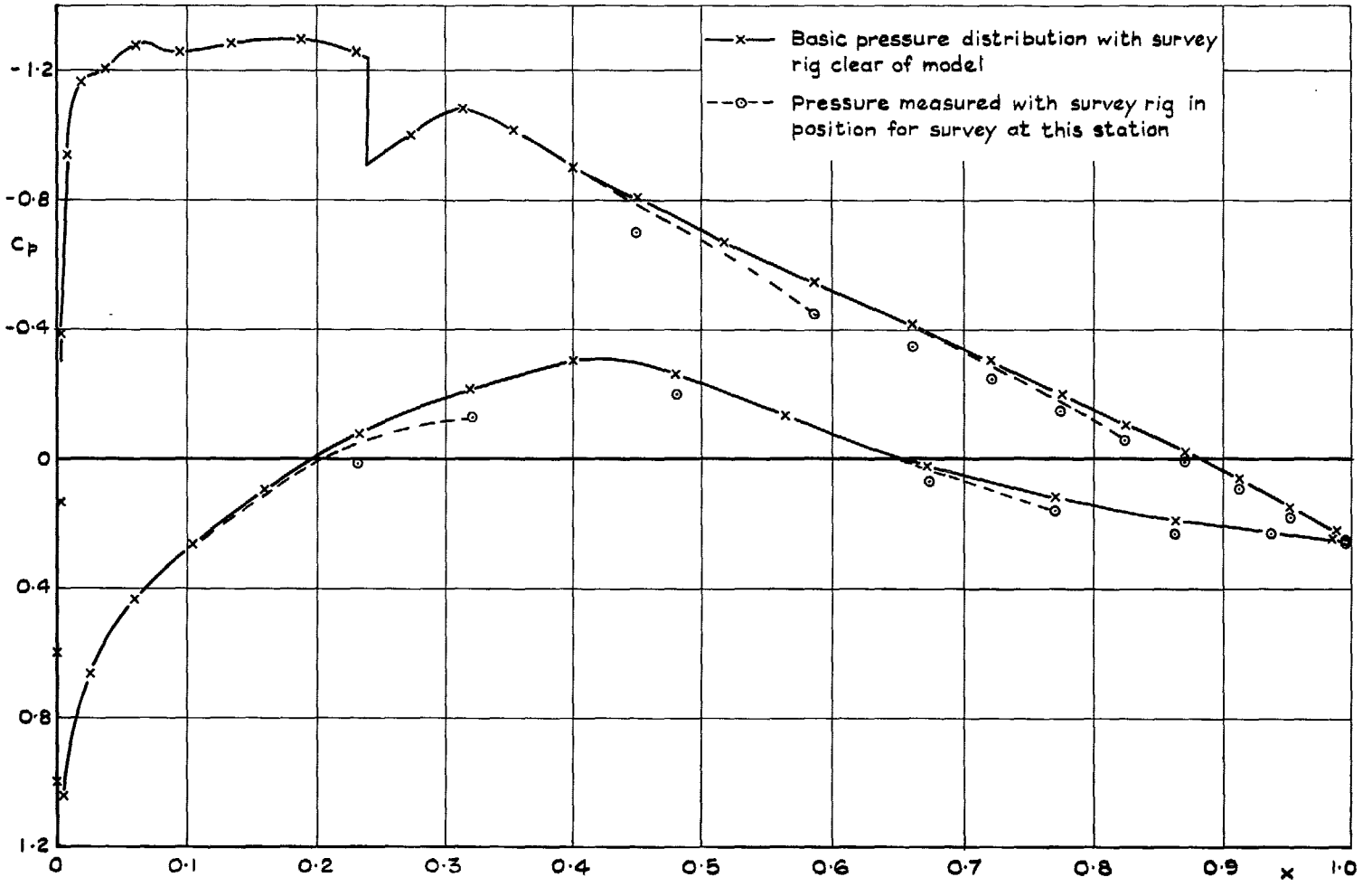

FIG. 9. Pressure distribution on section 2815; $C_L = 0{\cdot}70$, $M = 0{\cdot}664$, $R = 15{\cdot}6 \times 10^6$.

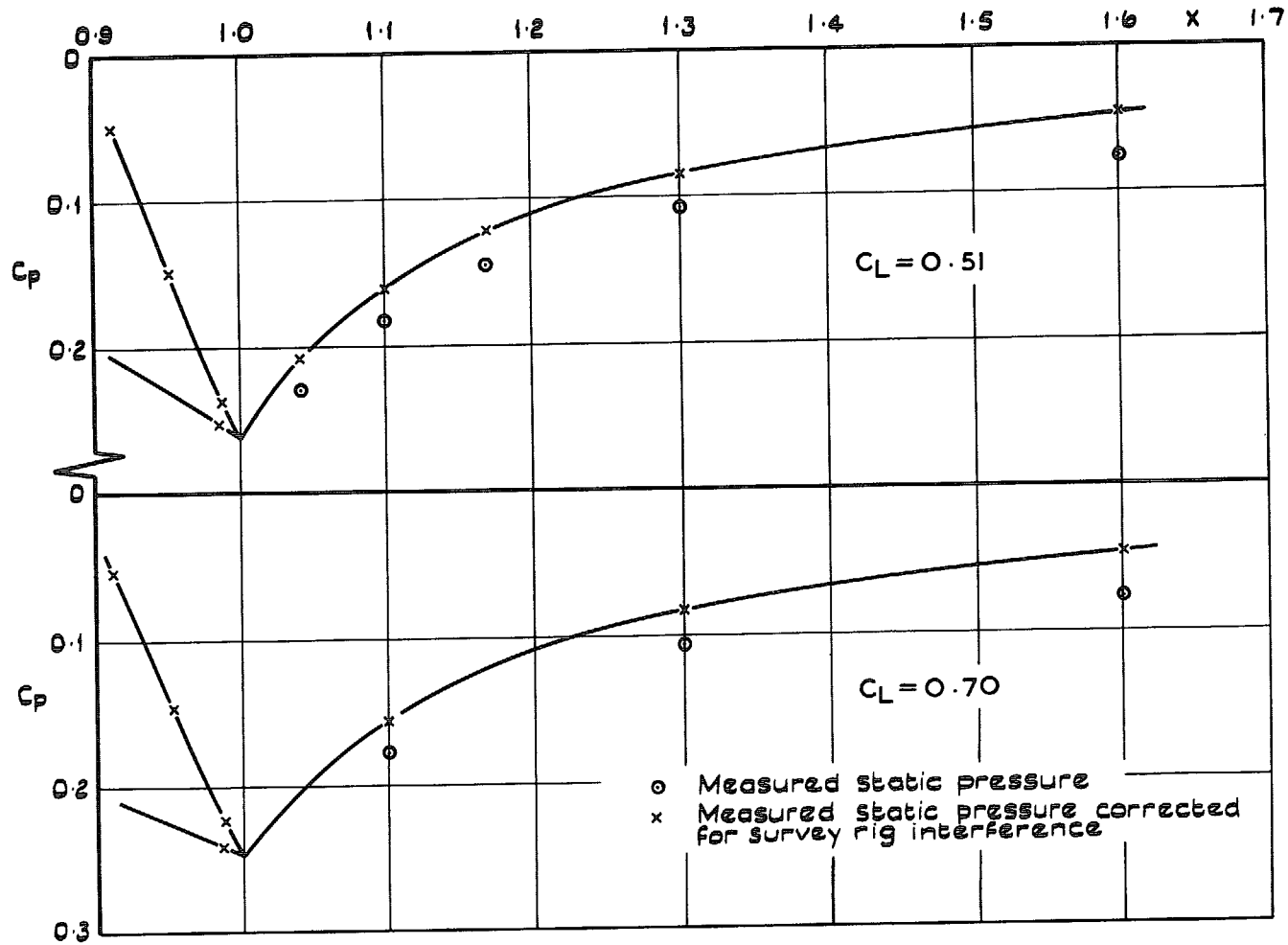

FIG. 10. Pressure distributions in wake of section 2815; $M = 0{\cdot}66$, $R = 15{\cdot}6 \times 10^6$.

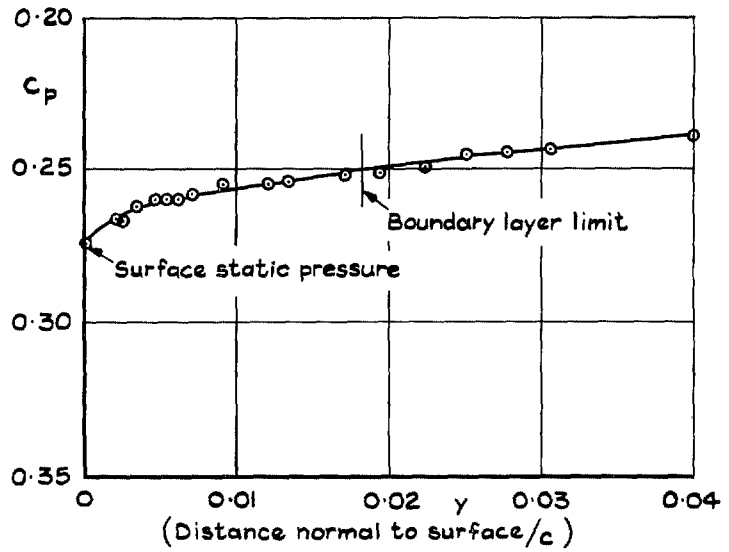

a Boundary layer on lower surface at x = 0·9970

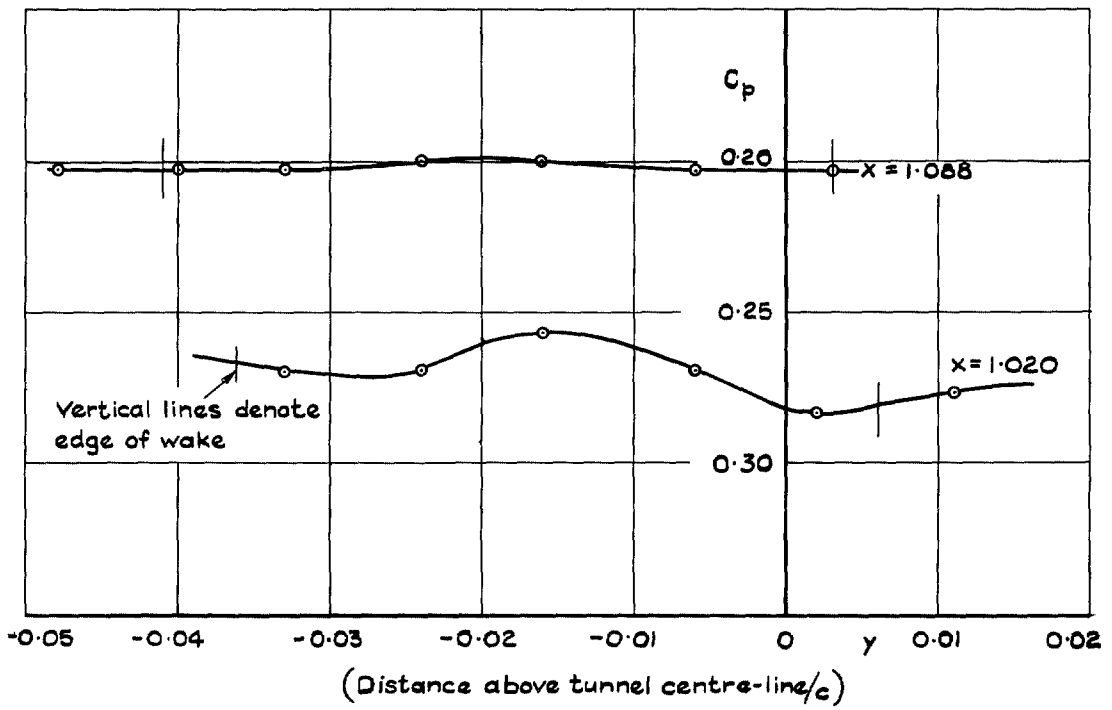

b Wake

FIG. 11(a) and (b). Static pressure variations across wake and boundary layer near trailing edge of section 2814.

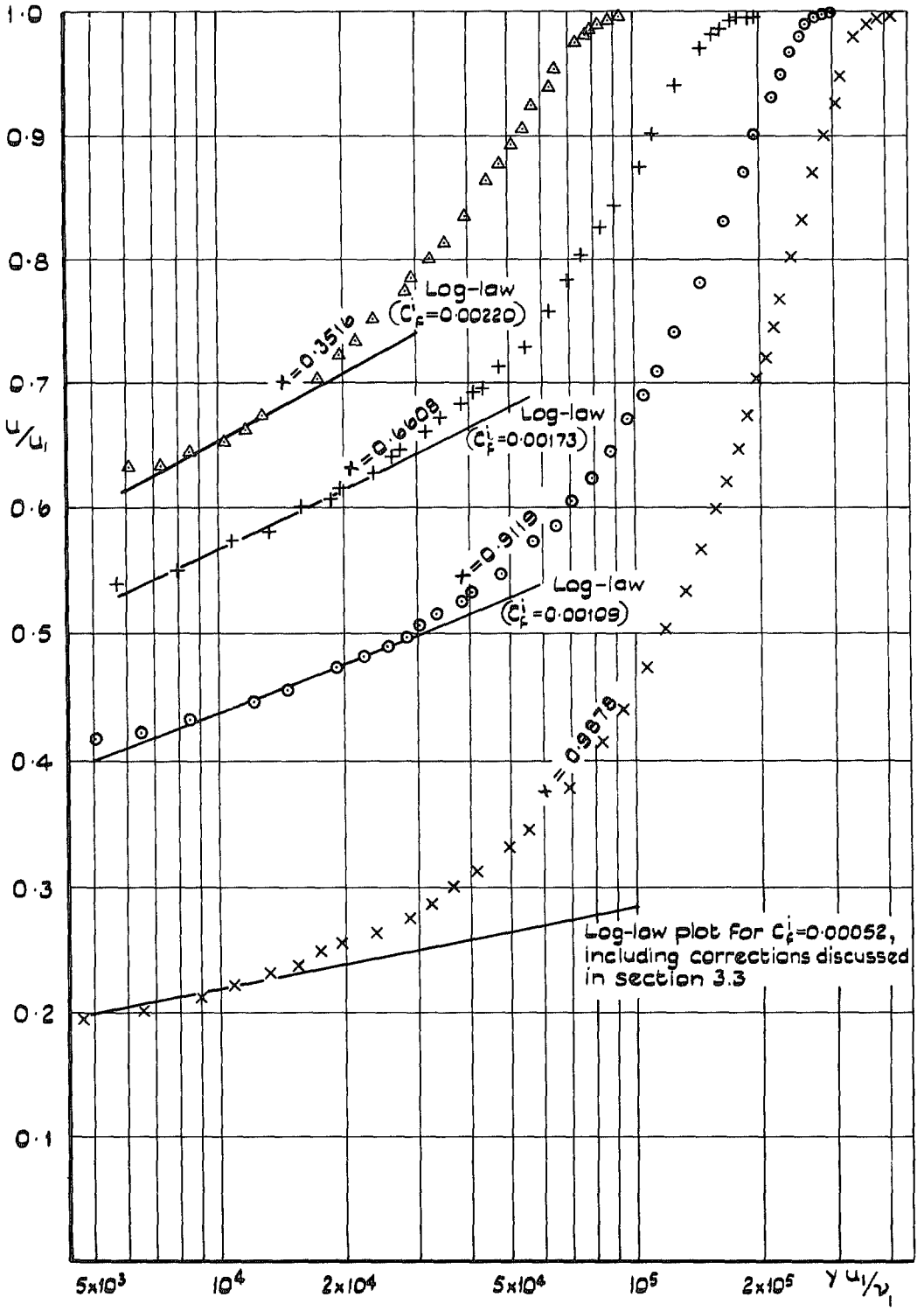

FIG. 12. Comparisons of expt[1] profile data with log–law: section 2815, $C_L = 0{\cdot}51$, upper surface.

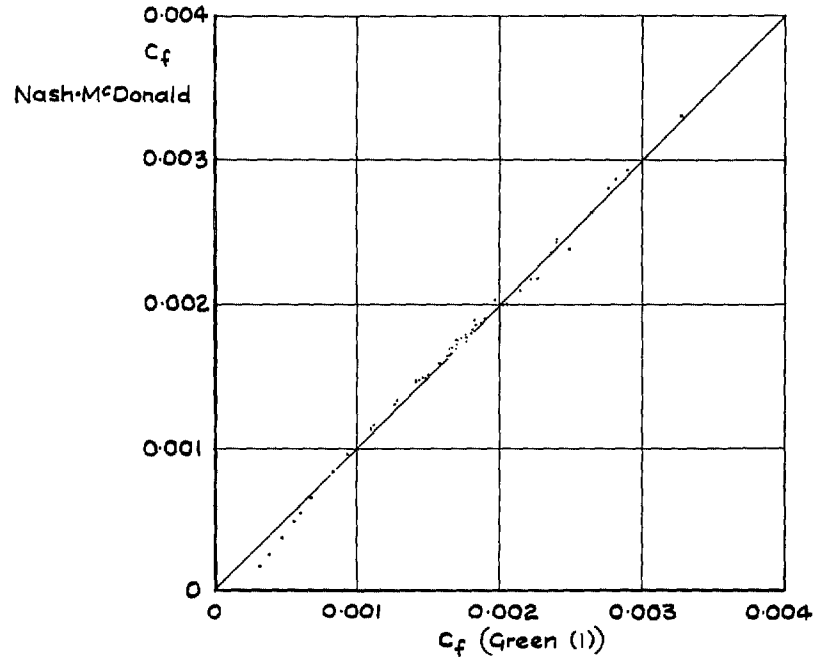

a Integral laws: Nash & McDonald v Green (1)

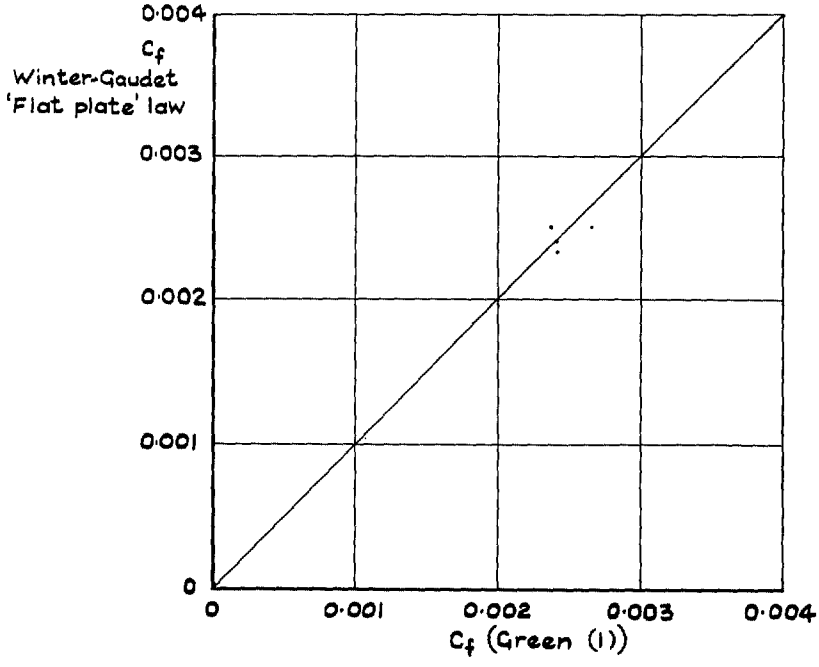

b Integral laws: Winter-Gaudet 'flat plate' law v Green (1)

FIG. 13(a) and (b). Comparisons of skin–friction results.

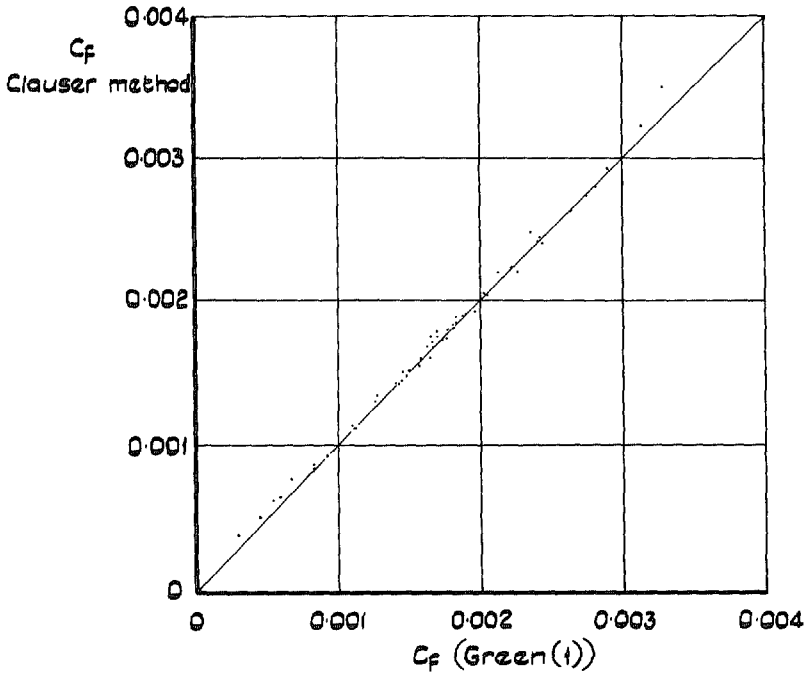

c Clauser method v Green(1) integral law

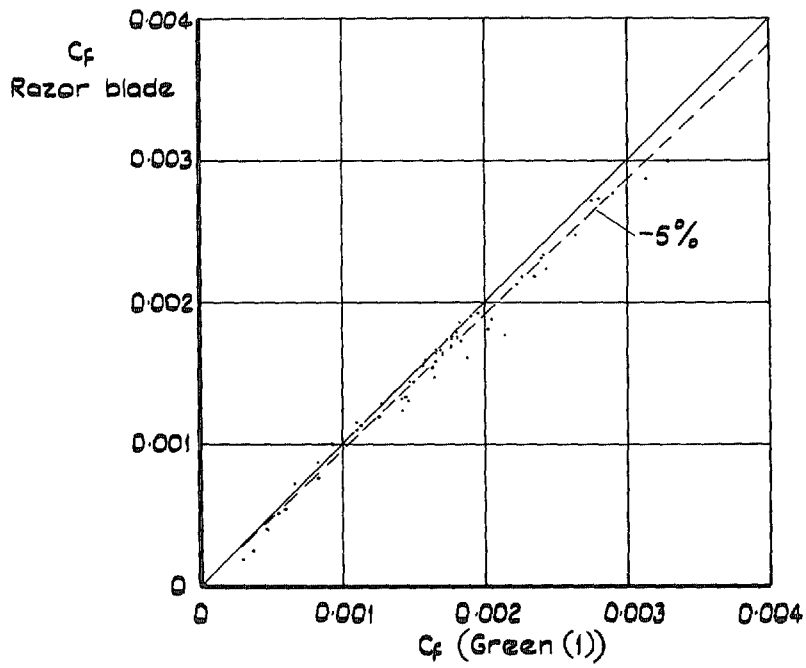

d Razor blade method v Green (1) integral law

FIG. 13(c) and (d).

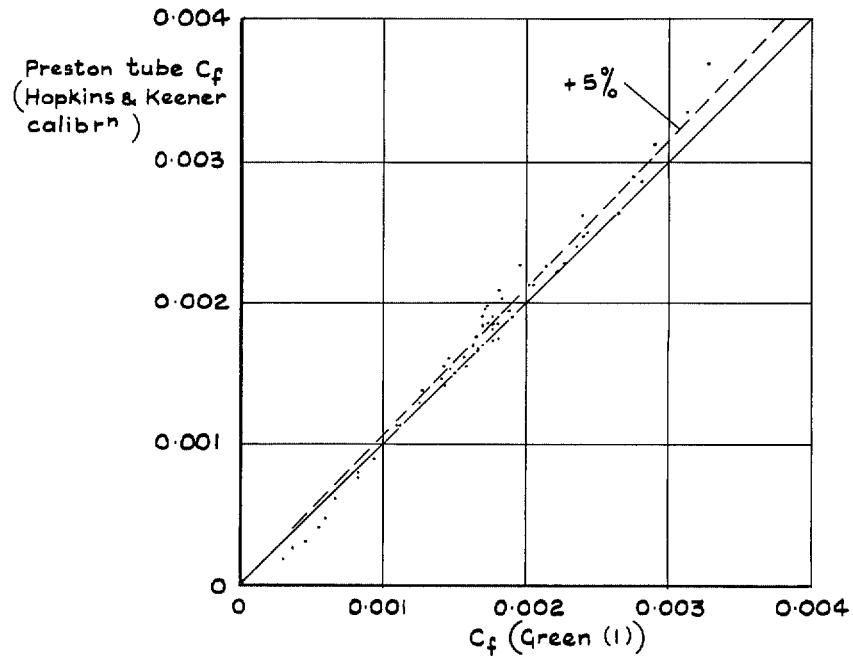

e Preston tube (Hopkins & Keener calibrⁿ) v Green (1) integral law

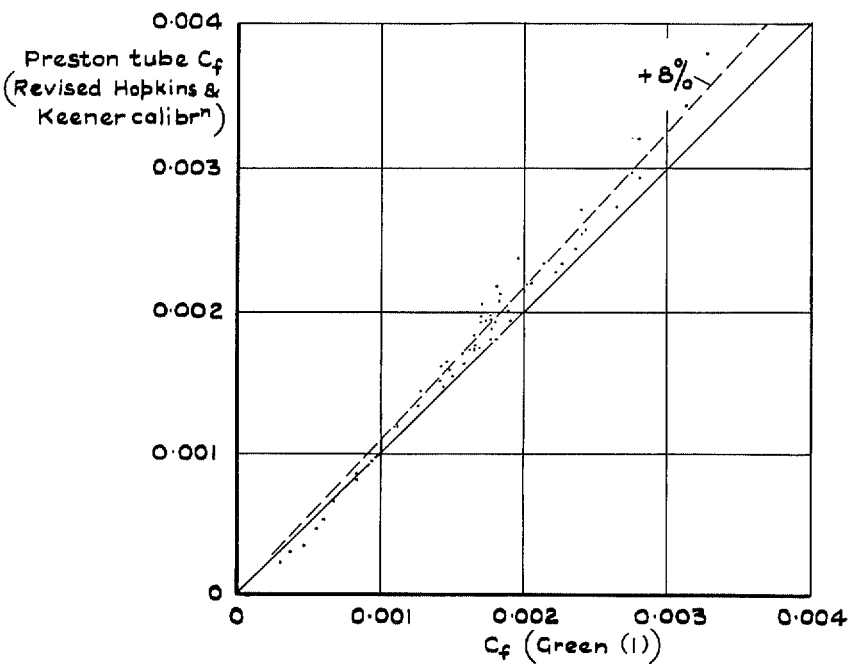

f Preston tube (revised Hopkins & Keener calibrⁿ) v Green (1) integral law

FIG. 13(e) and (f).

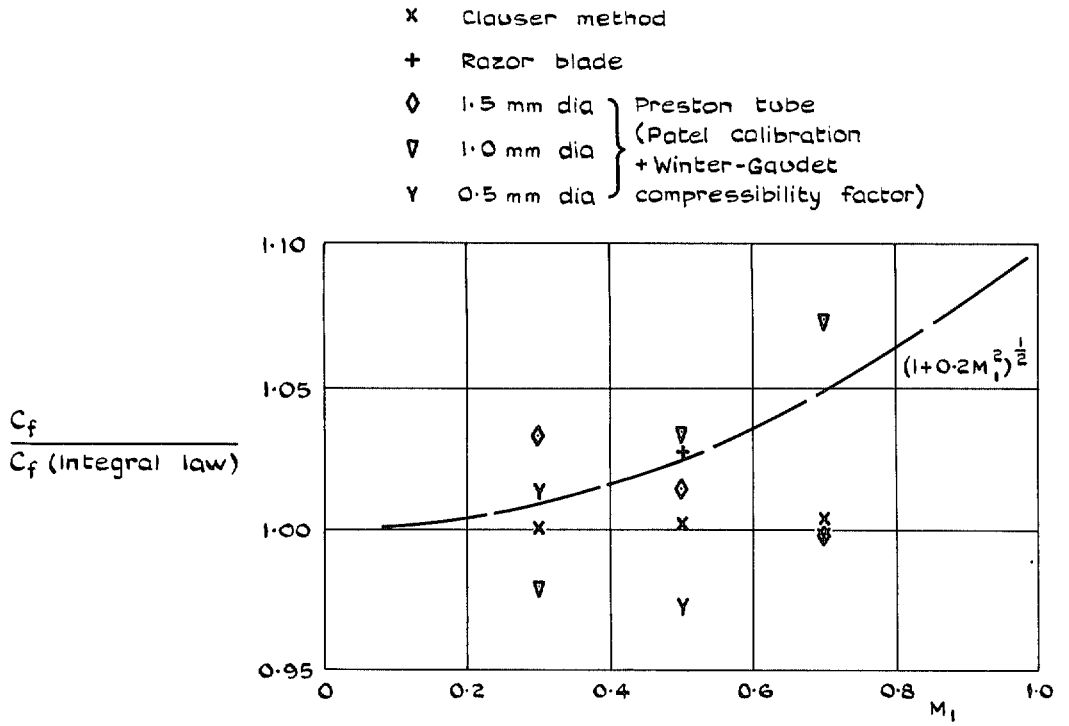

g. Skin-friction measurements made in RAE 9 in. x 8 in. tunnel at total pressure of 27 kN / m² (8 in. Hg)

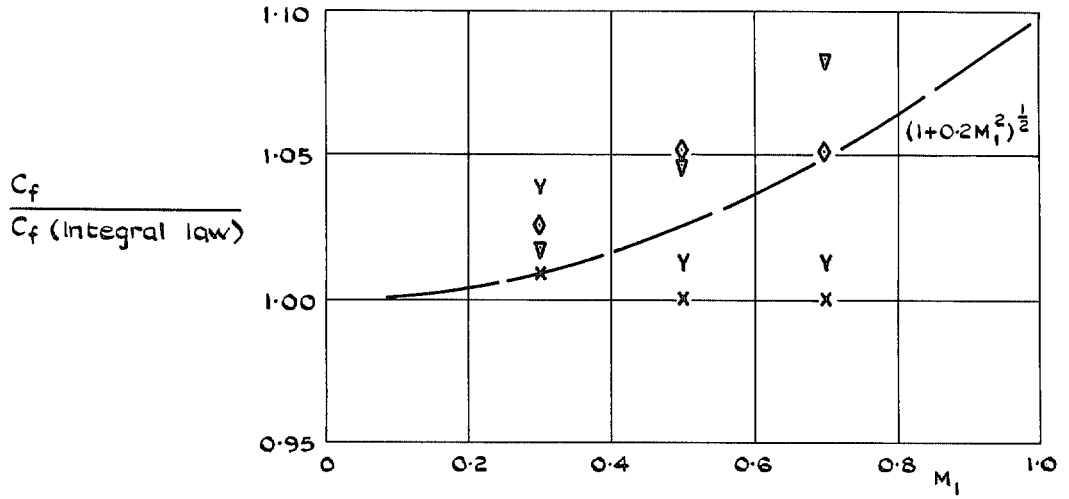

h. Skin-friction measurements made in RAE 9 in. x 8 in. tunnel at pressure of 169 kN/m² (50 in.Hg)

FIG. 13(g) and (h).

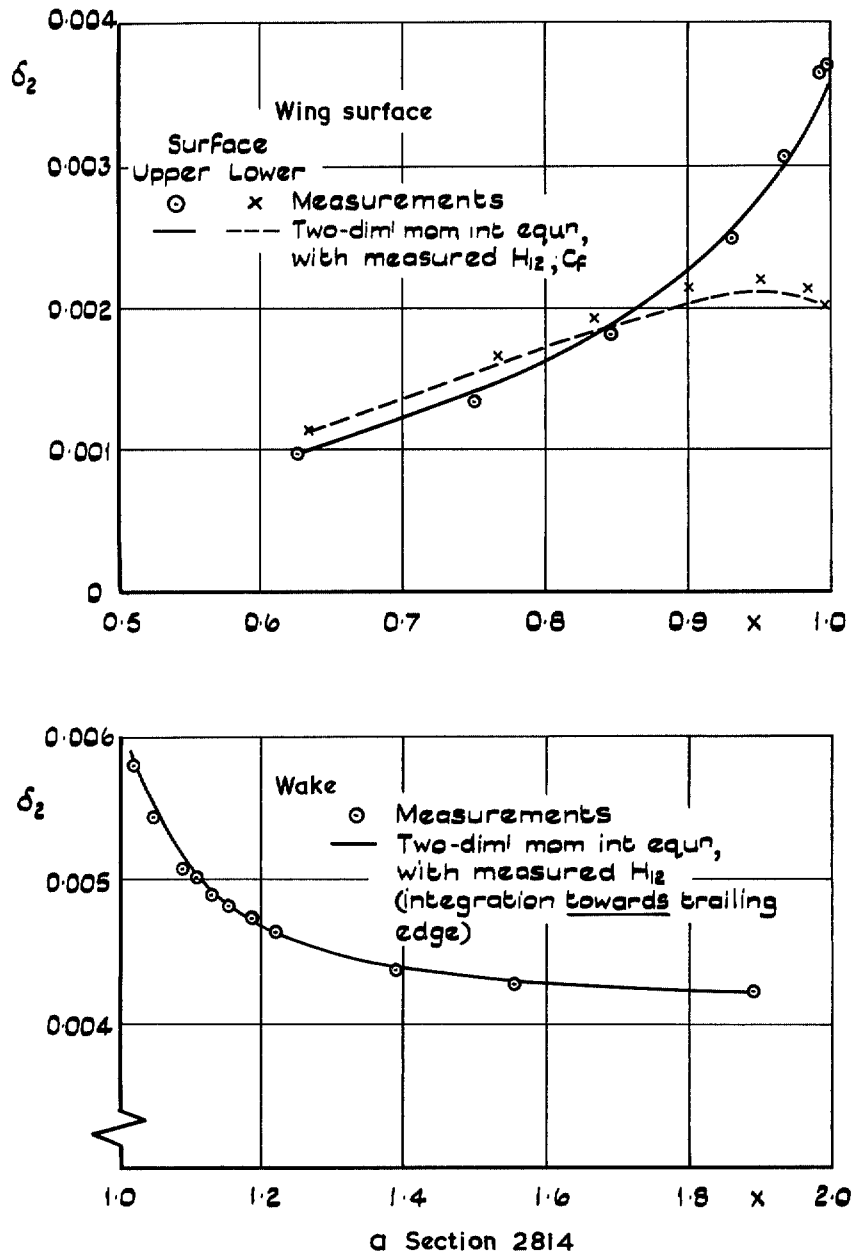

a Section 2814

FIG. 14(a). Comparisons with calculations using two-dimensional momentum integral equation.

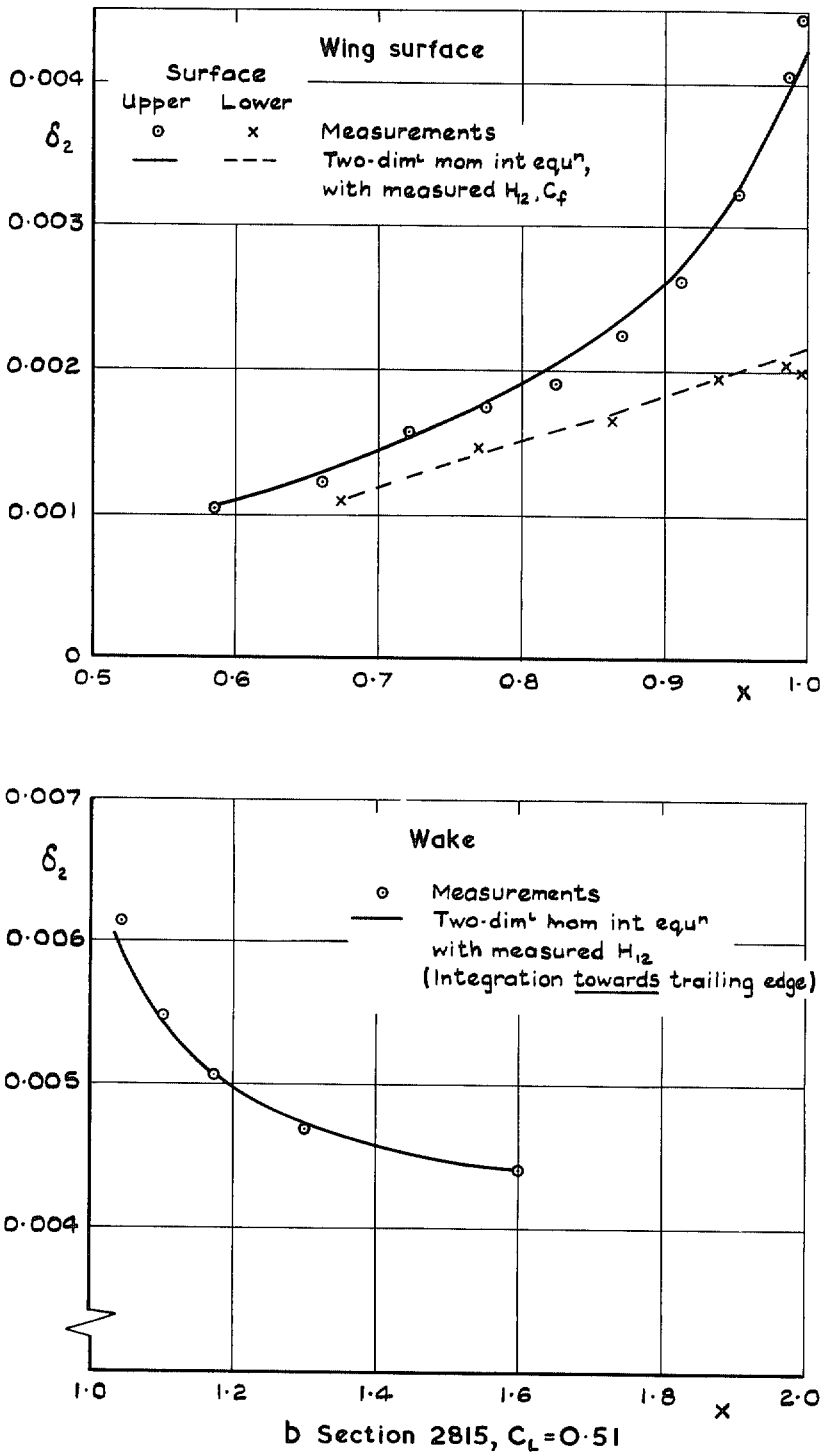
Wing surface
Surface
Upper
Lower
Measurements
Two-dimˡ mom int equⁿ,
with measured H12, Cf
δ2
0·004
0·003
0·002
0·001
0
0·5
0·6
0·7
0·8
0·9
x
1·0
Wake
Measurements
Two-dimˡ mom int equⁿ
with measured H12
(Integration towards trailing edge)
δ2
0·007
0·006
0·005
0·004
1·0
1·2
1·4
1·6
1·8
x
2·0
b Section 2815, CL=0·51

FIG. 14(b).

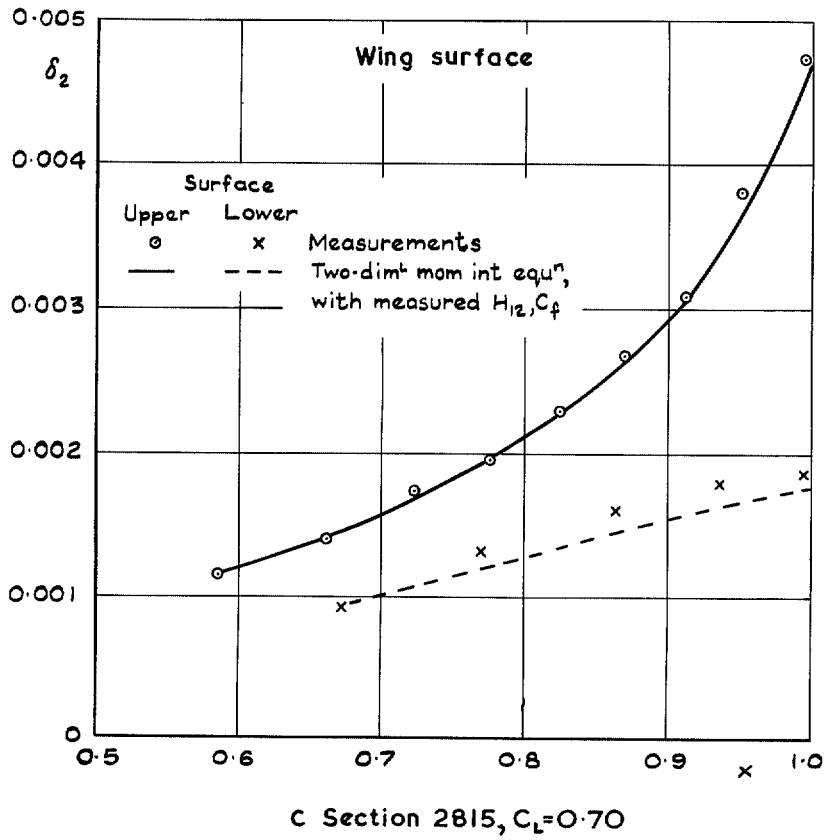

C Section 2815, C_L=0·70

FIG. 14(c).

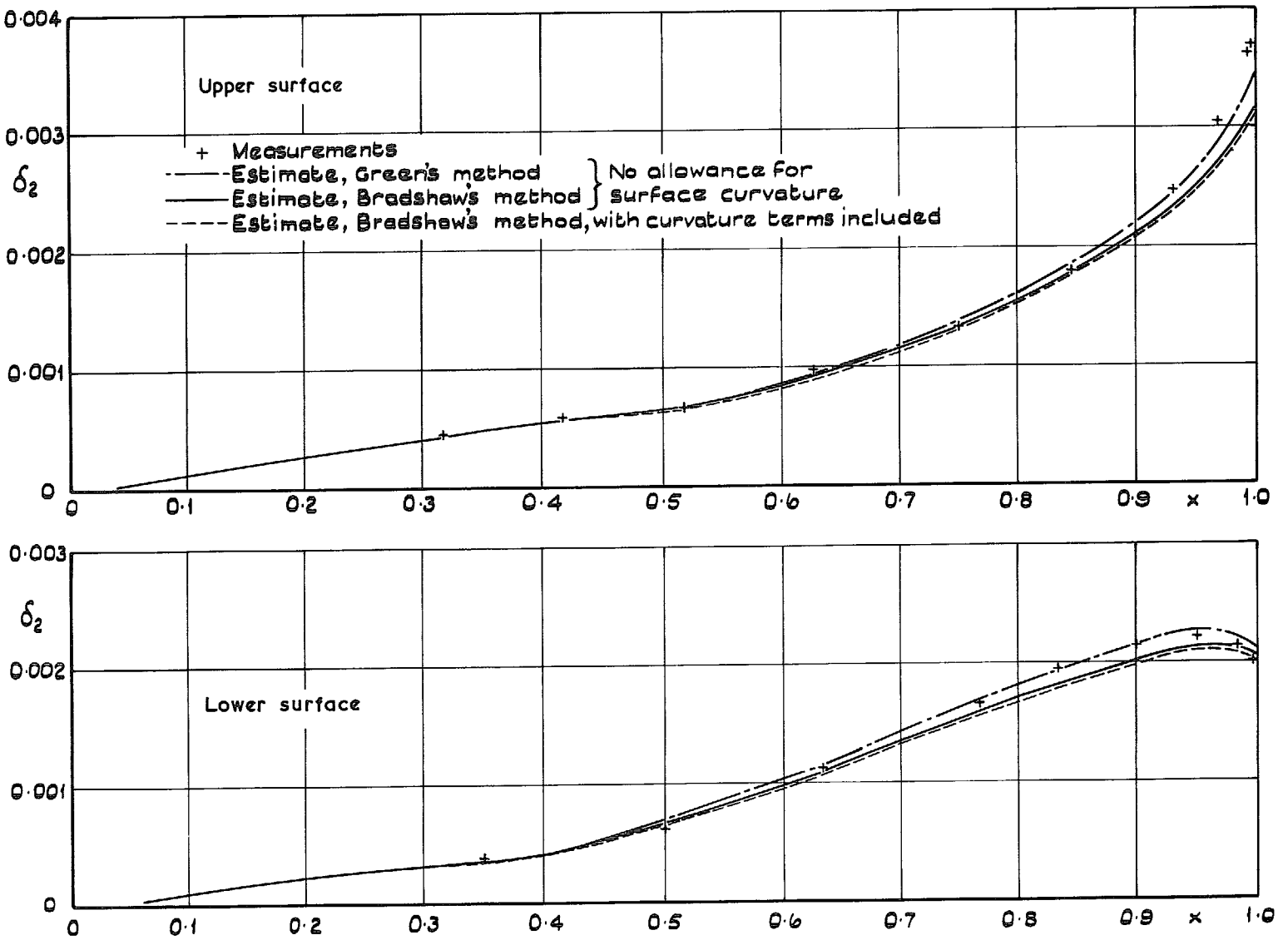

FIG. 15. Section 2814: boundary layer momentum thickness.

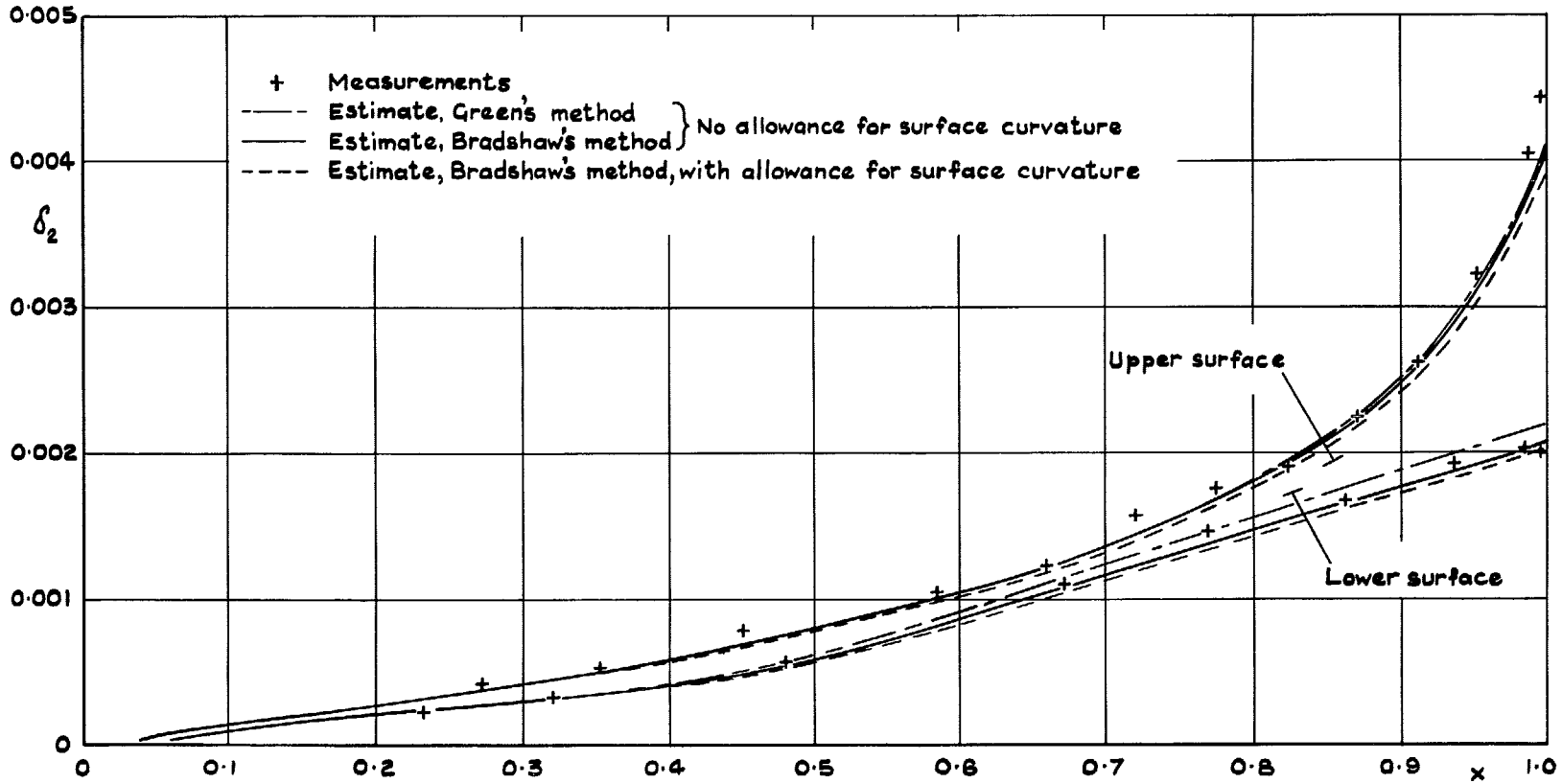

FIG. 16. Section 2815, $C_L = 0{\cdot}51$: boundary layer momentum thickness.

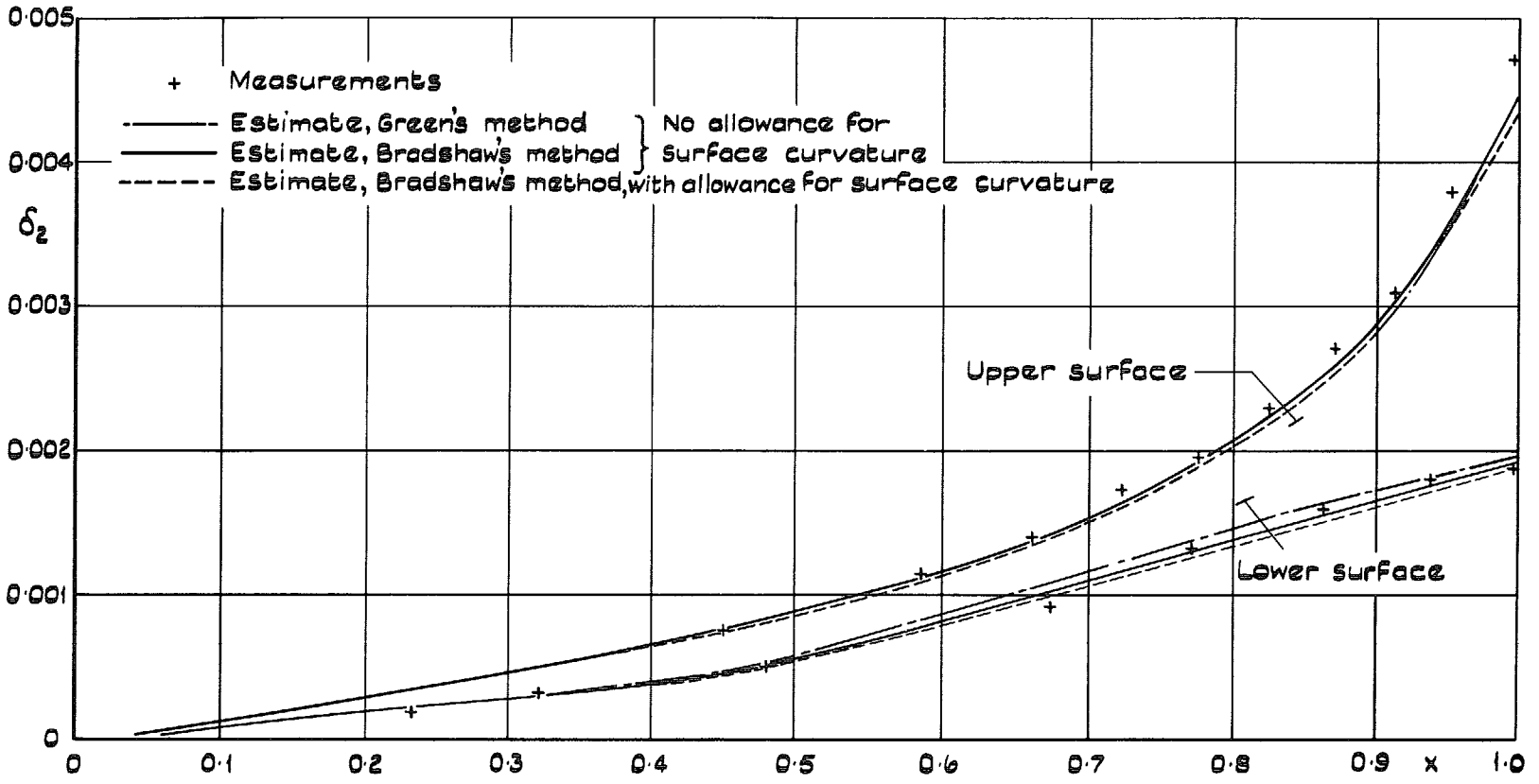

FIG. 17. Section 2815, $C_L = 0{\cdot}70$: boundary layer momentum thickness.

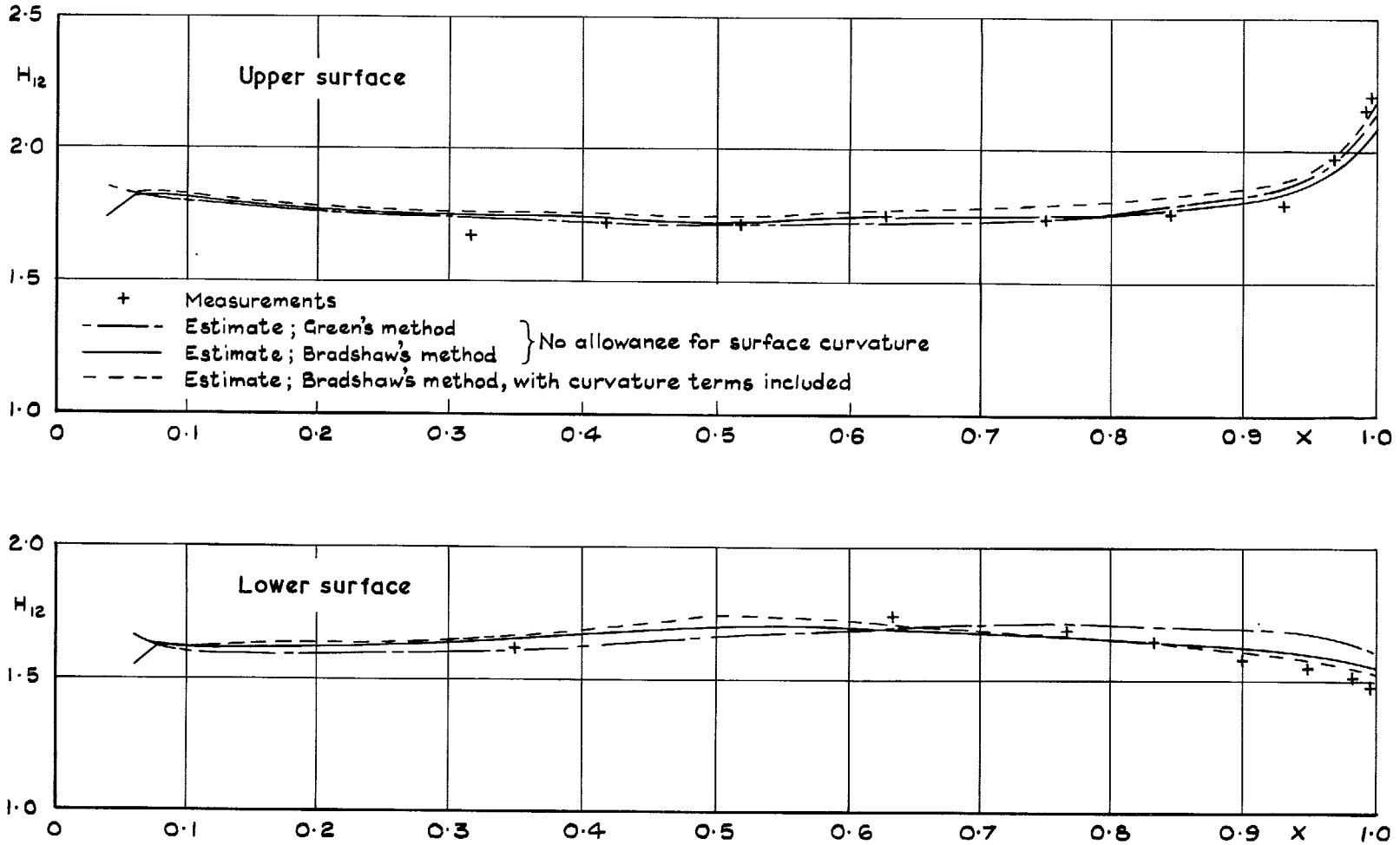

FIG. 18. Section 2814; boundary layer shape parameter, H_{12}.

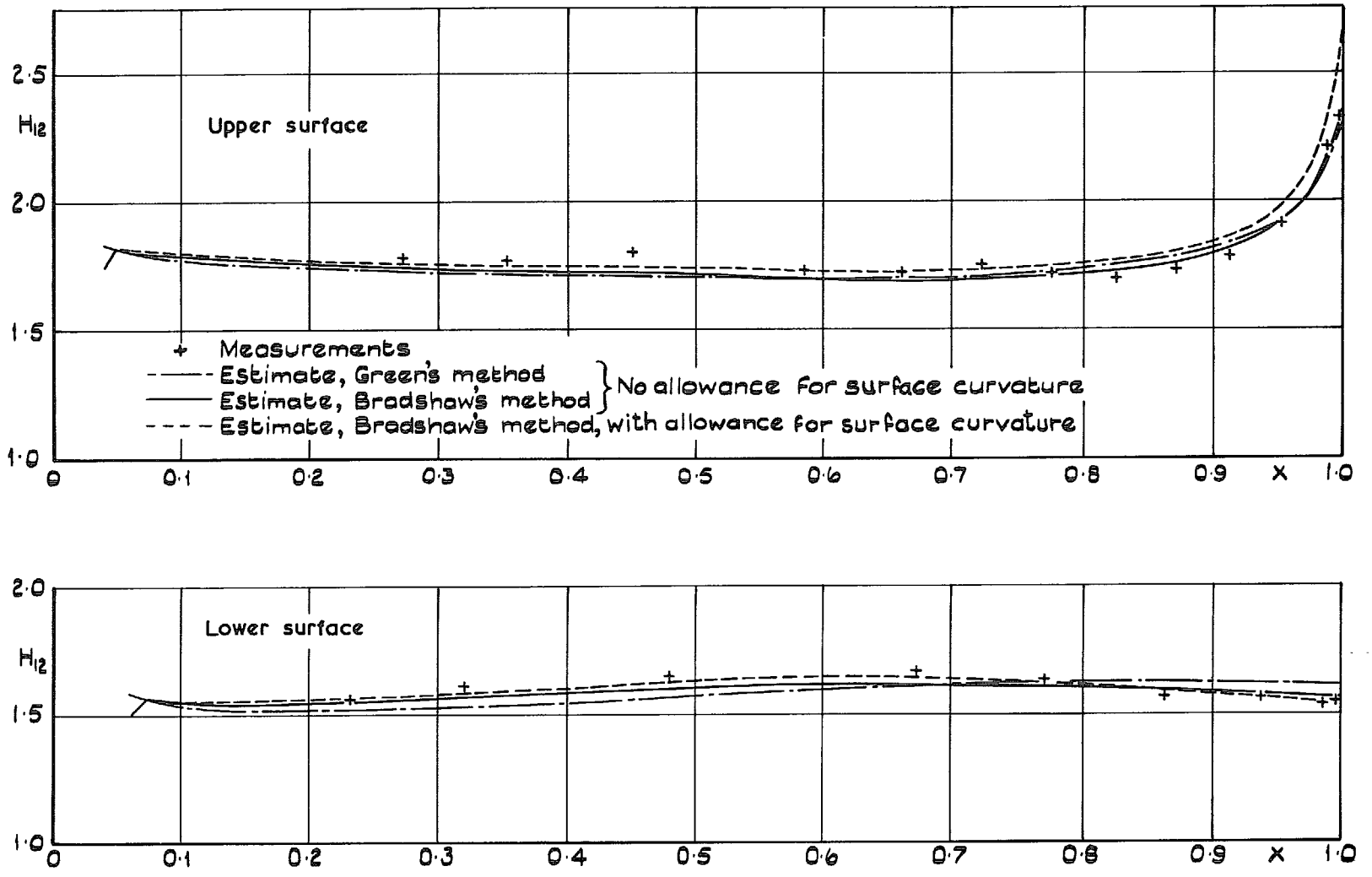

FIG. 19. Section 2815, $C_L = 0{\cdot}51$: boundary layer shape parameter.

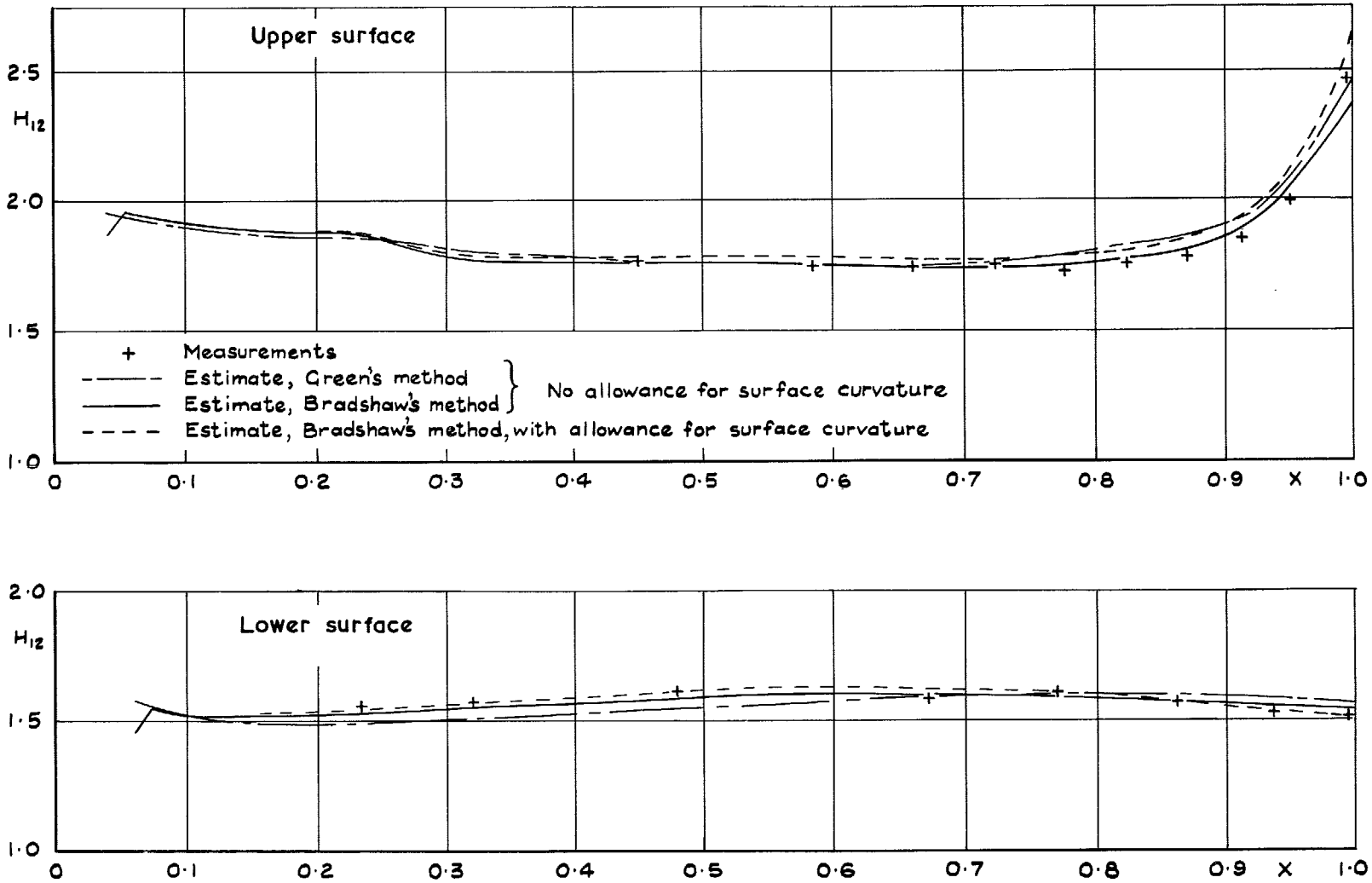

FIG. 20. Section 2815, $C_L = 0{\cdot}70$: boundary layer shape parameter.

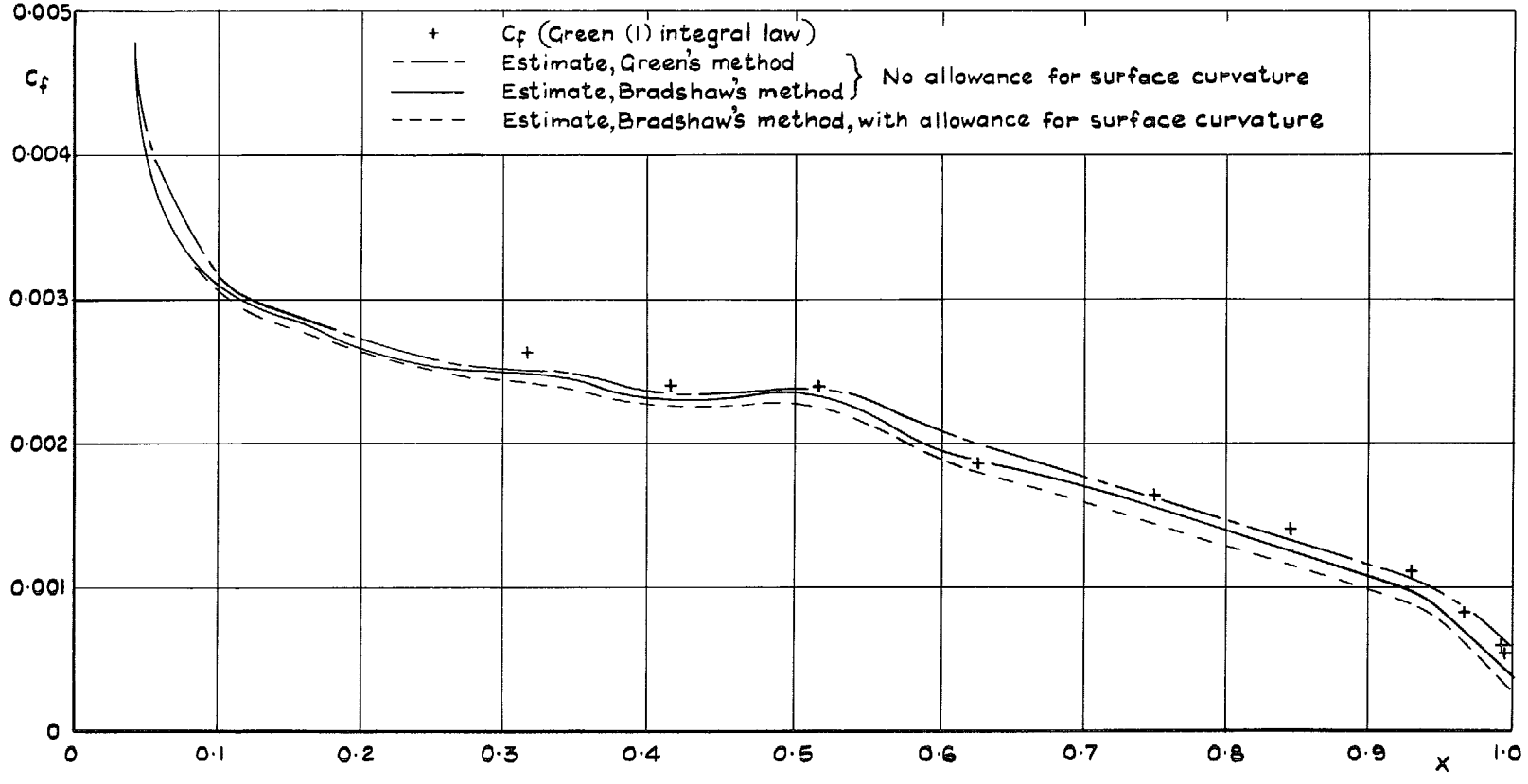

FIG. 21. Section 2814, upper surface: skin friction.

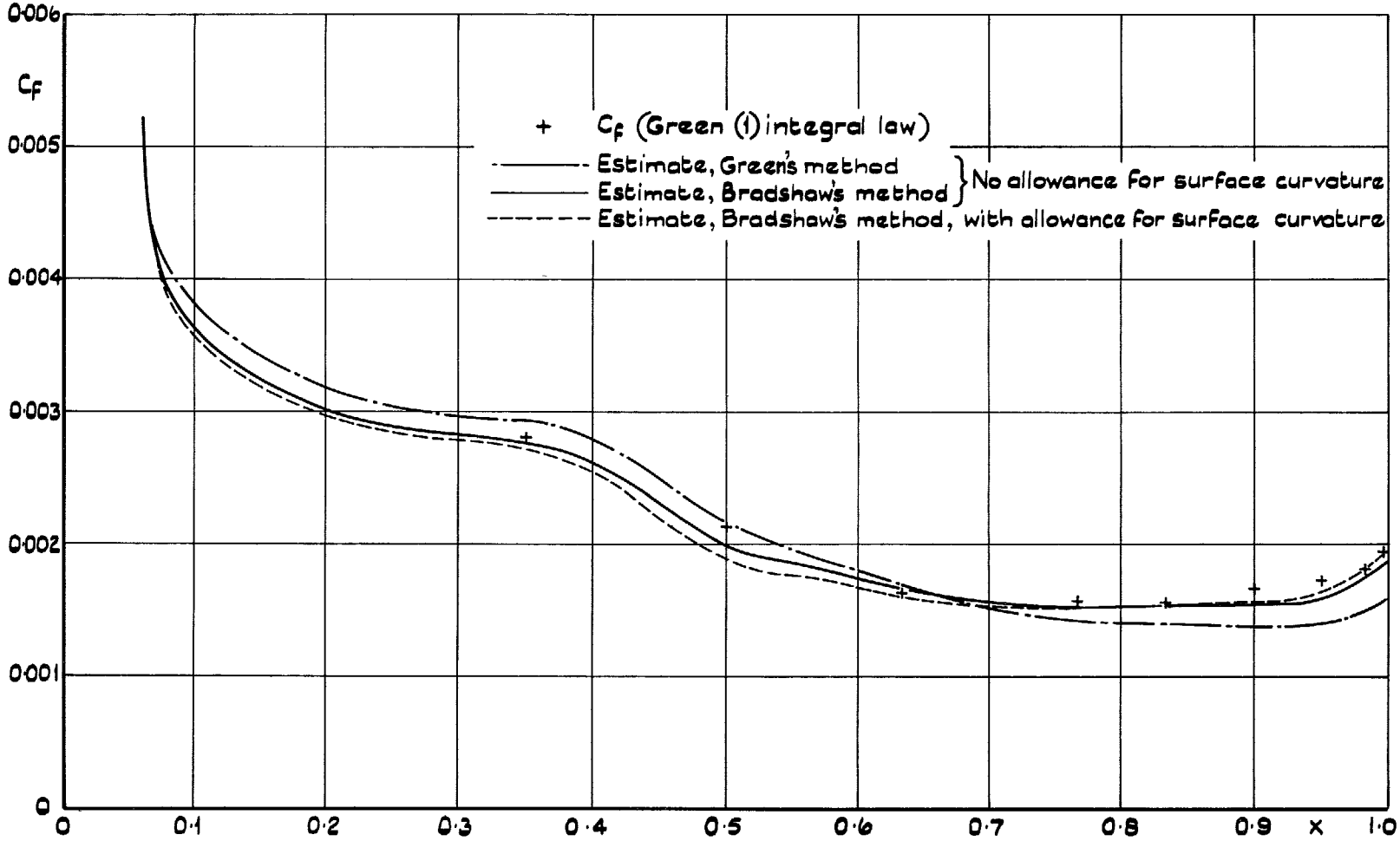

FIG. 22. Section 2814, lower surface: skin friction.

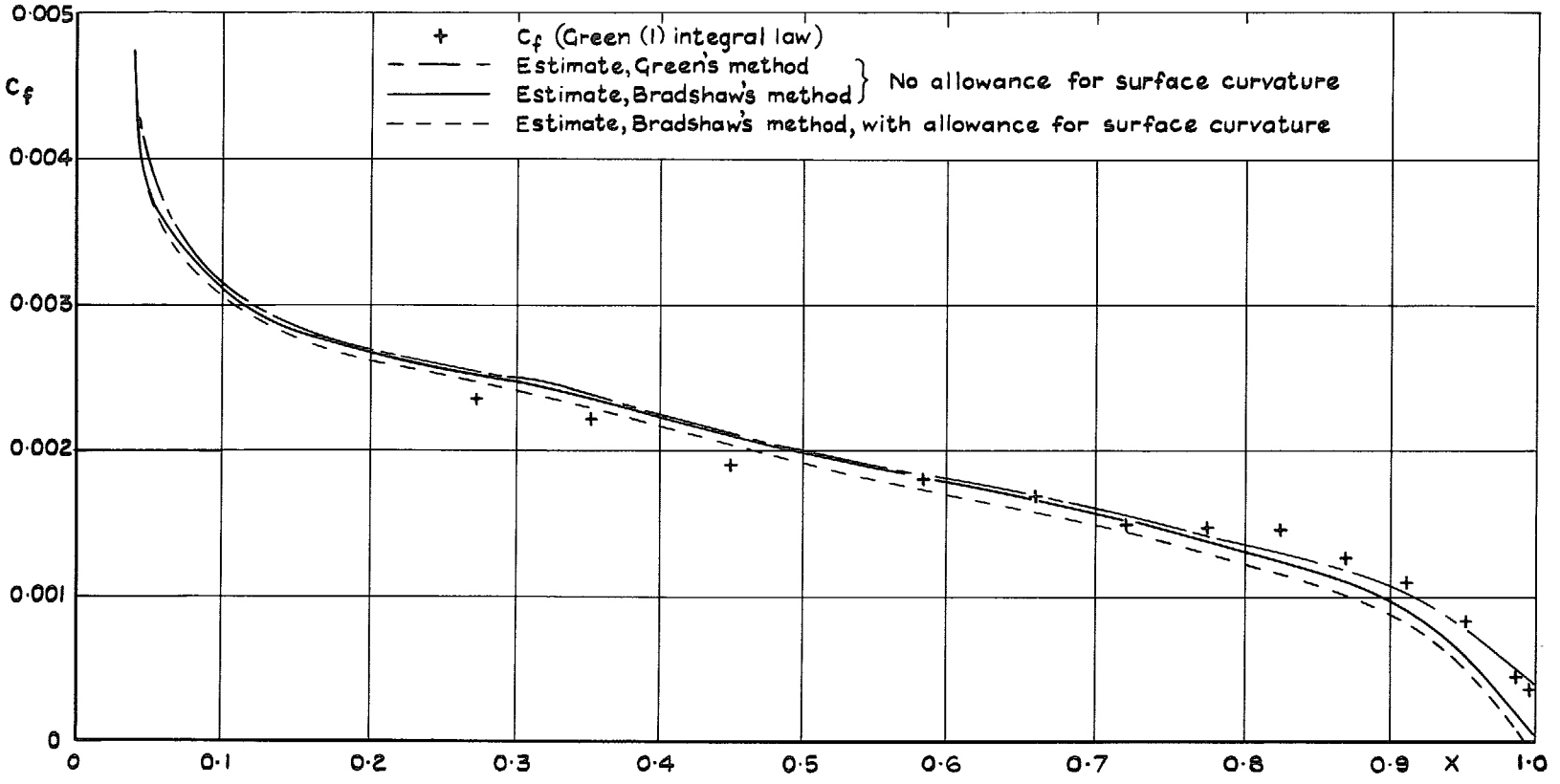

FIG. 23. Section 2815, $C_L = 0{\cdot}51$, upper surface: skin friction.

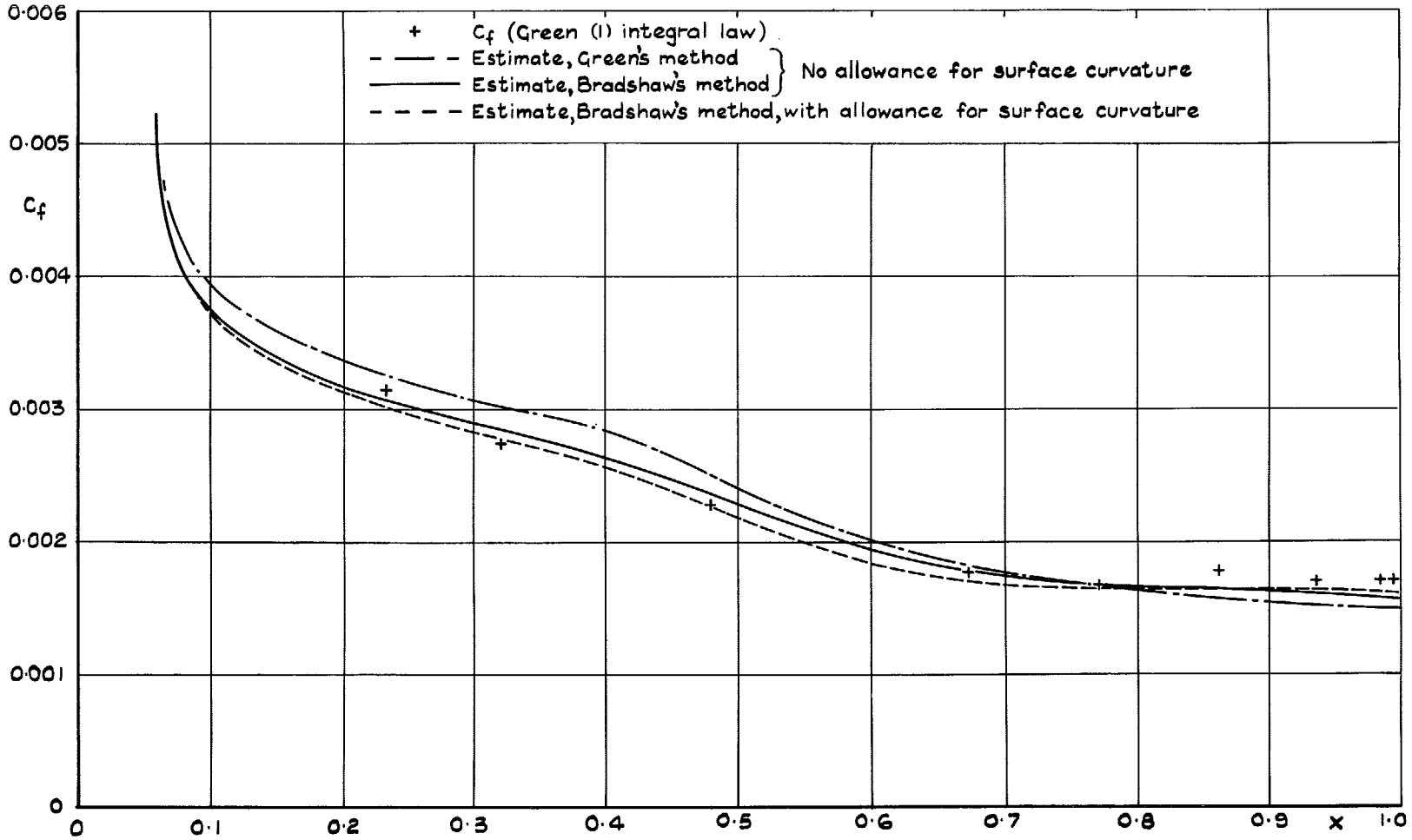

FIG. 24. Section 2815, $C_L = 0{\cdot}51$, lower surface: skin friction.

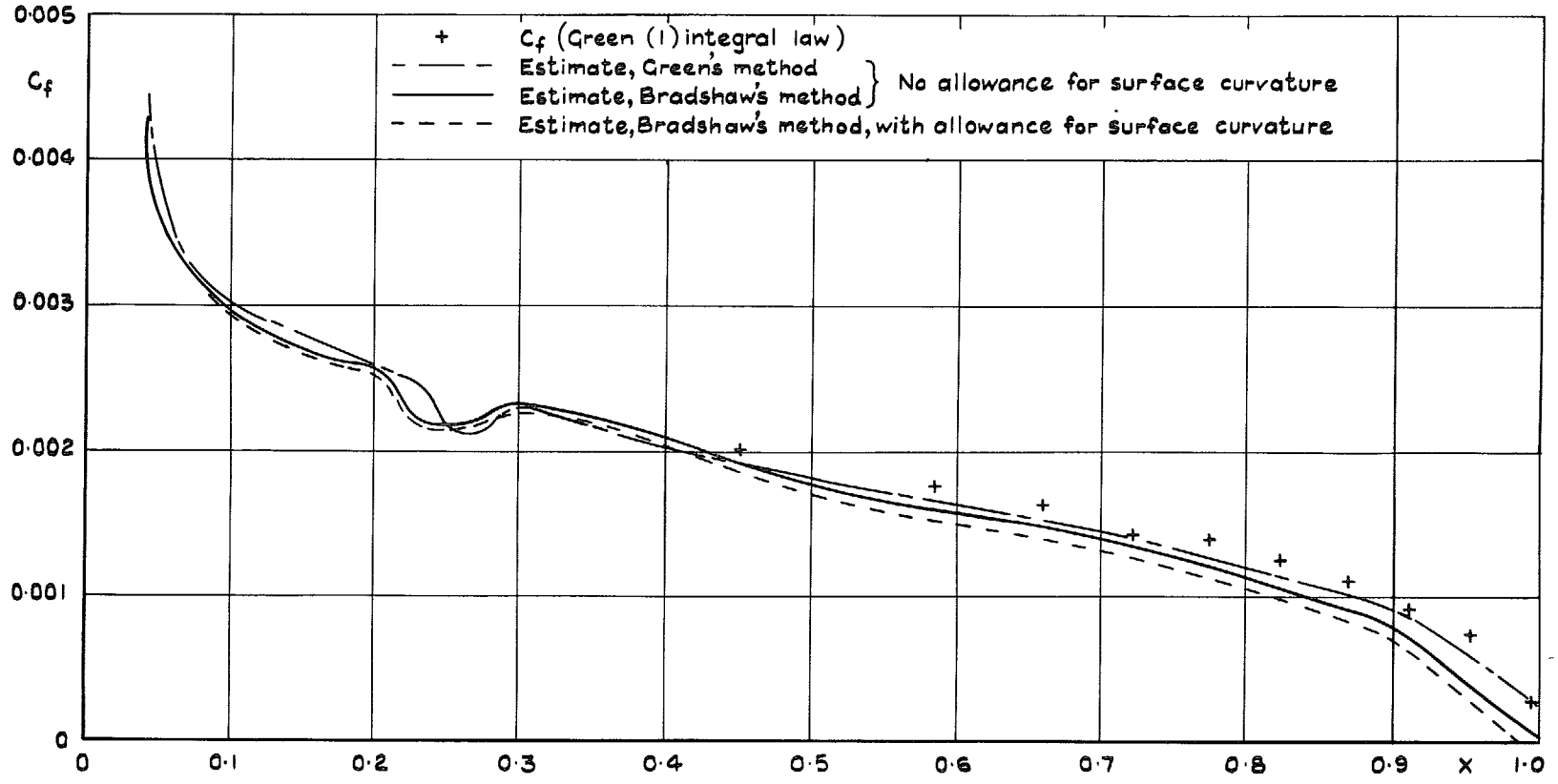

FIG. 25. Section 2815, $C_L = 0{\cdot}70$, upper surface: skin friction.

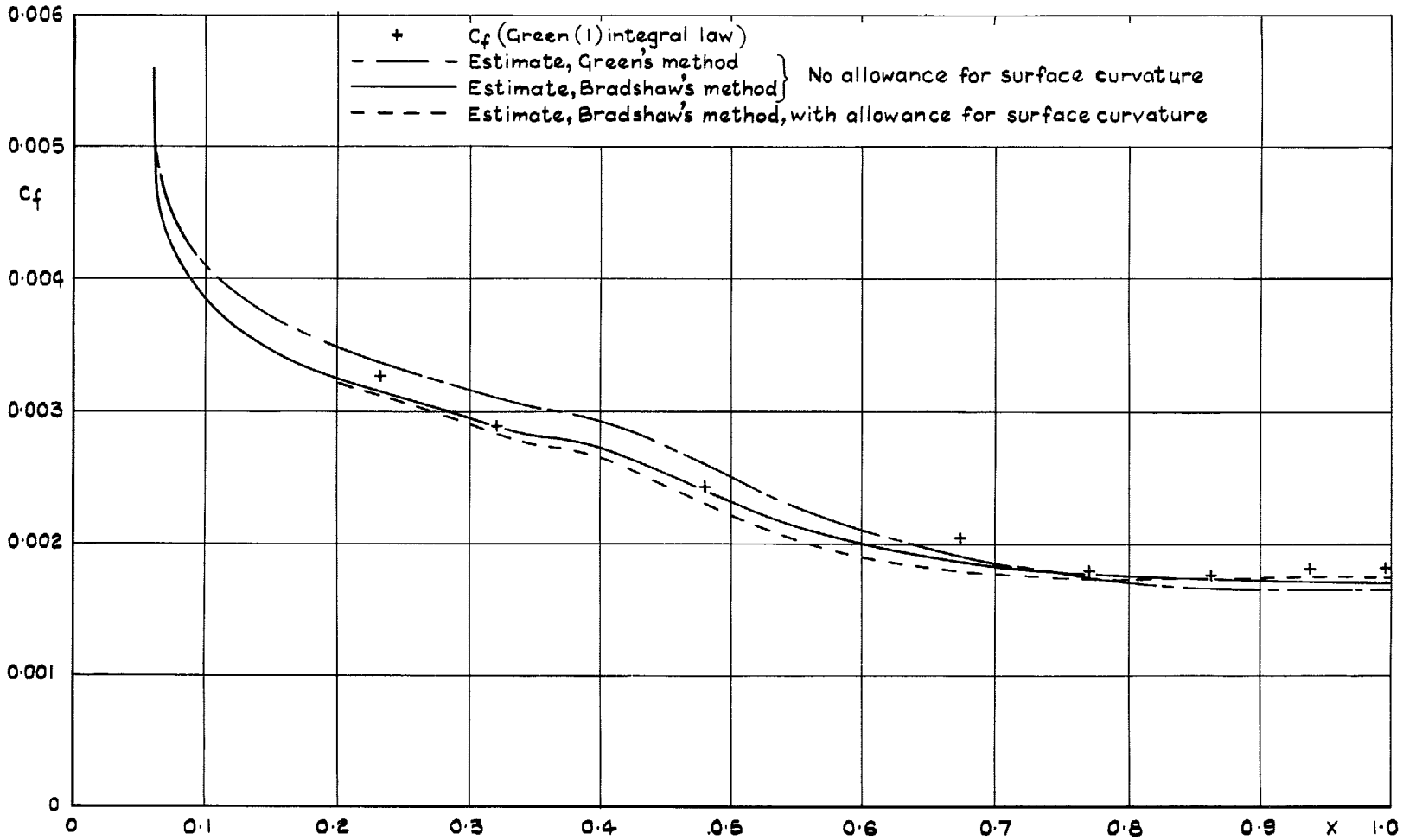

FIG. 26. Section 2815, $C_L = 0{\cdot}70$, lower surface: skin friction.

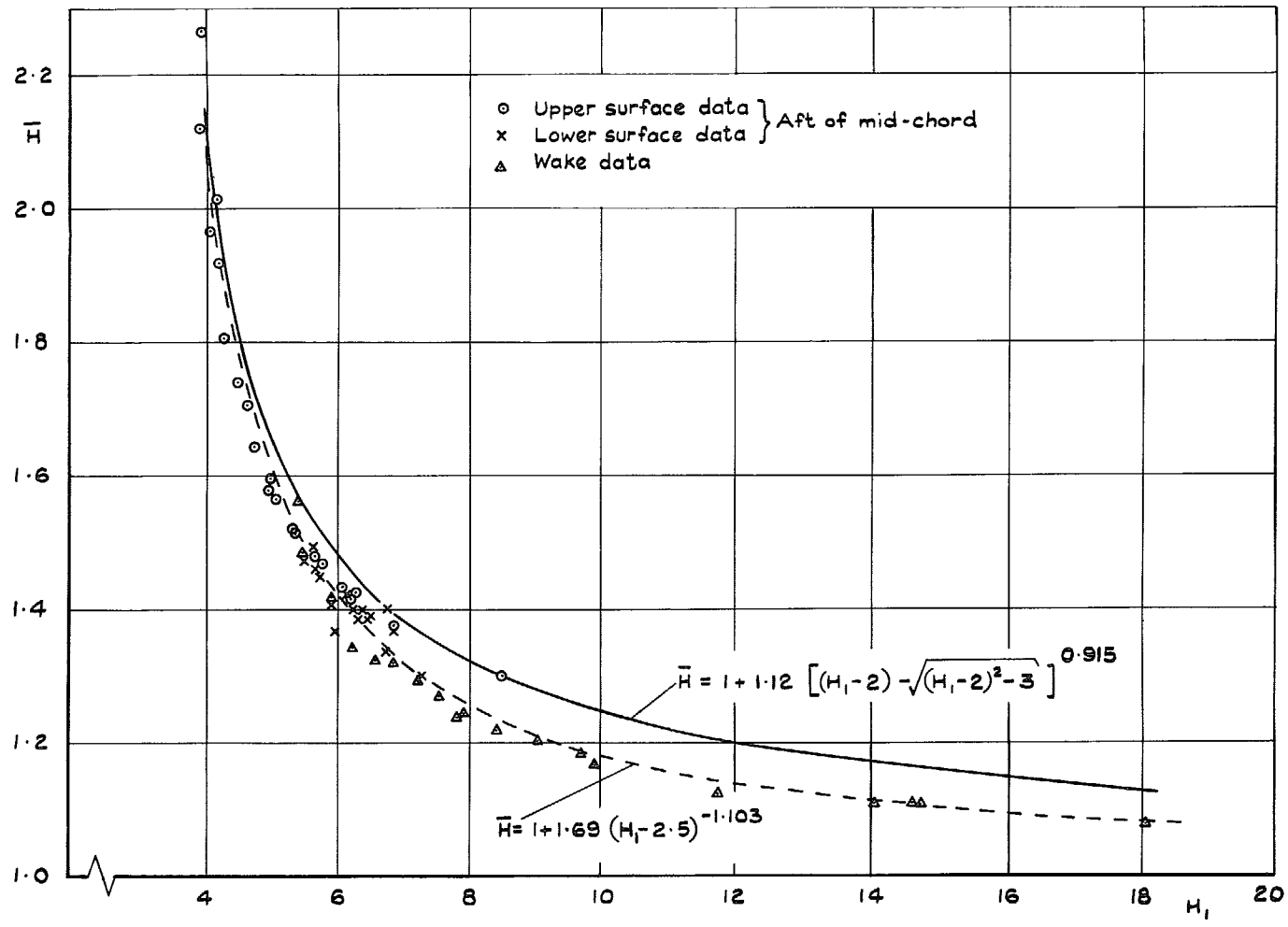

FIG. 27. $\bar{H} \sim H_1$ correlation.

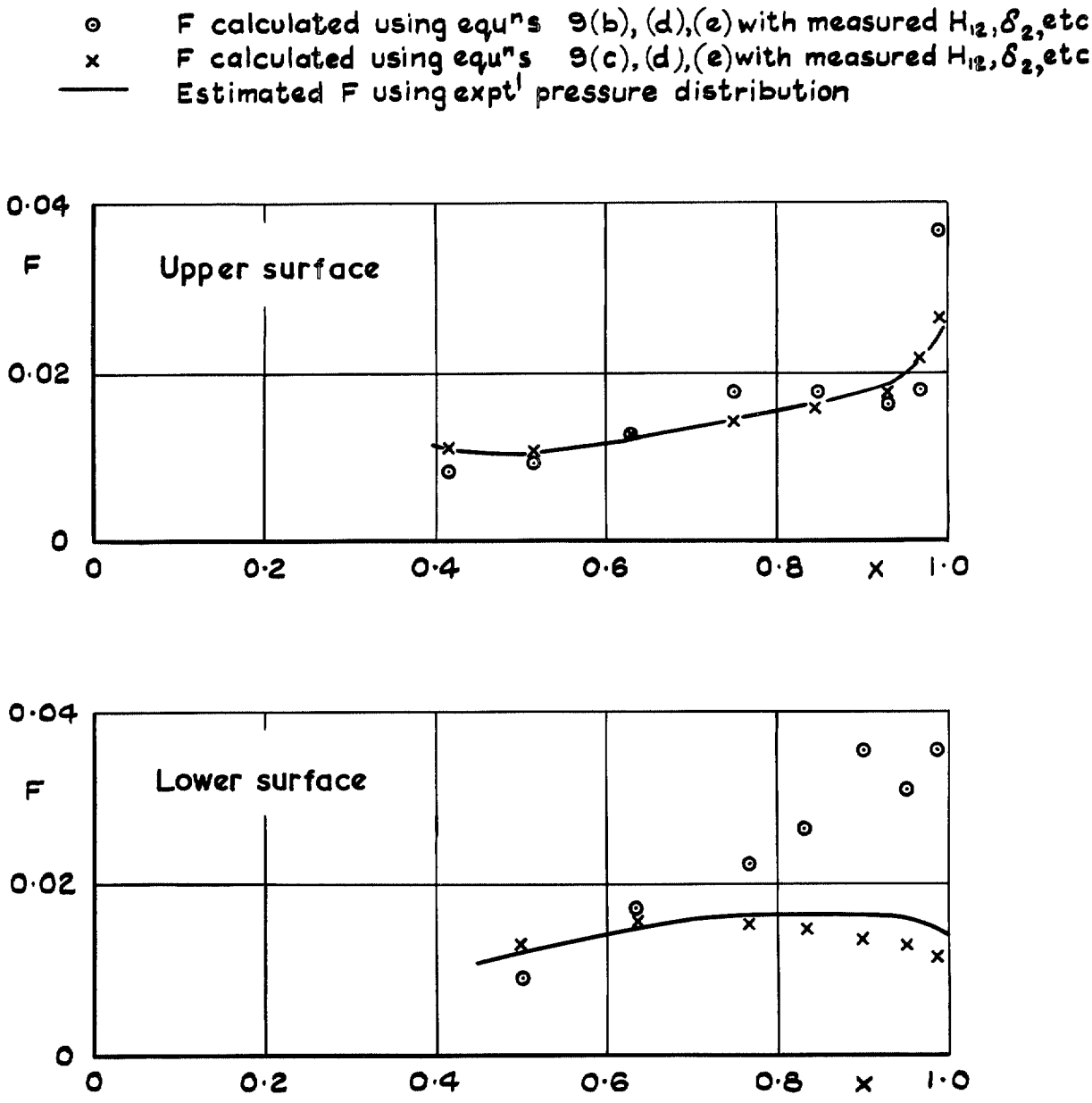

FIG. 28. Boundary layer entrainment-section 2814.

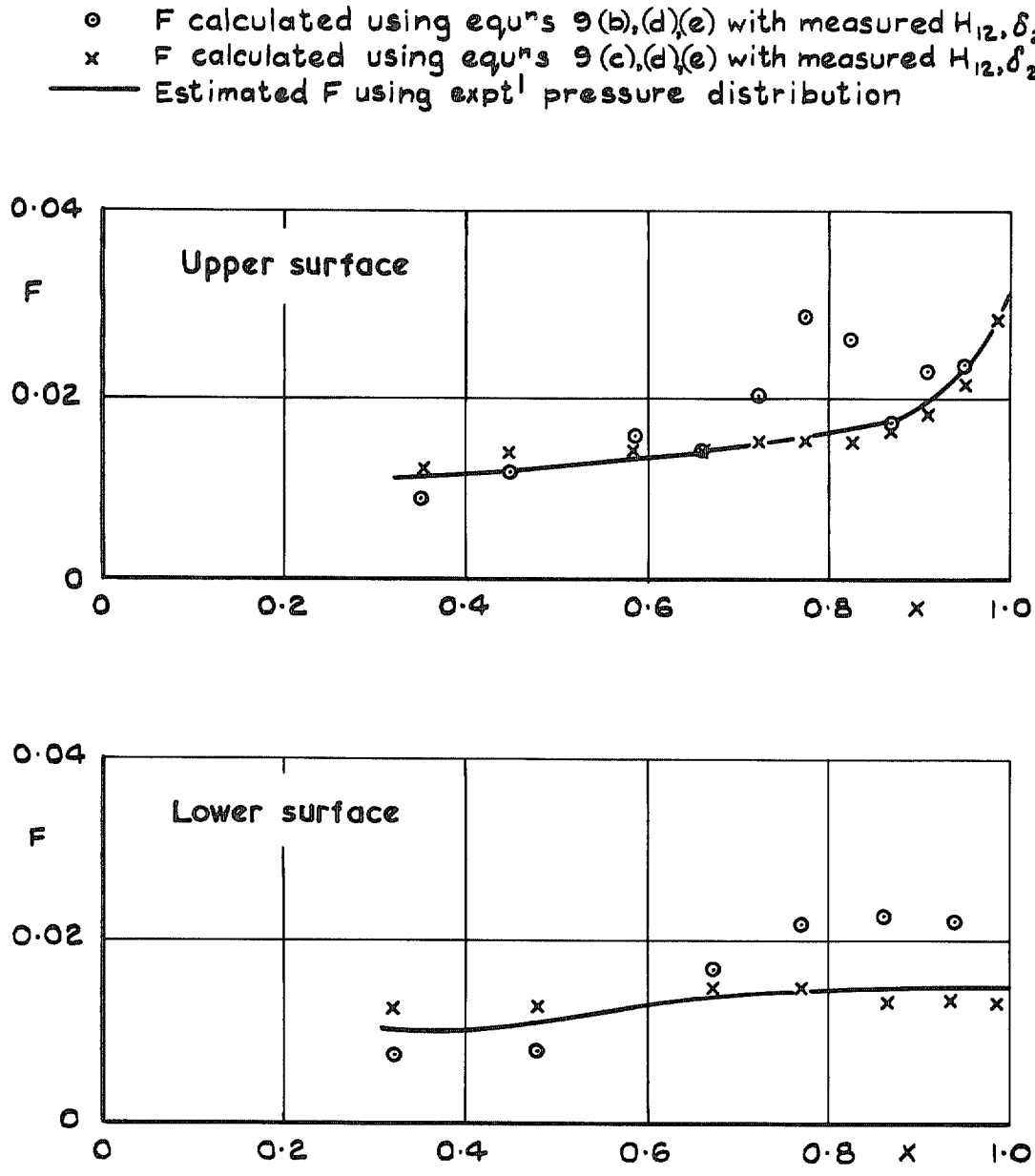

FIG. 29. Boundary layer entrainment-section 2815, $C_L = 0{\cdot}51$.

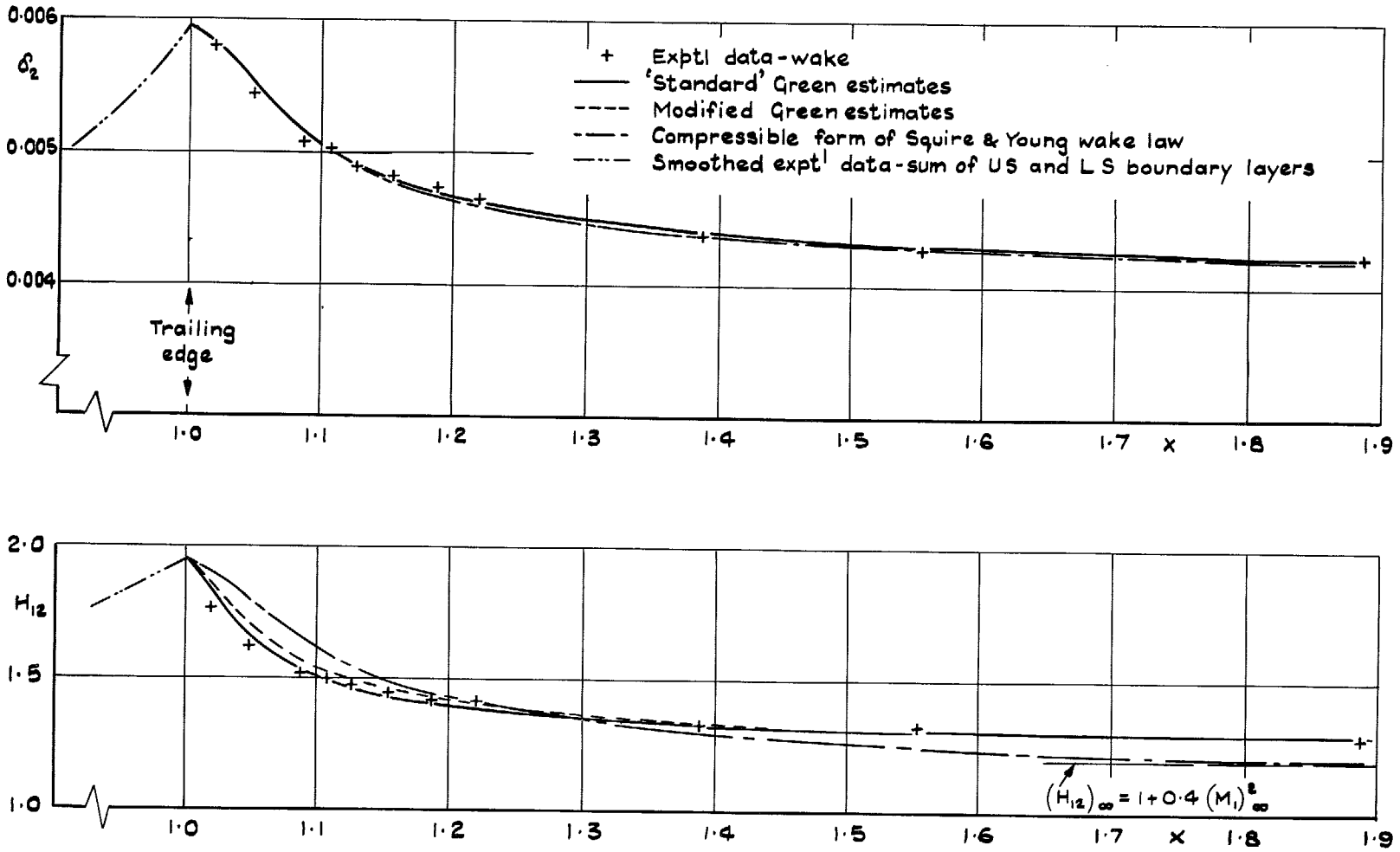

FIG. 30. Section 2814: wake development.

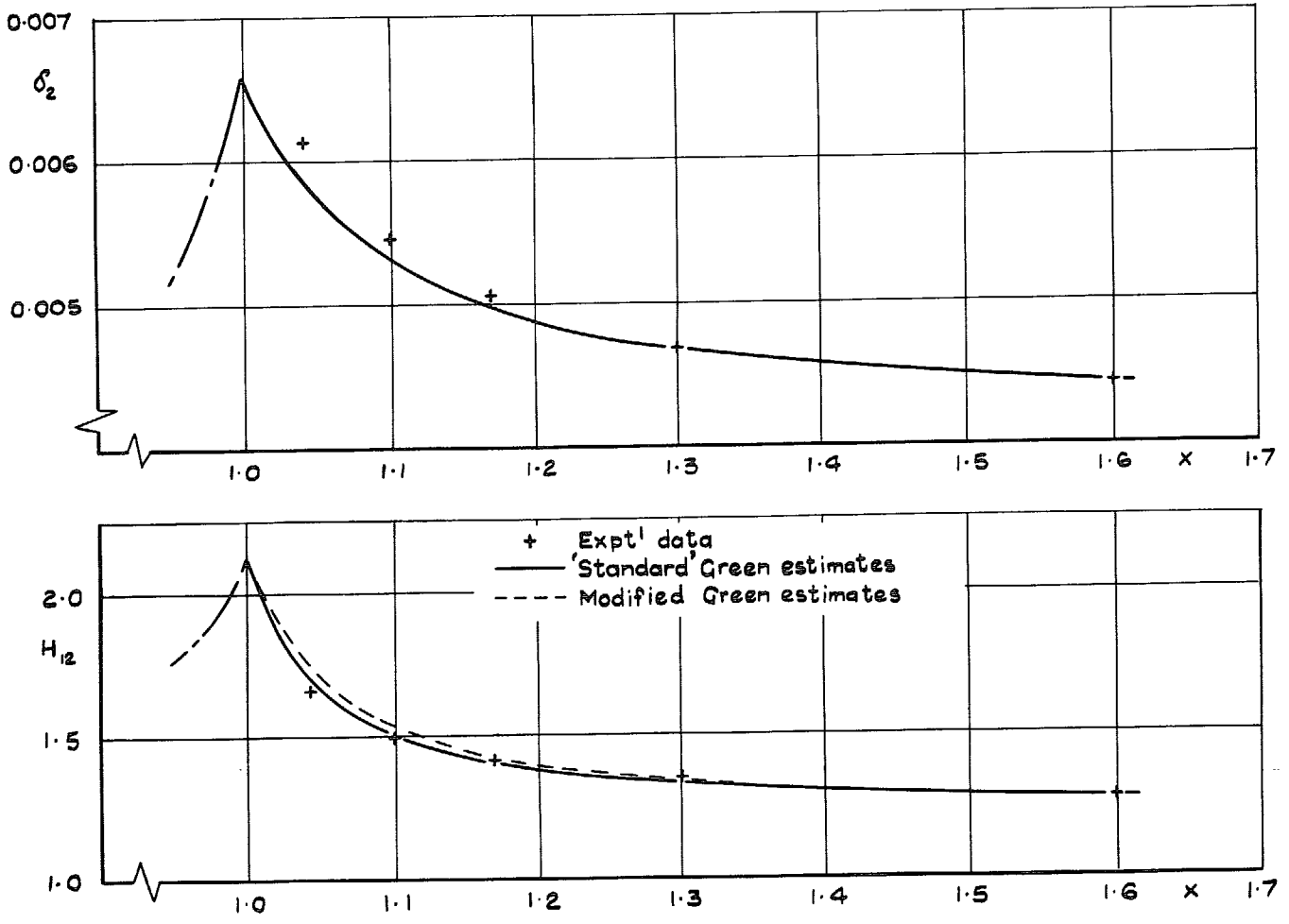

FIG. 31. Section 2815, $C_L = 0{\cdot}51$: wake development.

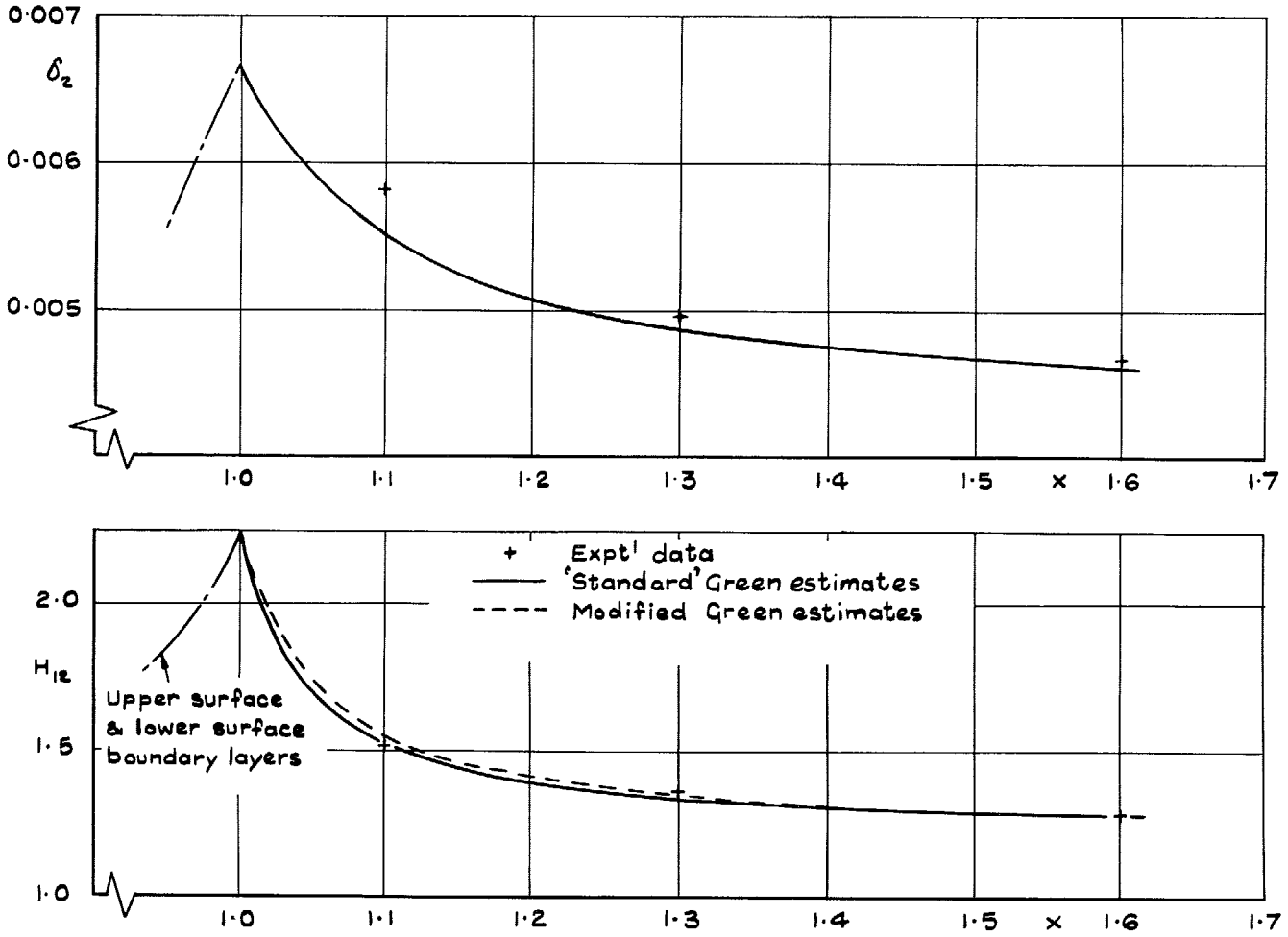

FIG. 32. Section 2815, $C_L = 0{\cdot}70$: wake development.

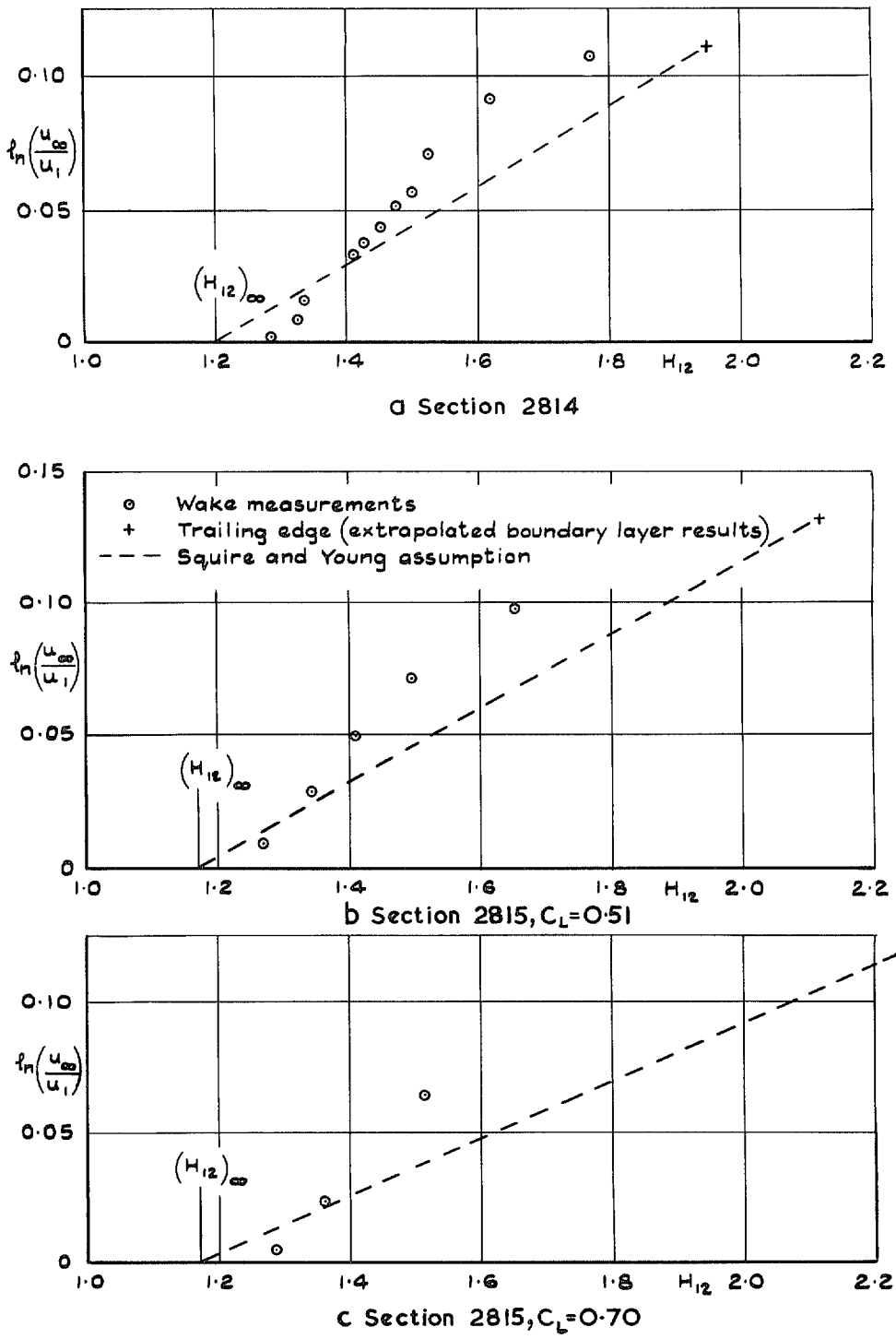

FIG. 33(a)–(c). Comparison of wake data with Squire and Young assumption.

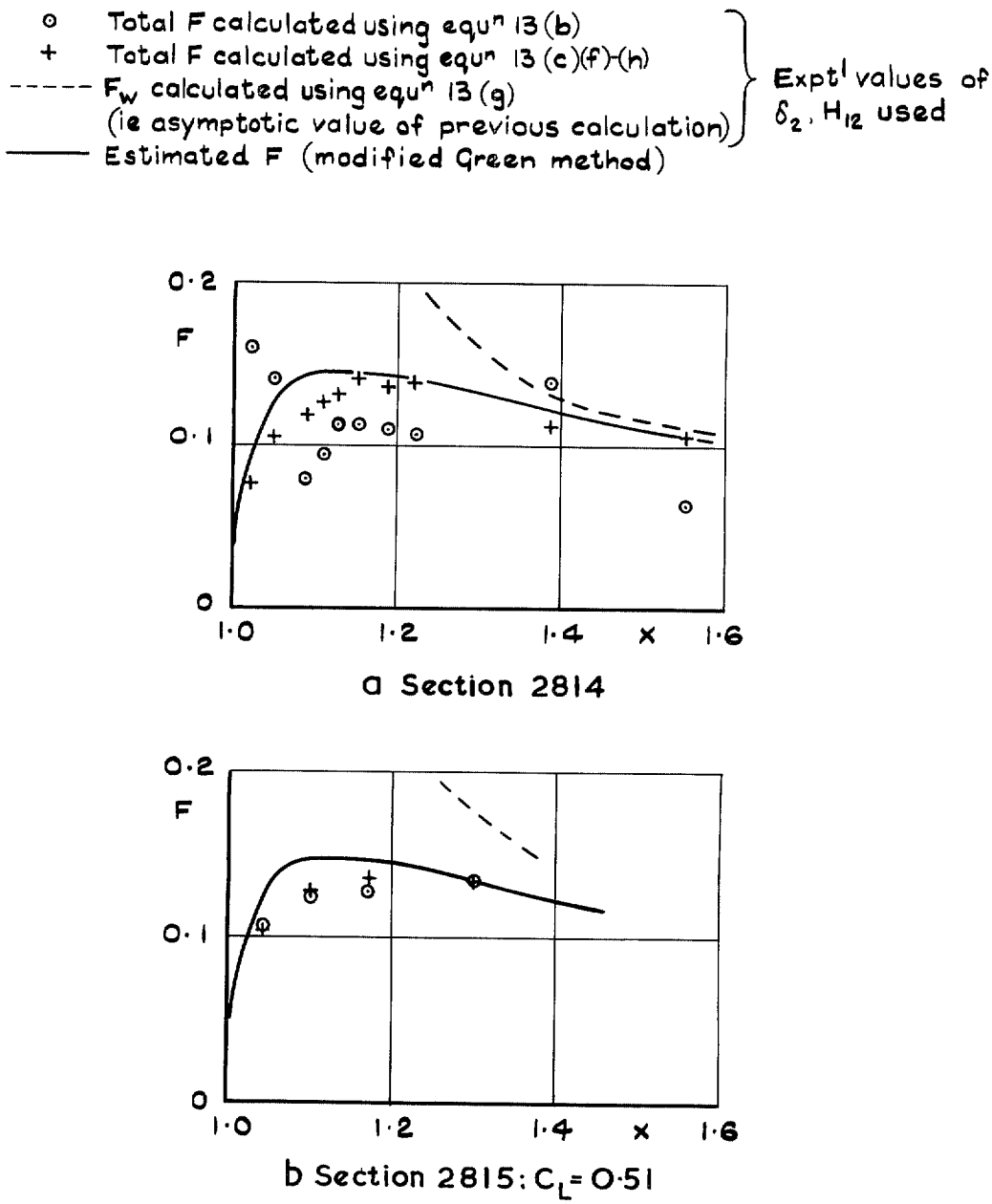

FIG. 34(a) and (b). Wake entrainment parameter.

Printed in England for Her Majesty's Stationery Office by J. W. Arrowsmith Ltd., Bristol BS3 2NT
Dd. 503426 K5 5/73

HER MAJESTY'S STATIONERY OFFICE

Government Bookshops

49 High Holborn, London WC1V 6HB
13a Castle Street, Edinburgh EH2 3AR
109 St Mary Street, Cardiff CF1 1JW
Brazennose Street, Manchester M60 8AS
50 Fairfax Street, Bristol BS1 3DE
258 Broad Street, Birmingham B1 2HE
80 Chichester Street, Belfast BT1 4JY

Government publications are also available through booksellers

SBN 11 470522 4*